Summer 7-30-2021

Efficient Polyhydroxyalkanoate Production by *Rhodopseudomonas palustris* from Lignocellulosic Biomass

Brandi Brown
University of Nebraska-Lincoln, bbrown25@huskers.unl.edu

EFFICIENT POLYHYDROXYALKANOATE PRODUCTION BY RHODOPSEUDOMONAS PALUSTRIS FROM LIGNOCELLULOSIC BIOMASS

by

Brandi J. Brown

A DISSERTATION

Presented to the Faculty of the

Graduate College at the

University of Nebraska

In Partial Fulfillment of Requirements

For the Degree of Doctor of Philosophy

Major: Biological Engineering

(Agricultural and Biological Systems Engineering)

Under the Supervision of Professors Rajib Saha and Mark Wilkins

Lincoln, Nebraska

July, 2021

EFFICIENT POLYHYDROXYALKANOATE PRODUCTION BY RHODOPSEUDOMONAS PALUSTRIS FROM LIGNOCELLULOSIC BIOMASS

Brandi Brown, Ph.D.

University of Nebraska-Lincoln, 2021

Advisors: Rajib Saha and Mark Wilkins

Polyhydroxyalkanoates (PHAs) are biopolymers produced by bacteria with the potential to replace conventional plastics. However, the relatively high production costs of PHAs are keeping them from market acceptance, with approximately half of the production costs derived from the feedstock. Thus, engineering a microbe for PHA production from cheaper and renewable carbon sources is necessary to promote the valorization of PHAs. Lignocellulosic biomass is considered to be one of the most economic carbon sources in the world, and is thus an attractive candidate for cheaper production of bioplastics. *Rhodopseudomonas palustris* CGA009 is a metabolically robust bacterium capable of catabolizing lignin breakdown products (LBPs), and also has the ability to produce several high-value bioproducts like bioplastics and biohydrogen. Thus, the goal of this research was aimed at producing and optimizing PHA production from *R. palustris* from LBPs. The first study produced poly-3-hydroxybutyrate (PHB) from *R. palustris* from the LBP *p*-coumarate with a PHB titer of 0.41 g/L and 68.4% carbon conversion efficiency. This study also optimized a high-throughput quantification method for PHB that employed flow cytometry. The second study produced poly(3-hydroxybutyrate-co-3-hydroxyvalerate) (PHBV) from the LBPs *p*-coumarate and coniferyl alcohol, and utilized an integrated experimental and computational modeling approach to infer metabolic factors controlling PHB production that can be expanded to

any PHB-producing microbe with similar metabolic features. The third study expressed the *phaP1* phasin gene from the PHB-producing model bacterium *Cupriavidus necator* H16 in *R. palustris* for the overproduction of PHBV on LBPs. Expression of *phaP1* yielded PHBV production from *R. palustris* aerobically (0.7 g/L), which does not occur in the wild type strain and provides more flexibility for industrial production. The 3-hydroxyvalerate fractions were also significantly increased under both anaerobic and aerobic conditions, which boosts thermomechanical properties compared to PHB alone. Taken together, these studies contributed to development of *R. palustris* as a biotechnology chassis for the production of bioplastics from lignocellosic biomass.

ACKNOWLEDGEMENTS

My dissertation and all the achievements during my program would not have been possible without a strong support network. Firstly, I'd like to thank my advisors, Dr. Mark Wilkins and Dr. Rajib Saha, for providing steadfast mentorship and for always believing in me. Having served as an officer in the United States Air Force for five years, I had to take prerequisite engineering courses before starting the program. Dr. Wilkins steered me through these, and also fostered me to work in Dr. Saha's Systems and Synthetic Biology (SSBio) Laboratory to gain experience in synthetic biology and metabolic analysis. I was pregnant twice during my program to have our first and second child, and neither of my advisors showed any signs of remorse when I informed them. They kept total faith in me, which gave the me encouragement to know that I could accomplish these hurdles while also growing my family. Furthermore, they have mentored and sponsored me to go to many conferences and other opportunities, which has enabled me to grow my technical communication, analysis, and other skills. Since my spouse is active duty in the military still, I knew I needed to accomplish this dissertation within three years. My advisors vectored me to accomplishing this on time, and I will be eternally grateful.

I dedicate this dissertation to my husband, Niall Brown, and our children. I could not have accomplished this without your love and support. We knew we would have to make some sacrifices as a family in order to get this done in three years, and you were always supportive. We always made the most of the situation as a family. For example, we would travel down to Lincoln together as a family on some weekends so that I could process some samples and then take Andromeda to visit Archie the mammoth or to the

Children's Museum afterwards. This has been the most adventurous three years of my life, and I cannot thank you enough for supporting me and being on this roller coaster with me the entire ride.

I would also like to thank my colleagues in Dr. Saha's SSBIO lab for their support and comradery. Dr. Cheryl Immethun (postdoctoral scholar) has been a phenomenal mentor to me during my program. It had been quite some time since I had stepped foot into a laboratory, and Cheryl was never condescending about giving me refreshers for the simpler tasks. She was patient, sincere, and provided just enough oversight and direction to enable me to grow as a researcher. I have learned so much from Cheryl, and will be forever indebted to her. I thank my fellow graduate students in the lab for being such a great team to be part of, such that everyone was looking out and supportive of one another (Adil Al-Siyabi, Mohammad Mazharul Islam, Mark Kathol, Dianna Long, and Wheaton Schroeder).

Furthermore, I thank Dr. Wilkins' Industrial Agricultural Products Center (IAPC) and its staff. I would not have been able to accomplish this dissertation without Anjeza Erickson, who mentored me on gas chromatography analysis and deconflicted between all of the clients and projects we had. Dr. Sibel Irmak and Boanerges Elías Bamaca mentored me in the methods they were working with regarding biohydrogen production. Lisbeth Vallecilla Yepez showed me how to process lignocellulosic biomass to obtain the pretreated liquor and to conduct enzymatic hydrolysis.

Finally, I would like to thank my close fiend Alyssa Timm, who was like my family-away-from family during this time. We were transplanted in Nebraska as a military family, and did not have family near us for support. Alyssa and the rest of the

Timms became our family here. I am thankful for having your friendship during my program, and especially for knowing there was someone I could rely on when Niall was deployed to look after Andromeda in case something happened and I was not able to make it back to Omaha on time. You have laughed and cried alongside me through these times, and I will forever value our friendship.

DISSERTATION DECLARATION

Chapter II was in progress to submission for peer review at the time of dissertation completion, no conflict of interest has been declared to this date.

Chapter III was published in Journal: Bioresource Technology Reports. Volume 11, 100474.

Chapter IV was submitted for peer review at the time of dissertation completion, no conflict of interest has been declared to this date.

Chapter V was submitted for peer review at the time of dissertation completion, no conflict of interest has been declared to this date.

TABLE OF CONTENTS

LIST OF TABLES

LIST OF FIGURES

CHAPTER I

1. Research objectives and brief description of studies

The overall objective was to produce and optimize polyhydroxyalkanoate (PHA) production from *R. palustris* grown on lignin breakdown products (LBPs). This objective was realized by the following studies:

i) ***Rhodopseudomonas palustris* CGA009 polyhydroxybutyrate (PHB) production from a lignin aromatic and quantification via flow cytometry (chapter III):** Although *R. palustris* is known to grow on lignin aromatics and lignocellulosic biomass, PHB production on phenolic LBPs had yet to be assessed (Larimer et al., 2004; McKinlay, Oda, Ruhl, et al., 2014). PHB metabolism serves as a redox sink for the bacterium, and since the LBP *p*-coumarate has more reducing potential than acetate it was hypothesized that *R. palustris* PHB production would increase using *p*-coumarate as a substrate (Kleiner et al., 2012; McKinlay, Oda, Rühl, et al., 2014). Hence, the first objective of this study was to produce PHB from *R. palustris* using *p*-coumarate, which yielded a PHB titer of 0.41 g/L with a 68.4% carbon conversion efficiency compared to no PHB titer from acetate (Brown et al., 2020). This study also optimized a high-throughput quantification method for PHB that employed flow cytometry. Extraction and quantification of PHB generally entails depolymerization so that the monomers can subsequently be analyzed with gas chromatography. This typically involves solvent extraction via acidic methanolysis with chlorinated hydrocarbons, which is time consuming and includes toxic solvents that are nonrecyclable (Anis et al., 2013; Kunasundari and Sudesh, 2011). Quantification of PHB via flow cytometry

was conducted with *R. palustris* for the first time, and this study delivered an optimized protocol using either Nile Red or BODIPY 493/503 lipophilic stains. Fluorescence intensity yielded high linear fitness with PHB titers for Nile Red (R^2 = 0.9384) and BODIPY 493/503 (R^2 = 0.9747). Unlike previous studies, the use of a permeabilizer yielded high linear fitness for cell counts when combined with Nile Red (R^2 = 0.9383) and BODIPY 493/503 (R^2 = 0.9955). Thus, a quick and non-destructive method for quantifying PHB production was optimized for this non-model bacterium grown on a lignin aromatic compound.

ii) **Synergistic Experimental and Computational Approach Identifies Novel Strategies for Polyhydroxybutyrate (PHB) Overproduction (chapter IV):** The second research study produced PHB from *R. palustris* on the LBP coniferyl alcohol for the first time and utilized an integrated experimental and computational modeling approach to decipher metabolic factors controlling PHB production. Comparison of the PHB profiles between *p*-coumarate and sodium butyrate showed that coniferyl alcohol's higher carbon content resulted in a higher rate of PHB production. However, coniferyl alcohol did not yield a higher titer than p-coumarate, and combined experimental results revealed that cytoplasmic space may be a limiting factor for maximum PHB titer. In order to obtain a systems-level understanding of factors driving PHB yield, a model-driven investigation was performed. The model yielded several engineering design strategies for PHB production, including utilizing reduced, high molecular weight substrates that bypass the thiolase reaction. The generality of the derived

design rules allows them to be applied to any PHB-producing microbe with similar metabolic features.

iii) **Heterologous Phasin Expression in *Rhodopseudomonas palustris* CGA009 for Bioplastic Production from Lignocellulosic Biomass (chapter V):** The third research study expressed the *phap1* gene (PhaP1 phasin protein) from the PHB-producing model bacterium *C. necator* H16 for the overproduction of PHAs by *R. palustris* using LBPs as substrate. Our recent efforts with *R. palustris* suggest intracellular space is a limiting factor of maximum production of the bioplastic poly(3-hydroxybutyrate-co-3-hydroxyvalerate) (PHBV) (Alsiyabi et al., 2021). PhaP1 leads to smaller and more abundant PHB granules in *C. necator*, and it was hypothesized that expression of this phasin would increase overall titers from *R. palustris* (Pötter et al., 2004; Sharma et al., 2016). Thus, *phaP1* was expressed in *R. palustris* with the aim of overproducing PHBV to foster smaller and more abundant granules and maximize the use of intracellular space. Expression of *phaP1* yielded PHBV production from *R. palustris* aerobically (0.7 g/L), which does not occur in the wild-type strain, and to a greater titer than wild-type anaerobic production (0.41 g/L). The 3HV fractions were also significantly increased under both anaerobic and aerobic conditions. Thus, heterologous phasin expression in *R. palustris* provides flexibility for industrial processing and fosters compositional changes in copolymers with better thermomechanical properties compared to PHB alone.

1.1 References

Alsiyabi, A., Brown, B., Immethun, C., Wilkins, M., Saha, R. (2021). *Synergistic Experimental and Computational Approach Identifies Novel Strategies for PHB Overproduction*. https://doi.org/10.21203/rs.3.rs-334477/v1

Anis, S. N. S., Iqbal, N. M., Kumar, S., Al-Ashraf, A. (2013). Increased recovery and improved purity of PHA from recombinant Cupriavidus necator. *Bioengineered*. https://doi.org/10.4161/bioe.22350

Brown, B., Immethun, C., Wilkins, M., Saha, R. (2020). Rhodopseudomonas palustris CGA009 polyhydroxybutyrate production from a lignin aromatic and quantification via flow cytometry. *Bioresource Technology Reports*, *11*, 100474. https://doi.org/https://doi.org/10.1016/j.biteb.2020.100474

Kleiner, M., Wentrup, C., Lott, C., Teeling, H., Wetzel, S., Young, J., … Dubilier, N. (2012). Metaproteomics of a gutless marine worm and its symbiotic microbial community reveal unusual pathways for carbon and energy use. *Proceedings of the National Academy of Sciences of the United States of America*. https://doi.org/10.1073/pnas.1121198109

Kunasundari, B., Sudesh, K. (2011). Isolation and recovery of microbial polyhydroxyalkanoates. *Express Polymer Letters*. https://doi.org/10.3144/expresspolymlett.2011.60

Larimer, F. W., Chain, P., Hauser, L., Lamerdin, J., Malfatti, S., Do, L., … Harwood, C. S. (2004). Complete genome sequence of the metabolically versatile photosynthetic bacterium Rhodopseudomonas palustris. *Nature Biotechnology*. https://doi.org/10.1038/nbt923

McKinlay, J. B., Oda, Y., Ruhl, M., Posto, A. L., Sauer, U., Harwood, C. S. (2014). Non-growing rhodopseudomonas palustris increases the hydrogen gas yield from acetate by shifting from the glyoxylate shunt to the tricarboxylic acid cycle. *Journal of Biological Chemistry*. https://doi.org/10.1074/jbc.M113.527515

McKinlay, J. B., Oda, Y., Rühl, M., Posto, A. L., Sauer, U., Harwood, C. S. (2014). Non-growing Rhodopseudomonas palustris Increases the Hydrogen Gas Yield from Acetate by Shifting from the Glyoxylate Shunt to the Tricarboxylic Acid Cycle* *Experimental aspects of this research were supported equally by the Division of Chemical Sciences,. *Journal of Biological Chemistry*, *289*(4), 1960–1970. https://doi.org/https://doi.org/10.1074/jbc.M113.527515

Mezzina, M. P., Pettinari, M. J. (2016). Phasins, Multifaceted Polyhydroxyalkanoate Granule-Associated Proteins. *Applied and Environmental Microbiology*, *82*(17), 5060 LP – 5067. https://doi.org/10.1128/AEM.01161-16

Pötter, M., Müller, H., Reinecke, F., Wieczorek, R., Fricke, F., Bowien, B., … Steinbüchel, A. (2004). The complex structure of polyhydroxybutyrate (PHB) granules: Four orthologous and paralogous phasins occur in Ralstonia eutropha. *Microbiology*. https://doi.org/10.1099/mic.0.26970-0

Sharma, P. K., Fu, J., Spicer, V., Krokhin, O. V, Cicek, N., Sparling, R., Levin, D. B. (2016). Global changes in the proteome of Cupriavidus necator H16 during poly-(3-hydroxybutyrate) synthesis from various biodiesel by-product substrates. *AMB Express*, *6*(1). https://doi.org/10.1186/s13568-016-0206-z

CHAPTER II

2. Literature review: *Rhodopseudomonas palustris*: A Biotechnology Chassis

Abstract

Rhodopseudomonas palustris is an attractive option for biotechnical applications and industrial engineering due to its metabolic versatility and its ability to catabolize a wide variety of feedstocks and turn them into several high-value products. Due to its adaptable metabolism, *R. palustris* has been studied and applied in an extensive variety of applications such as systems-level analysis of metabolic tradeoffs for environmental perturbations, biodegradation of aromatic compounds, environmental remediation, biofuel production, agricultural biostimulation, and electricity production. This review provides a holistic summary of the commercial applications for *R. palustris* as a biotechnology chassis and suggests future perspectives for research and engineering.

2.1 Introduction

Rhodopseudomonas palustris is a very metabolically robust bacterium that has the ability to catabolize a wide variety of feedstocks and turn them into several high-value products, making it an attractive option for biotechnical applications and industrial engineering. This gram-negative purple photosynthetic bacterium is renowned for its ability to function in the four known metabolisms of life: photosynthetic, photoheterotrophic, chemoheterotrophic, and chemoautotrophic (Larimer et al., 2004). It is commonly found in a wide variety of environments, and has been isolated from sources such as sludge, soils, aquatic sediments, alkaline waters, rice straw, leaf litters, and

eutrophic ponds (Rayyan et al., 2018). *R. palustris* was first identified by van Niel in 1944, and the first genome sequence of strain CGA009 was deciphered in 2004 (Larimer et al., 2004). This was followed by the complete genome sequence of strain JSC-3b in 2014, which is a strain known for degrading pyrethroid pesticides (Zhang et al., 2014). The essential genome of strain CGA009 was determined in 2016, and provides a detailed synopsis of the genes that are absolutely necessary for viability (Pechter et al., 2015). The complete genome sequence of strain ELI 1980 was obtained in 2017, and this strain has been applied as a commercial agricultural biostimulant (Crovadore et al., 2017). In 2018, the draft whole-genome sequence for strain XCP was accomplished, which was notable to have variations in cytochrome C2 compared to other strains (Rayyan et al., 2018). However, there have been many other strains isolated across the globe that have been applied in a variety of biotechnical applications that have yet to be sequenced (Table 1.1). Due to its versatile metabolism, *R. palustris* has been studied and applied in a wide variety of applications such as regulation of nitrogen fixation, photophosphorylation, biodegradation of aromatic compounds, environmental remediation, biofuel production, agricultural biostimulation, and electricity production. This review provides a holistic summary of the commercial applications for *R. palustris,* as well as future perspectives.

2.2 *R. palustris* as a model organism for flexible metabolism

R. palustris has emerged as a model organism for understanding how microbes respond to environmental perturbations on a systems level. The ability of *R. palustris* to switch between four modes of metabolism (photoautotrophy, photoheterotrophy, chemoautotrophy, and chemoheterotrophy) make it an ideal candidate for developing a deeper fundamental understanding of how organisms adapt to their environments.

Furthermore, *R. palustris* can grow both aerobically and aerobically, use light and organic compounds for its energy sources, use either organic or inorganics compounds for electron accumulation, and fix carbon dioxide and nitrogen gas (Oda et al., 2005; Rey and Harwood, 2010). During aerobic respiration, *R. palustris* can conduct aerobic respiration by oxidizing carbon compounds for carbon and energy. Known to straddle oxic and anoxic transitions zones, *R. palustris* can switch between aerobic respiration in atmospheric levels of oxygen to photosynthesis in anaerobic conditions (2-6% oxygen). As a result, *R. palustris* produces light absorbing pigments it needs for photosynthesis, turning the deep purple color it is known for. However, *R. palustris* differs from plants and cyanobacteria since it can perform photoheterotrophy in which it conducts anoxygenic photosynthesis (does not generate oxygen and CO_2 fixation is obligatory) (Rey and Harwood, 2010). *R. palustris* has also served as a model for adapting to changes in light conditions via employing phytochromes that alter gene expression, which ultimately provides insight into various strategies for responding to solar energy and optimizing photon capture (Evans K., Georgiou T., Hillon T., Fordham-Skelton A., 2009). Under low levels of oxygen *R. palustris* conducts nitrogen fixation and is capable of using atmospheric nitrogen as its sole nitrogen source (Rey and Harwood, 2010). As a byproduct of nitrogen fixation, *R. palustris* produces hydrogen and ammonium and has thus been extensively studied for biohydrogen fuel production (*Section 2.4*). *R. palustris* employs two forms of the enzyme ribulose-1,5-bisphosphate carboxylase/oxygenase (Rubisco), which is responsible for the majority of biologically-fixed CO_2 on Earth. There has been significant effort to engineer Rubisco since it is a relatively inefficient biocatalyst for the critical reaction in the Calvin-Benson-Bassham (CBB) reductive

pentose phosphate pathway (Rey and Harwood, 2010). *R. palustris* has served as a means to better understand this reaction mechanism and for deciphering differences in the forms of Rubisco enzymes (Satagopan et al., 2014). Due to *R. palustris'* ability to adapt to a wide variety of environments, it has also served as a platform for investigating biofilm formation under various conditions since the impact of biofilm formation during various metabolic growth modes can be investigated in a single species (Kernan et al., 2015). Findings, such as a novel quorum sensing synthase employed by *R. palustris* that is not tied to fatty acid metabolism (Schaefer et al., 2008), have expanded our understanding of biofilm formation in other organisms as well. Being able to either limit or encourage biofilm formation is key to optimized engineering for many applications in the biomedical and bioprocess engineering industries. Lastly, *R. palustris'* genome consists of 15% genes that encode for transport systems, which is triple that of most bacterial genomes (Larimer et al., 2004; Pechter et al., 2015). *R. palustris* has therefore been studied extensively for the transport and degradation of a wide variety of compounds (*Section 2.3*).

The "omics" revolution combined with advances in metabolic modelling have provided a platform for understanding *R. palustris* from a systems-level approach. Newer genome-scale metabolic modelling techniques enable simultaneous comparisons of biological trade-offs from several objectives and constraints. A recent metabolic model identified that phototrophic metabolism in *R. palustris* is limited by light and not the availability of carbon, and that *R. palustris* will still strive for maximum carbon efficiency even if this efficiency results in lower growth rates (Navid et al., 2019). A genome-scale metabolic model was employed in order to decipher tradeoffs and

connections between photosynthesis, CO_2 fixation, and the quinone pool by *R. palustris* (Alsiyabi et al., 2019). This model identified several key factors for employing excess electrons produced during metabolic processes that can be further exploited. These findings included the presence of an unidentified sink responsible for the oxidation of excess quinols generated by the tricarboxylic acid (TCA) cycle, that the quinol oxidation rate governs light-dependent energy production, and the amount of ATP generated in the electron transport chain directly impacts the extent of CO_2 fixation (Alsiyabi et al., 2019). In summary, *R. palustris* is an excellent candidate for studying the systems-level metabolic tradeoffs between major forms of metabolisms. As more information is available that can feed into increasingly sophisticated metabolic modeling, such as the availability of metabolic flux analysis models, deeper understandings about tradeoffs between modes of metabolism can be found from a systems perspective.

2.3 *R. palustris* biodegradation applications

The biodegradation of aromatic compounds has received much attention due to their persistence, toxicity, and renewability. *R. palustris* is renowned for its ability to catabolize a wide variety of aromatic compounds, which makes it an excellent candidate for applications in bioremediation and utilizing renewable aromatics like those from lignocellulosic biomass. The biochemical pathways for anaerobic benzoate and 4-hydroxybenzoate degradation have been characterized extensively, and have illuminated novel steps in the biodegradation pathway (Egland et al., 1995; Hirakawa et al., 2015). For example, the AadR and HbaR members of the fumarate and nitrate reductase (FNR) family of transcriptional regulators have been characterized (Díaz and Prieto, 2000). This

characterization provides a platform of bacterial promotors for further engineering the biodegradation of aromatic pollutants.

Aromatic hydrocarbon contamination is found in environments worldwide, and microbial degradation has become a promising strategy for remediation and recovery. Petroleum is the base material for many of today's products from plastics to cosmetics. *R. palustris* has been applied to mitigate aromatic hydrocarbon contamination through petroleum removal in marine environments via the transformation of toluene to benzoyl-CoA (Harayama et al., 1999; Rhee et al., 2004), flame retardants (Chang et al., 2020; Li et al., 2021; R. Wang et al., 2019), and polycyclic aromatic hydrocarbon degradation (Zhao et al., 2011). Another approach to remediate the impacts of petroleum-based products is through promoting processes for biodegradable and sustainable plastics. Enzymes employed by *R. palustris* are capable of degrading polyesters such as the bioplastic poly(lactic) acid (PLA), which is a potential replacement for conventional plastics (Hajighasemi et al., 2016; Qi et al., 2017; X. Wang et al., 2019). Thus, *R. palustris* has been employed as a robust chassis for the remediation of aromatic hydrocarbon contaminations.

As a photosynthetic bacterium with high tolerance and flexible metabolic modes, *R. palustris* has also been employed for waste water remediation. Sustainable waste water treatment has reached a paradigm shift from removing unwanted pollutants to salvaging resources and producing energy. Alternative methods to replace conventional activated sludge methods are arising to develop more sustainable protocols and combat some of the leading challenges associated with waste water treatment such as nutrient recovery and

degradation efficiency. The feasibility of utilizing photosynthetic bacteria for wastewater treatment has been extensively studied since they can be used to deliver more complete nutrient capture in waste water, absorb CO_2, deliver diversification of products, and their biomass can be recycled for downstream processing (J. Chen et al., 2020). A recent review provides an overview of photosynthetic-based technology for wastewater treatment, and details the photosynthetic membrane bioreactor systems in which *R. palustris* has been applied (J. Chen et al., 2020). *R. palustris* has been specifically studied for removal of heavy metals from waste water (Gao et al., 2017), consumption of oils (Padovani et al., 2018; Phongjarus et al., 2018), decolorization and mineralization of dyes (Liu et al., 2006; Rumin et al., 2015; Wang et al., 2008), processing farm chemicals and wastewaters (Dong et al., 2017; Kim et al., 2004; Mutharasaiah et al., 2012a; Phongjarus et al., 2018; Wu et al., 2019), salinity tolerance (Qin et al., 2017), efficient culture using landfill leachate (Qing Wang, Lijun Shen, Zhenzhen Zhao, Hai Yan, Qianqian Xu, Chunhua Yin, Xiaolu Liu, 2018), dechlorination (Egland et al., 2001; Kamal and Wyndham, 1990), and the degradation of chemicals used in fuel processing (Berne et al., 2007, 2005).

R. palustris is also a promising biotechnology chassis for the production of high-value productions from the biodegradation of lignocellulosic biomass. Lignocellulosic biomass from plants is a common agricultural waste and highly renewable carbon source, and is thereby considered to have the most economic potential (Ponnusamy et al., 2019; Qian, 2013). Lignin comprises a large portion of lignocellulosic biomass and is the most abundant aromatic polymer on Earth, but unfortunately many microbes are unable to catabolize it and are often inhibited by it due to its toxicity and inhibition of enzymes

(Lee et al., 2019). The production of biopolymers from lignin has emerged as one of the most promising routes for valorizing lignin, and thus engineering a microbe that can catabolize it for high-value products is ideal (Rajesh Banu et al., 2019). As a very metabolically robust bacterium, *R. palustris*' genome includes pathways for three of the four known microbial lignin degradation strategies, incorporating both aerobic and anaerobic photosynthetic catabolism (Larimer et al., 2004). Thus, *R. palustris* cannot only break down numerous aromatic compounds derived from lignin but could also potentially accomplish complete degradation of lignin breakdown products to intermediates in the citric acid cycle that are important building blocks for multiple cell functions (Harwood and Gibson, 1988; Larimer et al., 2004). Thus far, it has been shown that *R. palustris* can catabolize over two dozen aromatic compounds from lignin (Austin et al., 2015; Harwood and Gibson, 1988). *R. palustris* has emerged as model organism for anaerobic catabolism of aromatic compounds, in particular for the major lignin breakdown product *p*-coumarate (Doud and Angenent, 2016; Pan et al., 2008; Salmon et al., 2013). Employing *R. palustris* as a means to remove these aromatics so that another microbe may consume sugars or other breakdown products has proved to be a promising strategy for efficiently utilizing pretreated lignocellulosic biomass (Austin et al., 2015). Another study identified that single-genotype syntropy is not an ideal strategy to aid the redox balance during anaerobic degradation of lignin monomers (Doud and Angenent, 2016). Recent kinetic modeling of anaerobic degradation of lignin aromatics by *R. palustris* highlights the dynamics between the co-metabolism of multiple lignin aromatics and proposes new mechanisms for substrate channeling (Ma et al., 2021). Lastly, although Strain CGA009 was shown to be unable to metabolize meta-methoxylated phenolic

compounds from lignin, Strain SA008.1.07 was recently adapted to grow on syringic acid as a sole carbon source (Oshlag et al., 2020). However, many lignin breakdown products remain uncharacterized for this bacterium, and there is a large gap in our understanding of degradation pathways. Furthermore, optimizing co-culture systems whereby multiple organisms can consume different parts of lignocellosic biomass could provide for more holistic processing into high-value products.

2.4 *R. palustris* is a biohydrogen powerhouse

There have been attempts to produce biofuels from *R. palustris*, such as n-butanol (Bai et al., 2020; Doud et al., 2017), but the majority of research is aimed at biohydrogen production due to *R. palustris'* native capabilities for hydrogen production and its flexibility as a chassis. Hydrogen combustion produces no CO_2 emission, is efficiently converted to electricity, and produces 2.72 times greater energy yield than gasoline, making it one of the cleanest possible energy alternatives to fossil fuels (Levin et al., 2004). Biological hydrogen production technologies are considered to be one of the leading options for hydrogen production. Photo-hydrogen production by photosynthetic bacteria is ranked highest in these promising biological conversion technologies due to the high purity of the hydrogen produced, high theoretical conversion, and the ability to use a variety of feedstocks.

R. palustris is one of the very few prokaryotes characterized thus far that encodes three different nitrogenases, the enzyme responsible for converting nitrogen gas into ammonia with the obligatory production of hydrogen. A molybdenum cofactor (Mo) nitrogenase is encoded by the *nif* genes, and two alternative vanadium cofactor (V) and

iron cofactor (Fe) nitrogenases are encoded by the *vnf* and *anf* genes respectively (Oda et al., 2005). Thus, *R. palustris* has multiple enzymatic options for nitrogen-fixation and is not repressed by the presence of transition metals like many other bacteria (Oda et al., 2005). Furthermore, the ability of *R. palustris* to generate H_2 without producing O_2 provides an opportune production system for purer hydrogen fuel production. Significantly larger H_2 yields are overserved from *R. palustris* when it is starved for nitrogen and cells can utilize the available electrons to synthesize H_2 from nitrogenase (McKinlay et al., 2014). Many synthetic biology efforts have fostered a more fundamental understanding of *R. palustris'* H_2 production abilities under various conditions or created new strains for overproduction. Strains that produce H_2 constitutively even in the presence of ammonium have been selected, and produce up to five times the amount of H_2 compared to the wild-type strain under nitrogen fixing conditions (Rey et al., 2007). The selection strategy identified in this study can also be expanded to many species of anoxygenic photosynthetic bacteria to pinpoint fitness incentives for H_2 production. The regulatory paradox for why these mutants are able to resist posttranslational modifications that would normally inactive nitrogenases has been illuminated, which revealed that the mutants have insufficient levels of two posttranslational regulation proteins (DraT2 and GlnK2) (Heiniger et al., 2012). A strain containing a variant molybdenum nitrogenase was used to assess tradeoffs in intracellular ADP, light intensity, and gas production that hypothesized that rate limiting step for H_2 and CH_4 production is inhibition of nitrogenase by ADP. This study revealed several strategies for H_2 and even CH_4 production that included (i) increasing the amounts of electrons available to nitrogenase by providing cells with organic alcohols, (ii) using

nongrowing cells, blocking electrons from entering the Calvin cycle, and (iii) or blocking H_2 uptake (Zheng and Harwood, 2019). Another approach for H_2 overproduction was to delete the bioplastic poly-β-hydroxybutyrate (PHB) synthesis gene *phbC* in *R. palustris* WP3-5 to funnel carbon and reducing potential to H_2 production, which yielded 1.7 times more H_2 than the non-engineered strain (Yang and Lee, 2011). Since the O_2-fixing Calvin cycle competes with H_2 production for electrons, another study showed that deletion of the upstream phosphoribulokinase (PRK) resulted in both an increase in H_2 yield and specific production rate (McCully and McKinlay, 2016). This provides an alternative strategy to disrupting the Rubisco enzyme, which can cause negative impacts on growth and does not yield an increase in H_2 production rates. Thus, the robustness of *R. palustris'* H_2 production arsenal provides a platform for developing over-producing strains and for generating a more holistic understanding of H_2 production by photosynthetic bacteria in general.

R. palustris is an attractive microbial biocatalyst for hydrogen production since it can generate ATP from light and reductant necessary for nitrogen fixation from a wide variety of compounds including aromatic compounds (Alsiyabi et al., 2021; Archana et al., 2003; Fiβler et al., 1995), inorganic electron donors (e.g. thiosulfate) (Huang et al., 2010), industrial wastes (Adessi et al., 2018; Corneli et al., 2017; Lee et al., 2011, 2006; Pintucci et al., 2015, 2013), substrates with relatively high salt concentrations (Adessi et al., 2016), and carbon monoxide and water (Oh et al., 2005). For example, *R. palustris* has been shown to produce biohydrogen from crude glycerol (a byproduct of biodiesel manufacturing) to yields higher than other photosynthetic bacteria (Ghosh et al., 2012; Sabourin-Provost and Hallenbeck, 2009). Strains P4 and PT have the ability to grow to a

higher cell density, have a high specific H_2 production activity, and produce carbon monoxide-dependent H_2 production from the water-gas shift reaction (Hosseini et al., 2015; Oh et al., 2005, 2002). Perhaps the most promising biohydrogen production strategy thus far has been syntrophic metabolism of co-cultures. Table 1.2 provides an overview of some highlighted H_2 production systems involving *R. palustris*. Developing co-culture systems employing *R. palustris* enables the removal of inhibitory compounds or metabolic byproducts by the versatile bacterium that allow growth of the other organism(s) and more holistic consumption of feedstocks. Several co-culture systems have developed relatively high H_2 yields utilizing a combined dark-photo fermentation process from potato starch and glucose (Hitit et al., 2017a), cellulose (Hitit et al., 2017b), cheese whey (Azbar and Cetinkaya Dokgoz, 2010), cassava starch (Su et al., 2009a, 2009b), or bread wastes (Adessi et al., 2018). Yet, more research and development regarding H_2 production from renewable and cost-effective substrates is necessary. Lignocellulosic biomass has high potential as an ideal feedstock for photofermentative H_2 production. *R. palustris* shows resistance towards high phenolic concentrations derived from lignocellulosic biomass, and has been known to utilize lignin breakdown productions for H_2 production (Alsiyabi et al., 2021; Mabutyana and Pott, 2021). Advances in co-culture systems on lignocellulosic biomass whereby one organism consumes the sugars and *R. palustris* utilizes the inhibitory phenolic compounds could further valorize biohydrogen production from lignocellulosic biomass.

There have been numerous progressive techniques engineered for biohydrogen production involving *R. palustris*. Entrapment of cells in gels (Ross and Pott, 2021; Tian et al., 2009; Wang et al., 2013), support mediums like grid columnar flat panels (Y.

Wang et al., 2019), SiO2-chitosan support mediums (Liao et al., 2013), and reverse micelles (Pandey et al., 2007) have shown improved H_2 production compared to planktonic cultures. Biofilm photobioreactors using packed glass beads (Tian et al., 2010) and optical fiber-illuminating photobioreactors (Chen et al., 2006a) have also shown promise. *R. palustris* has also been used as a model organism for testing continuous reactors, and for employing ultrasonic treatment to boost H_2 production (Wang et al., 2012). Several modelling techniques such as statistical experimental design (Jamil et al., 2009) and response surface methodology and desirability function approaches (Hitit et al., 2017b, 2017c; Liu et al., 2015; Shi et al., 2014) have optimized H_2 production by *R. palustris* in a variety of conditions. A method of using light-activated materials and biocatalysts from *R. palustris* to produce H_2 with conjugated polymers has been developed recently (Wang et al., 2021). Plasmonic nanoparticles and near-infrared light offer a novel method for conversion of organic acids to H_2 by *R. palustris,* and increased the purity of H_2 produced (J. Craven, M.A. Sultan, R. Sarma, S. Wilson, N. Meeks, D.Y. Kim, 2019). A nanoscale organic-iron complex was shown to be more efficient than iron ions alone, and improved H_2 production in several strains of *R. palustris* (Kanwal et al., 2020). Sustained outdoors biohydrogen production from tubular photobioreactors has also been demonstrated (Adessi et al., 2012). Acclimation strategies like photo-acclimation (Muzziotti et al., 2017), photo-evolution (Pintucci et al., 2015), and heat-acclimation (Pintucci et al., 2015) have generated new strains with significantly improved H_2 production.

In summary, *R. palustris* is a robust and diverse powerhouse for biohydrogen production. However, there is still room for growth to further valorize biohydrogen

production for industrial-scale production. The main bottleneck of H_2 production is production efficiency, and either sequential or co-culture systems offer a possibility to boost efficiency. A combination of dark and photo-fermentation may be the solution to converting organic acids, removing chemical oxygen demand, and enabling more flexibility for using renewable and cheaper feedstocks. Either sequential or co-culture H_2 production systems provide possibilities to achieve higher efficiency, but more research is necessary for optimization. Furthermore, the photofermentation production aspect of the system needs to be optimized to increase the lower growth rates of the photosynthetic bacteria as well as boosting light conversion efficiencies. Genetically engineering *R. palustris* to optimize H_2 production on various light intensities, reducing the lag phase, and increase H_2 production rates are all examples of ways to boost production in a combined dark and photo-fermentative system (Kour et al., 2019). Combined dark and photofermentative H_2 production from wastes (e.g. waste waters and lignocellosic biomass) provide a unique opportunity to utilize cheap and renewable feedstocks in which more holistic conversion can be accomplished by multiple organisms.

2.5 *R. palustris* electricity generation

Bioelectrochemical systems have emerged as a promising means for developing sustainable electricity generation, waste removal, recovering valuable resources, producing chemicals, and much more (Bajracharya et al., 2016). These systems utilize microbes as biocatalysts to convert chemical energy into electrical energy (and vice versa), and rely on the ability of the microbe to transport electrons. As a facultative phototroph, *R. palustris* offers distinct advantages regarding engineering toward more efficient bioelectrical systems. Under photoautotrophic conditions, *R. palustris* utilizes

electrons from inorganic donors to generate reducing equivalents. However, under photoheterotrophic conditions *R. palustris* can obtain these electrons from organic donors and balances the excess reducing power through CO_2 fixation or via other electron acceptors. Thus, *R. palustris'* flexible metabolism enables it to either accept or supply electrons to an electrode. For example, *R. palustris* Azul can perform direct and indirect electron uptake during phototrophic conditions, and can transfer charge from redox molecules to extracellular space (Guardia et al., 2020). It has also been shown recently that the nitrogen ratio can be customized to direct what fraction of electron flux is directed towards biosynthesis, biohydrogen, and extracellular electron transfer (Pankan et al., 2020). To fill the knowledge gap of how microbes use solid-phase conductive substances as electron donors, *R. palustris* was employed to take up electrons from substances like metal oxides (Guzman et al., 2019). *R. palustris* TIE-1 has served as a model organism for the development of bioelectrochemical systems since it can generate electricity and higher power density relative to mixed cultures and can use a wide variety of substates (Xing et al., 2008). Its electron uptake ability and growth under photoelectroautotrophic conditions has been further optimized by iron-mediated uptake strategies like the addition of immobilized iron-based redox mediators (e.g. Prussian Blue) (Doud and Angenent, 2014; Rengasamy et al., 2018). Deletion of the genes encoding Rubisco in *R. palustris* TIE-1 led to a reduction in extracellular electron uptake, which highlights that phototrophic electron uptake is linked to CO_2 fixation (Guzman et al., 2019). This demonstrates that phototrophs can directly use solid-phase substances for electron transfer, energy transduction, and CO_2 fixation. Consequently, *R. palustris* was the first purple no sulfur bacterium demonstrated to perform direct contact and electron

transfer following biofilm growth. Another tactic genetically suppressed hydrogen production to render more availability to reducing equivalents, thereby improving electricity generation by *R. palustris* (Morishima et al., 2007). Taken together, these studies highlight how *R. palustris* has been used as a model organism for developing a deeper fundamental understanding of how photosynthetic bacteria can be manipulated to cater to bioelectrochemical production.

Microbial fuel cells (MFCs) are a type of bioelectrochemical system where heterotrophic bacteria metabolize exogenous organic nutrients and generate external electrical currents (Howe and Bombelli, 2020). In comparison, in biophotovoltaics (BPVs) the electrical current comes from electrons generated by the light-driven oxidation of water that are passed through the photosynthetic electron transfer chain (rather than via heterotrophic metabolism) (Howe and Bombelli, 2020). Sometimes referred to as photosynthetic microbial fuel cells (photo-MFCs), BPVs do not require supply of an added organic substrate like MFCs, and thus mass transfer is not a limiting factor of BPVs. *R. palustris* has been applied in MFCs and photo-MFCs using corn stover (Wang et al., 2009), soil paddy soils (Liu et al., 2021), poly(lactic)acid (Qi et al., 2018a, 2018b), and whole-cell cyanobacteria (Inglesby et al., 2012) as feedstocks. For example, *R. palustris* strain PS3 is a plant-based strain that has been studied for electricity generation in paddy soil-based MFCs (Liu et al., 2021). The essential factors affecting bioelectricity generation were illuminated, which revealed improved power performance arises from the biofilm acting as a living electrode in the system, CO_2 fixation, and oxidation of ferrous iron in the soil. Complementary metal-oxide-semiconductor technology was also implemented, which is expected to deliver a potentially lower-cost

system with higher power output for practical applications. In another study, a portable, paper-based MFC was fabricated using *R. palustris*, which could be preserved for long-term usage with only 10% performance degradation after four weeks (Otani et al., 2020). Syntropy between microbial consortia of *R. palustris* and hydrogen oxidizing bacteria has also been proposed as a strategy to produce higher power densities in MFCs (Park et al., 2014). *R. palustris* has also been applied in MFCs employing microbial electrochemical remediation systems (MERS). MERS are strategies that exploit microorganisms' abilities for remediation (e.g., treating contaminants) in the environmental while also producing electricity. *R. palustris* RP2 is a strain isolated from anodic biofilms of MERS with the capability for direct electrode respiration, anaerobic nitrate reduction, dissimilarity metal oxide reduction, and degradation of petroleum hydrocarbons (Venkidusamy and Megharaj, 2016).

Despite the advances in bioelectrochemical production and MFCs, there is still limited knowledge in our understanding of the molecular components involved in the associated mechanisms. For example, *R. palustris'* genome has an arsenal of electron transport mechanisms that have yet to be explored in great detail, such as the porin-cytochrome complexes that facilitate movement of electron acceptors (e.g. MtrA/MtrB cytochrome: porin homologues MtoA/MtoB) (Larimer et al., 2004; McCormick et al., 2015). Advances in our understanding of the critical components and mechanisms factored into electrochemical production, the development of improved genetic tools, and initiatives in scale-up feasibility should progress the possibilities of utilizing *R. palustris* as a versatile platform for power production, especially from cheaper and renewable feedstocks like wastes or lignocellulosic biomass.

2.6 *R. palustris* bioplastic production

Since the 1950s, an estimated 18.2 trillion tons of fossil-fuel derived plastics have been created, with only 9% of it being recycled (Geyer et al., 2017). Thus there, has been much attention towards finding sustainable and renewable alternatives to conventional plastics. Polyhydroxyalkonoates (PHAs) are a type of biopolymer created by a variety of microbes under certain environmental conditions that are stored as granules inside the cell. PHAs are an ideal substitute for conventional plastics since they are produced by a wide array of microorganisms, biodegradable, renewable, show biocompatibility with cells and tissues, and have a wide range of diverse structures (G.-Q. Chen et al., 2020a). Unfortunately the widespread adoption of PHAs is hampered by higher production costs, which is largely attributed to feedstock costs (G.-Q. Chen et al., 2020b). Due to *R. palustris'* flexible metabolism and ability to utilize a wide array of feedstocks, it offers a unique opportunity to generate bioplastics from cheaper feedstocks and render PHAs more cost-effective for market acceptance.

R. palustris has been shown to produce PHAs from waste products, such as lignocellulosic biomass. For example, *R. palustris* accumulates the most common PHA, called poly-3-hydrdoxybutyrate (PHB), from several lignin breakdown products (Alsiyabi et al., 2021; Brown et al., 2020) and nutrient recovery from cyanobacteria blooms (Tian et al., 2017). It has also been revealed that *R. palustris* is capable of creating a copolymer of PHB called poly-3-hydroxybutyrate-co-hydroxyvalerate (PHBV) that has better thermomechanical properties compared to PHB alone (Alsiyabi et al., 2021). PHA production in each bacterium is governed by *in vivo* substrate specificity of

enzymes and specific metabolic and regulatory network characteristics. PHA metabolism influences other cell activities and is usually controlled by a group of proteins called granule associated proteins (GAPs). These GAPs include PHA synthases, PHA depolymerase, PHA repressor proteins, acyl-CoA synthase, and phasins. Phasins are the dominant protein surrounding PHA granules, and a recent study expressed the dominant phasin from the PHB-producing model bacterium *Cupriavidus necator* H16 into *R. palustris* for the overproduction of PHB on lignin breakdown products (Chapter V).

As previously described, there are tradeoffs in utilizing reducing power between biomass, PHA, and H_2 production by *R. palustris* (Chen et al., 2012; McKinlay et al., 2014; Touloupakis et al., 2021), and identifying how to capitalize on these tradeoffs is critical for engineering over-producing strains. A recent study delivered a synergistic experimental and computational biology approach that identified key design strategies for PHB overproduction in *R. palustris* and other organisms with similar metabolisms (Alsiyabi et al., 2021). Combined experimental results including PHB production on various substrates (e.g., lignin breakdown products), H_2 production, and electron microscopy suggested that the rate of PHB production is mainly controlled by metabolic factors. Thermokinetic analysis identified a bottleneck in the thiolase reaction (*phaA*) in the PHB production pathway. Application of a novel genome-scale metabolic model rendered four major findings including (i) a very high AcCoA/CoA ratio is required to drive the thiolase reaction, (ii) substrates with high carbon uptake rates accumulate higher amounts of acyl-CoA, (iii) the rate through PhaB (reductase) is linearly dependent on the NADPH/NADP ratio, and (iv) PhaB will likely be rate-limiting even under optimal metabolic conditions due to the very low catalytic efficiency (Alsiyabi et al., 2021, 2019).

Ultimately, *R. palustris* was used a model organism for deciphering generalized design strategies that could be expanded to other organisms with similar metabolism for the over-production of PHB. Emerging techniques with microbial electrosynthesis have also capitalized on tradeoffs between PHB and H_2 production from available reducing potential. The ability to produce PHB *by R. palustris* TIE-1 via bioelectrochemical generation became the first study to systematically quantify PHB production by photoelectroautotrophy and photoferrautotrophy (Ranaivoarisoa et al., 2019). Other studies employing TIE-1 have utilized immobilized iron complexes and Magnetite nanoparticle anchored graphene cathodes to enhance PHB production vial microbial electrosynthesis (Rengasamy et al., 2020, 2017).

Despite these advances in PHB production from *R. palustris*, many studies focus on H_2 production rather than PHB production due to *R. palustris'* native ability as a powerhouse for biohydrogen generation. *R. palustris* is still emerging as non-model bacteria for bioplastic production, and thus there are gaps in our understanding regarding its PHA production mechanisms. For example, characterizing *R. palustris'* native phasins employed for PHA production or engineering methods for increased fractions of valerate in PHBV production are ideal stepping stones.

2.7 *R. palustris'* environmental remediation and agricultural production

As a naturally-occurring bacterium found in a wide variety of environments, *R. palustris* has been used as a bio-based method for applications in agricultural for bioremediation and to boost plant production. Industrial and agricultural activity can often be detrimental to soils and other environments, making it necessary to find effective

and sustainable remediation methods. Bioremediation of contaminated soils has been demonstrated by several strains such as degradation of chlorobenzoic acids by Strain RCB100 (Haq and Fixen, 2021), removal of heavy metals and metalloids by Strain CGA009 (Batool et al., 2017; Llorens et al., 2012; Zhao et al., 2015), and elimination of acrylamide by *S*train Ac1 (Wampler and Ensign, 2005). Several strains of *R. palustris* have been applied for waste water treatment and nutrient recovery for detoxifying pesticides (Luo et al., 2018; Wu et al., 2019; L. Yin et al., 2012), removing halogenated compounds (Mutharasaiah et al., 2012b; Tomei et al., 2021), decreasing the chemical oxygen demand, nitrates, and H_2S in the system (Bogarapu et al., 2019), and cleaning aquaculture pond waters (Xiao et al., 2020). A shift from employing monocultures for bioremediation to microbial communities using advancing techniques like machine learning are enabling artificial selection of optimal consortia the can be applied in certain conditions (Borchert et al., 2021). Future efforts employing optimized systems of microbial consortia could further improve microbial remediation of waste water and even promote the production of high-value products (Nagadomi et al., 2000).

With the stark increase in global population, the need to find more effective and sustainable methods to feed the growing populous is ever-pressing. Agricultural biostimulants have emerged as an ideal method for using biologically-derived fertilizer additives or other products that are applied to boost plant health, growth, and productivity during crop production. *R. palustris* has shown great promise as a commercialized biostimulant for enhancing agricultural production. Notably, Strain ELI 1980 has been used as a component of Quantum Light, a biofertilizer commercialized by Ecological Laboratories, Inc. (FL, USA) (Crovadore et al., 2017). A recent review on purple non-

sulfur bacteria and plant production provides a nice overview of the many benefits several strains of *R. palustris* have had for numerous crops (Sakarika et al., 2020). Strains P3 and BCRC16408 have a promoting effect on *Brassica rapa chinensis* (Chinese cabbage) with reduced fertilizer input, the ability to use poorer-quality seeds, and higher crop yields (Hsu et al., 2021; Wong et al., 2014). A strategy for quicker and cheaper fermentation of Strain P3 using corn steep liquor and molasses has also been developed, which further promotes it for large-scale industrial production (Lo et al., 2020). Strain GJ-22 yielded systemic protection of tobacco plants against tobacco mosaic virus (Su et al., 2017), and a genetic tool was developed recently enabling visualization of bacterial colonization on tobacco and rice leaves (Zhai et al., 2019). Stevia plants (Wu et al., 2013; XU et al., 2018) and Chinese Dwarf Cherry seedlings (Z. P. Yin et al., 2012) are also among the plants known to have positive effects from *R. palustris*. Several strains of *R. palustris* have potential for biofertilizers for rice production as well. Strain PSB06 promotes rice growth and enhances stress resistance at the seedling stage, and both Strain PSB06 and Strain CGA006 increase the length of length of stems (Luo et al., 2019). Strains TK103, PP803, and P1 have several beneficial attributes to rice production including increased rice grain yield, reduce inhibition of rice straw and hucks, increased root dry weight, and increased plant height under salt stress (Kantachote et al., 2016; Kantha et al., 2015). *R. palustris* also shows potential as a biofertilizer for plant growth at sites with heavy metal contamination, as demonstrated in with Strain CS2 on *Vigna mungo* (bean) in soil contaminated with arsenic and heavy metals (Batool et al., 2017). Hence, *R. palustris* has been investigated and applied in a variety of biostimulant applications. However, deciphering the implications for abiotic stress tolerance,

agronomic and physiological traits of crops, interaction with non-microbial biostimulants, and improvements in nutrient usage associated with *R. palustris* are all necessary to continue to develop it as a commercialized biostimulant (Rouphael and Colla, 2020).

2.8 Conclusions

R. palustris is a purple non sulfur bacteria that is an attractive option for biotechnical applications and industrial engineering since it is among the most metabolically robust bacteria with the ability to catabolize a wide variety of feedstocks and turn them into several high-value products. Due to its versatile metabolism, *R. palustris* has been studied and applied in a wide variety of applications such as systems-level analysis of metabolic tradeoffs for environmental perturbations, biodegradation of aromatic compounds, environmental remediation, biofuel production, agricultural biostimulation, and electricity production (Fig. 2.1). Although *R. palustris* holds great potential as a commercial biotechnology chassis, further research and application that combines emerging technologies is necessary for optimization and cost-competitiveness. Engineering systems-level approaches that capitalize on more than one aspect of *R. palustris'* capabilities will be the key to developing more efficient and sustainable industrial processes. For example, a recent study combined *R. palustris'* biodegradation capabilities of recalcitrant ethinylestradiol in a novel hybrid photo-MFC to enhance biohydrogen production (Sogani et al., 2021). The commercial application of *R. palustris* as a versatile biotechnology chassis will continue to rise as advances in our understanding of systems-level tradeoffs in metabolic capacities are coupled with synthetic biology and emerging technologies that utilize renewable substrates.

Table 2.1 Highlighted *R. palustris* strains and their applications

Strain	Application(s)	Reference(s)
42OL	H_2 production	(Adessi et al., 2012)
AS1.2352	Azo dyes decolorization	(Liu et al., 2006)
ATH2.1.37	Heat-acclimated, H_2 production	(du Toit and Pott, 2021)
Azul	Electricity generation	(Guardia et al., 2020)
CGA009	Genome-scale modeling for studying photoheterotrophy; H_2 production, bioplastic production; bioremediation; biostimulant for agriculture; complete genome sequence available	(Alsiyabi et al., 2021, 2019; Brown et al., 2020; Egland et al., 2001; Gosse et al., 2010; Oshlag et al., 2020)
CS2	Biostimulant for agriculture (*Vigna mungo*)	(Batool et al., 2017)
CQK 01	H_2 production	(Liao et al., 2013; Tian et al., 2010, 2009; Wang et al., 2013, 2012)
DSM 127	H_2 production	(Azbar and Cetinkaya Dokgoz, 2010)
DSM 131	H_2 production	(Fiβler et al., 1995)
DX-1	Electricity generation	(Rengasamy et al., 2020; Xing et al., 2008)
ELI 1980	Biostimulant for agriculture; genome sequence available	(Crovadore et al., 2017)
GJ-22	Biodegradation of pesticides; Biostimulant for agriculture (resistance against tobacco mosaic virus)	(Su et al., 2017; L. Yin et al., 2012)
JA1	H_2 production	(Archana et al., 2003)
JSC-3b	Pyrethroid degradation	(Zhang et al., 2014)
RCB-100	Degradation of 3-chlorobenzoate environmental pollutant; complete genome sequence available	(Haq and Fixen, 2021)
P1	Biostimulant for agriculture (rice)	(Kantachote et al., 2016; Kantha et al., 2015)
P4	H_2 production from syngas (carbon monoxide)	(Hosseini et al., 2015; Oh et al., 2005)
PBUM001	H_2 production	(Jamil et al., 2009)
PP803	Biostimulant for agriculture (rice)	(Kantachote et al., 2016; Kantha et al., 2015)

PS3	Biostimulant for Chinese cabbage; electricity production	(Hsu et al., 2021; Liu et al., 2021; Lo et al., 2020; Wong et al., 2014)
PSB07-21	Biodegradation of pesticides	(Luo et al., 2018)
PSB-S	Biodegradation of pesticides	(Luo et al., 2018)
PT	H_2 production from syngas (carbon monoxide)	(Hosseini et al., 2015; Oh et al., 2005)
TIE-1	Electricity production	(Bai et al., 2020; Guzman et al., 2019; Rengasamy et al., 2018, 2017)
TK103	Biostimulant for agriculture (rice)	(Kantachote et al., 2016; Kantha et al., 2015)
WS17	Dechlorination	(Kamal and Wyndham, 1990)
WKU-KDNS3	Skatole degradation from animal wastes	(Sharma et al., 2015)
XCP	Variations in cytochrome C2 compared to other strains; draft whole-genome sequence available	(Rayyan et al., 2018)
YSC3	Biodegradation of hexabromocyclododecane	(Chang et al., 2020)

Table 2.2. Highlighted examples of biohydrogen production systems with *R. palustris*.

	Organism(s)	Substrate(s)	Total H_2 (mol H_2/mol substrate)	Notes	Reference(s)
Single Stage	*R. palustris* CGA009	Polyester substrate coating (reductant)	8.24	Nongrowing cells coated and stabilized with a novel latex coating	(Gosse et al., 2010; Piskorska et al., 2013)
	Clostridium butyricum CGS55 and *R. palustris* CGA009	Potato starch and glucose	6.4	Dark-photo fermentation; response surface methodology with a Box-Behnken design was used to optimize	(Hitit et al., 2017a)
	R. palustris CGA009	Glycerol	6.69	Stoichiometric conversion of biodiesel derived crude glycerol; Simpler operation; suitable for metabolism study; substrates limited to a few sugars and some organic acids	(Ghosh et al., 2012; Pott et al., 2014; Sabourin-Provost and Hallenbeck, 2009; Zhang et al., 2015)
	R. palustris CGA009	Butyrate	4.92	Incandescent light was found to be more effective	(Hu et al., 2018)

	R. palustris CGA009 and *Cellulomonas fimi*	Cellulose (glucose)	3.84	Effective H_2 production from cellulose by co-cultures without previous pre-treatment	(Hitit et al., 2017b)
	R. palustris CGA009	Ethanol	2.0	Optimized by response surface methodology	(Liu et al., 2015)
Two Stage	*Mixed culture with R. palustris DSM 127*	Cheese whey (lactose)	10	Combined dark-photo fermentation process	(Azbar and Cetinkaya Dokgoz, 2010)
	Thermotoga neapolitana DSM 4359^T and *R. palustris* 42OL	Glucose	9.4	Combined dark-photo fermentation process; Broad substrate range; addition operational cost from treatment of fermentation effluents of first stage	(Dipasquale et al., 2015)
	Clostridium butyricum CGS55 and *R. palustris* WP3-5	Sucrose	5.6	Sequential dark-photo fermentation and autotrophic microbial growth for high yield and CO_2-free biohydrogen production	(Lo et al., 2010)

	Lactobacillus amylovorus DSM 20532 and *R. palustris 42OL*	Bread waste (glucose)	3.1	Sequential lactic and photo-fermentation; among the highest yields obtained on starch containing substrates; No hydrolytic pretreatment necessary	(Adessi et al., 2018)
	R. palustris P4	Acetate	2.8	Combined dark-photo fermentation process	(Oh et al., 2004; Padovani et al., 2016)
	Klebsiella sp. TR17 and *R. palustris* TN1	Glycerol	0.8	Combined dark-photo fermentation process of crude glycerol	(Chookaew et al., 2015)
Semi-Continuous or Continuous	*R. palustris* GCA009	Acetate	3.15	Optical-fiber-assisted illumination systems	(Chen et al., 2006b)
	R. palustris 42OL	Malic acid	3.03	High irradiance under a semicontinuous regime	(Carlozzi, 2012)
	R. palustris GCA009	Glucose	1.15	Grid columnar flat panel photobioreactor with immobilized cells	(Y. Wang et al., 2019)

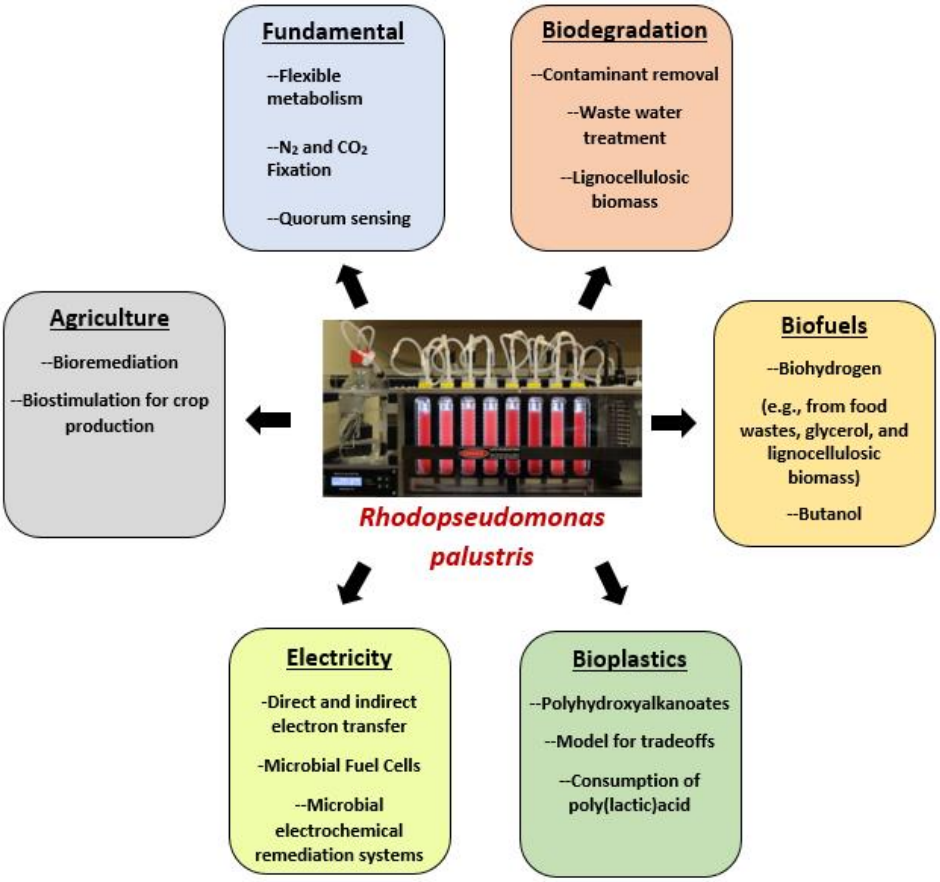

Fig. 2.1: *R. palustris* as a biotechnology chassis. *R. palustris* is a very metabolically diverse purple non sulfur bacterium and a developing biotechnology chassis that has been applied in many applications such as developing a deeper fundamental understanding of tradeoffs between metabolisms, biodegradation, biofuels, bioplastics, electricity systems, and agricultural production.

2.9 References

Adessi, A., Concato, M., Sanchini, A., Rossi, F., De Philippis, R., 2016. Hydrogen production under salt stress conditions by a freshwater Rhodopseudomonas palustris strain. Appl. Microbiol. Biotechnol. 100, 2917–2926. https://doi.org/10.1007/s00253-016-7291-4

Adessi, A., Torzillo, G., Baccetti, E., De Philippis, R., 2012. Sustained outdoor H2 production with Rhodopseudomonas palustris cultures in a 50L tubular photobioreactor. Int. J. Hydrogen Energy 37, 8840–8849. https://doi.org/https://doi.org/10.1016/j.ijhydene.2012.01.081

Adessi, A., Venturi, M., Candeliere, F., Galli, V., Granchi, L., De Philippis, R., 2018. Bread wastes to energy: Sequential lactic and photo-fermentation for hydrogen production. Int. J. Hydrogen Energy 43, 9569–9576. https://doi.org/https://doi.org/10.1016/j.ijhydene.2018.04.053

Alsiyabi, A., Brown, B., Immethun, C., Wilkins, M., Saha, R., 2021. Synergistic Experimental and Computational Approach Identifies Novel Strategies for PHB Overproduction. https://doi.org/10.21203/rs.3.rs-334477/v1

Alsiyabi, A., Immethun, C.M., Saha, R., 2019. Modeling the Interplay between Photosynthesis, CO2 Fixation, and the Quinone Pool in a Purple Non-Sulfur Bacterium. Sci. Rep. https://doi.org/10.1038/s41598-019-49079-z

Archana, A., Sasikala, C., Ramana, C.V., 2003. Augmentation of H2 photoproduction in Rhodopseudomonas palustris by N-heterocyclic aromatic compounds. Biotechnol. Lett. 25, 79–82. https://doi.org/10.1023/A:1021717424268

Austin, S., Kontur, W.S., Ulbrich, A., Oshlag, J.Z., Zhang, W., Higbee, A., Zhang, Y., Coon, J.J., Hodge, D.B., Donohue, T.J., Noguera, D.R., 2015. Metabolism of Multiple Aromatic Compounds in Corn Stover Hydrolysate by Rhodopseudomonas palustris. Environ. Sci. Technol. https://doi.org/10.1021/acs.est.5b02062

Azbar, N., Cetinkaya Dokgoz, F.T., 2010. The effect of dilution and l-malic acid addition on bio-hydrogen production with Rhodopseudomonas palustris from effluent of an acidogenic anaerobic reactor. Int. J. Hydrogen Energy 35, 5028–5033. https://doi.org/https://doi.org/10.1016/j.ijhydene.2009.10.044

Bai, W., Ranaivoarisoa, T.O., Singh, R., Rengasamy, K., Bose, A., 2020. Sustainable

Production of the Biofuel n-Butanol by Rhodopseudomonas palustris TIE-1. bioRxiv 2020.10.13.336636. https://doi.org/10.1101/2020.10.13.336636

Bajracharya, S., Sharma, M., Mohanakrishna, G., Dominguez Benneton, X., Strik, D.P.B.T.B., Sarma, P.M., Pant, D., 2016. An overview on emerging bioelectrochemical systems (BESs): Technology for sustainable electricity, waste remediation, resource recovery, chemical production and beyond. Renew. Energy 98, 153–170. https://doi.org/https://doi.org/10.1016/j.renene.2016.03.002

Batool, K., tuz Zahra, F., Rehman, Y., 2017. Arsenic-Redox Transformation and Plant Growth Promotion by Purple Nonsulfur Bacteria *Rhodopseudomonas palustris* CS2 and *Rhodopseudomonas faecalis* SS5. Biomed Res. Int. 2017, 6250327. https://doi.org/10.1155/2017/6250327

Berne, C., Allainmat, B., Garcia, D., 2005. Tributyl phosphate degradation by Rhodopseudomonas palustris and other photosynthetic bacteria. Biotechnol. Lett. 27, 561–566. https://doi.org/10.1007/s10529-005-2882-7

Berne, C., Pignol, D., Lavergne, J., Garcia, D., 2007. CYP201A2, a cytochrome P450 from Rhodopseudomonas palustris, plays a key role in the biodegradation of tributyl phosphate. Appl. Microbiol. Biotechnol. 77, 135–144. https://doi.org/10.1007/s00253-007-1140-4

Biodegradation of reactive red 195 azo dye by the bacterium Rhodopseudomonas palustris 51ATA, 2012. . African J. Microbiol. Res. Vol.6(1), 120–126.

Bogarapu, R., Kumar, R., Madanapally, U.D., Nayak, J., 2019. ROLE OF PURPLE NON-SULFUR BACTERIA RHODOPSEUDOMONAS PALUSTRIS RSOU000 AND RHODOPSEUDOMONAS THERMOTOLERANCE RSOU555 IN WASTE WATER TREATMENT. WORLD J. Pharm. Pharm. Sci. 5, 1379–1387. https://doi.org/10.20959/wjpps20168-7428

Borchert, E., Hammerschmidt, K., Hentschel, U., Deines, P., 2021. Enhancing Microbial Pollutant Degradation by Integrating Eco-Evolutionary Principles with Environmental Biotechnology. Trends Microbiol. https://doi.org/10.1016/j.tim.2021.03.002

Brown, B., Immethun, C., Wilkins, M., Saha, R., 2020. Rhodopseudomonas palustris

CGA009 polyhydroxybutyrate production from a lignin aromatic and quantification via flow cytometry. Bioresour. Technol. Reports 11, 100474. https://doi.org/https://doi.org/10.1016/j.biteb.2020.100474

Carlozzi, P., 2012. Hydrogen photoproduction by Rhodopseudomonas palustris 42OL cultured at high irradiance under a semicontinuous regime. J. Biomed. Biotechnol. 2012, 590693. https://doi.org/10.1155/2012/590693

Chang, T.-H., Wang, R., Peng, Y.-H., Chou, T.-H., Li, Y.-J., Shih, Y., 2020. Biodegradation of hexabromocyclododecane by Rhodopseudomonas palustris YSC3 strain: A free-living nitrogen-fixing bacterium isolated in Taiwan. Chemosphere 246, 125621. https://doi.org/https://doi.org/10.1016/j.chemosphere.2019.125621

Chen, C.-Y., Lee, C.-M., Chang, J.-S., 2006a. Hydrogen production by indigenous photosynthetic bacterium Rhodopseudomonas palustris WP3–5 using optical fiber-illuminating photobioreactors. Biochem. Eng. J. 32, 33–42. https://doi.org/https://doi.org/10.1016/j.bej.2006.08.015

Chen, C.-Y., Lee, C.-M., Chang, J.-S., 2006b. Feasibility study on bioreactor strategies for enhanced photohydrogen production from Rhodopseudomonas palustris WP3-5 using optical-fiber-assisted illumination systems. Int. J. Hydrogen Energy 31, 2345–2355. https://doi.org/https://doi.org/10.1016/j.ijhydene.2006.03.007

Chen, G.-Q., Chen, X.-Y., Wu, F.-Q., Chen, J.-C., 2020a. Polyhydroxyalkanoates (PHA) toward cost competitiveness and functionality. Adv. Ind. Eng. Polym. Res. 3, 1–7. https://doi.org/https://doi.org/10.1016/j.aiepr.2019.11.001

Chen, G.-Q., Chen, X.-Y., Wu, F.-Q., Chen, J.-C., 2020b. Polyhydroxyalkanoates (PHA) toward cost competitiveness and functionality. Adv. Ind. Eng. Polym. Res. https://doi.org/10.1016/j.aiepr.2019.11.001

Chen, J., Wei, J., Ma, C., Yang, Z., Li, Z., Yang, X., Wang, M., Zhang, H., Hu, J., Zhang, C., 2020. Photosynthetic bacteria-based technology is a potential alternative to meet sustainable wastewater treatment requirement? Environ. Int. 137, 105417. https://doi.org/https://doi.org/10.1016/j.envint.2019.105417

Chen, Y.-T., Wu, S.-C., Lee, C.-M., 2012. Relationship between cell growth, hydrogen production and poly-β-hydroxybutyrate (PHB) accumulation by Rhodopseudomonas palustris WP3-5. Int. J. Hydrogen Energy 37, 13887–13894.

https://doi.org/https://doi.org/10.1016/j.ijhydene.2012.06.024

Chookaew, T., O-Thong, S., Prasertsan, P., 2015. Biohydrogen production from crude glycerol by two stage of dark and photo fermentation. Int. J. Hydrogen Energy 40, 7433–7438. https://doi.org/https://doi.org/10.1016/j.ijhydene.2015.02.133

Corneli, E., Adessi, A., Olguín, E.J., Ragaglini, G., García-López, D.A., De Philippis, R., 2017. Biotransformation of water lettuce (Pistia stratiotes) to biohydrogen by Rhodopseudomonas palustris. J. Appl. Microbiol. 123, 1438–1446. https://doi.org/https://doi.org/10.1111/jam.13599

Crovadore, J., Xu, S., Chablais, R., Cochard, B., Lukito, D., Calmin, G., Lefort, F., 2017. Metagenome-Assembled Genome Sequence of Rhodopseudomonas palustris Strain ELI 1980, Commercialized as a Biostimulant. Genome Announc. 5, e00221-17. https://doi.org/10.1128/genomeA.00221-17

Dipasquale, L., Adessi, A., d'Ippolito, G., Rossi, F., Fontana, A., De Philippis, R., 2015. Introducing capnophilic lactic fermentation in a combined dark-photo fermentation process: a route to unparalleled H2 yields. Appl. Microbiol. Biotechnol. 99, 1001–1010. https://doi.org/10.1007/s00253-014-6231-4

Díaz, E., Prieto, M.A., 2000. Bacterial promoters triggering biodegradation of aromatic pollutants. Curr. Opin. Biotechnol. 11, 467–475. https://doi.org/https://doi.org/10.1016/S0958-1669(00)00126-9

Dong, Y., Li, L., Hu, X., Wu, C., 2017. Optimization of o-Chlorophenol Biodegradation by Combined Mycelial Pellets Using Response Surface Methodology. Water, Air, Soil Pollut. 228, 431. https://doi.org/10.1007/s11270-017-3606-z

Doud, D.F.R., Angenent, L.T., 2016. Single-Genotype Syntrophy by Rhodopseudomonas palustris Is Not a Strategy to Aid Redox Balance during Anaerobic Degradation of Lignin Monomers . Front. Microbiol. .

Doud, D.F.R., Angenent, L.T., 2014. Toward Electrosynthesis with Uncoupled Extracellular Electron Uptake and Metabolic Growth: Enhancing Current Uptake with Rhodopseudomonas palustris. Environ. Sci. Technol. Lett. 1, 351–355. https://doi.org/10.1021/ez500244n

Doud, D.F.R., Holmes, E.C., Richter, H., Molitor, B., Jander, G., Angenent, L.T., 2017. Metabolic engineering of Rhodopseudomonas palustris for the obligate reduction of

n-butyrate to n-butanol. Biotechnol. Biofuels 10, 178. https://doi.org/10.1186/s13068-017-0864-3

du Toit, J.-P., Pott, R.W.M., 2021. Heat-acclimatised strains of Rhodopseudomonas palustris reveal higher temperature optima with concomitantly enhanced biohydrogen production rates. Int. J. Hydrogen Energy 46, 11564–11572. https://doi.org/https://doi.org/10.1016/j.ijhydene.2021.01.068

Egland, P.G., Gibson, J., Harwood, C.S., 2001. Reductive, coenzyme A-mediated pathway for 3-chlorobenzoate degradation in the phototrophic bacterium Rhodopseudomonas palustris. Appl. Environ. Microbiol. 67, 1396–1399. https://doi.org/10.1128/AEM.67.3.1396-1399.2001

Egland, P.G., Gibson, J., Harwood, C.S., 1995. Benzoate-coenzyme A ligase, encoded by badA, is one of three ligases able to catalyze benzoyl-coenzyme A formation during anaerobic growth of Rhodopseudomonas palustris on benzoate. J. Bacteriol. 177, 6545–6551. https://doi.org/10.1128/jb.177.22.6545-6551.1995

Evans K., Georgiou T., Hillon T., Fordham-Skelton A., P.M., 2009. Bacteriophytochromes Control Photosynthesis in Rhodopseudomonas palustris, in: The Purple Phototrophic Bacteria. Advances in Photosynthesis and Respiration. Springer, Dordrecht.

Fiβler, J., Kohring, G.W., Giffhorn, F., 1995. Enhanced hydrogen production from aromatic acids by immobilized cells of Rhodopseudomonas palustris. Appl. Microbiol. Biotechnol. 44, 43–46. https://doi.org/10.1007/BF00164478

Gao, R., Wang, Y., Zhang, Y., Tong, J., Dai, W., 2017. Cobalt(II) bioaccumulation and distribution in Rhodopseudomonas palustris. Biotechnol. Biotechnol. Equip. 31, 527–534. https://doi.org/10.1080/13102818.2017.1292148

Geyer, R., Jambeck, J.R., Law, K.L., 2017. Production, use, and fate of all plastics ever made. Sci. Adv. 3, e1700782. https://doi.org/10.1126/sciadv.1700782

Ghosh, D., Sobro, I.F., Hallenbeck, P.C., 2012. Stoichiometric conversion of biodiesel derived crude glycerol to hydrogen: Response surface methodology study of the effects of light intensity and crude glycerol and glutamate concentration. Bioresour. Technol. 106, 154–160. https://doi.org/https://doi.org/10.1016/j.biortech.2011.12.021

Gosse, J.L., Engel, B.J., Hui, J.C.-H., Harwood, C.S., Flickinger, M.C., 2010. Progress toward a biomimetic leaf: 4,000 h of hydrogen production by coating-stabilized nongrowing photosynthetic Rhodopseudomonas palustris. Biotechnol. Prog. 26, 907–918. https://doi.org/https://doi.org/10.1002/btpr.406

Guardia, A.E., Beligni, M. V, Cortéz, N., Busalmen, J.P., 2020. Electrochemistry of R. palustris Azul during phototrophic growth. Electrochim. Acta 355, 136757. https://doi.org/https://doi.org/10.1016/j.electacta.2020.136757

Guzman, M.S., Rengasamy, K., Binkley, M.M., Jones, C., Ranaivoarisoa, T.O., Singh, R., Fike, D.A., Meacham, J.M., Bose, A., 2019. Phototrophic extracellular electron uptake is linked to carbon dioxide fixation in the bacterium Rhodopseudomonas palustris. Nat. Commun. https://doi.org/10.1038/s41467-019-09377-6

Hajighasemi, M., Nocek, B.P., Tchigvintsev, A., Brown, G., Flick, R., Xu, X., Cui, H., Hai, T., Joachimiak, A., Golyshin, P.N., Savchenko, A., Edwards, E.A., Yakunin, A.F., 2016. Biochemical and Structural Insights into Enzymatic Depolymerization of Polylactic Acid and Other Polyesters by Microbial Carboxylesterases. Biomacromolecules 17, 2027–2039. https://doi.org/10.1021/acs.biomac.6b00223

Haq, I.U., Fixen, K.R., 2021. Complete Genome Sequence of Rhodopseudomonas palustris RCB100, an Anoxygenic Phototroph That Degrades 3-Chlorobenzoate. Microbiol. Resour. Announc. 10, e00043-21. https://doi.org/10.1128/MRA.00043-21

Harayama, S., Kishira, H., Kasai, Y., Shutsubo, K., 1999. Petroleum biodegradation in marine environments. J. Mol. Microbiol. Biotechnol. 1, 63–70.

Harwood, C.S., Gibson, J., 1988. Anaerobic and aerobic metabolism of diverse aromatic compounds by the photosynthetic bacterium Rhodopseudomonas palustris. Appl. Environ. Microbiol. https://doi.org/10.1128/aem.54.3.712-717.1988

Heiniger, E.K., Oda, Y., Samanta, S.K., Harwood, C.S., 2012. How posttranslational modification of nitrogenase is circumvented in Rhodopseudomonas palustris strains that produce hydrogen gas constitutively. Appl. Environ. Microbiol. 78, 1023–1032. https://doi.org/10.1128/AEM.07254-11

Hirakawa, H., Hirakawa, Y., Greenberg, E.P., Harwood, C.S., 2015. BadR and BadM Proteins Transcriptionally Regulate Two Operons Needed for Anaerobic Benzoate

Degradation by Rhodopseudomonas palustris. Appl. Environ. Microbiol. 81, 4253–4262. https://doi.org/10.1128/AEM.00377-15

Hitit, Z.Y., Lazaro, C.Z., Hallenbeck, P.C., 2017a. Hydrogen production by co-cultures of Clostridium butyricum and Rhodospeudomonas palustris: Optimization of yield using response surface methodology. Int. J. Hydrogen Energy 42, 6578–6589. https://doi.org/https://doi.org/10.1016/j.ijhydene.2016.12.122

Hitit, Z.Y., Lazaro, C.Z., Hallenbeck, P.C., 2017b. Single stage hydrogen production from cellulose through photo-fermentation by a co-culture of Cellulomonas fimi and Rhodopseudomonas palustris. Int. J. Hydrogen Energy 42, 6556–6566. https://doi.org/https://doi.org/10.1016/j.ijhydene.2016.12.035

Hitit, Z.Y., Zampol Lazaro, C., Hallenbeck, P.C., 2017c. Increased hydrogen yield and COD removal from starch/glucose based medium by sequential dark and photo-fermentation using Clostridium butyricum and Rhodopseudomonas palustris. Int. J. Hydrogen Energy 42, 18832–18843. https://doi.org/https://doi.org/10.1016/j.ijhydene.2017.05.161

Hosseini, S.S., Aghbashlo, M., Tabatabaei, M., Najafpour, G., Younesi, H., 2015. Thermodynamic evaluation of a photobioreactor for hydrogen production from syngas via a locally isolated Rhodopseudomonas palustris PT. Int. J. Hydrogen Energy 40, 14246–14256. https://doi.org/https://doi.org/10.1016/j.ijhydene.2015.08.092

Howe, C.J., Bombelli, P., 2020. Electricity Production by Photosynthetic Microorganisms. Joule 4, 2065–2069. https://doi.org/https://doi.org/10.1016/j.joule.2020.09.003

Hsu, S.-H., Shen, M.-W., Chen, J.-C., Lur, H.-S., Liu, C.-T., 2021. The Photosynthetic Bacterium Rhodopseudomonas palustris Strain PS3 Exerts Plant Growth-Promoting Effects by Stimulating Nitrogen Uptake and Elevating Auxin Levels in Expanding Leaves . Front. Plant Sci. .

Hu, C., Choy, S.-Y., Giannis, A., 2018. Evaluation of Lighting Systems, Carbon Sources, and Bacteria Cultures on Photofermentative Hydrogen Production. Appl. Biochem. Biotechnol. 185, 257–269. https://doi.org/10.1007/s12010-017-2655-5

Huang, J.J., Heiniger, E.K., McKinlay, J.B., Harwood, C.S., 2010. Production of

hydrogen gas from light and the inorganic electron donor thiosulfate by Rhodopseudomonas palustris. Appl. Environ. Microbiol. 76, 7717–7722. https://doi.org/10.1128/AEM.01143-10

Inglesby, A., Beatty, D., Fisher, A., 2012. Rhodopseudomonas palustris purple bacteria fed Arthrospira maxima cyanobacteria: Demonstration of application in microbial fuel cells. RSC Adv. 2, 4829–4838. https://doi.org/10.1039/C2RA20264F

J. Craven, M.A. Sultan, R. Sarma, S. Wilson, N. Meeks, D.Y. Kim, et al., 2019. Rhodopseudomonas palustris-based conversion of organic acids to hydrogen using plasmonic nanoparticles and near-infrared light. RSC Adv 9, 41218–41227.

Jamil, Z., Mohamad Annuar, M.S., Ibrahim, S., Vikineswary, S., 2009. Optimization of phototrophic hydrogen production by Rhodopseudomonas palustris PBUM001 via statistical experimental design. Int. J. Hydrogen Energy 34, 7502–7512. https://doi.org/https://doi.org/10.1016/j.ijhydene.2009.05.116

Kamal, V.S., Wyndham, R.C., 1990. Anaerobic phototrophic metabolism of 3-chlorobenzoate by Rhodopseudomonas palustris WS17. Appl. Environ. Microbiol. 56, 3871–3873. https://doi.org/10.1128/aem.56.12.3871-3873.1990

Kantachote, D., Nunkaew, T., Kantha, T., Chaiprapat, S., 2016. Biofertilizers from Rhodopseudomonas palustris strains to enhance rice yields and reduce methane emissions. Appl. Soil Ecol. 100, 154–161. https://doi.org/https://doi.org/10.1016/j.apsoil.2015.12.015

Kantha, T., Kantachote, D., Klongdee, N., 2015. Potential of biofertilizers from selected Rhodopseudomonas palustris strains to assist rice (Oryza sativa L. subsp. indica) growth under salt stress and to reduce greenhouse gas emissions. Ann. Microbiol. 65, 2109–2118. https://doi.org/10.1007/s13213-015-1049-6

Kanwal, F., Tahir, A., Qadir Shah, S.A., Tsuzuki, T., Nisbet, D., Chen, J., Rehman, Y., 2020. Effect of phyto-fabricated nanoscale organic-iron complex on photo-fermentative hydrogen production by Rhodopseudomonas palustris MP2 and Rhodopseudomonas palustris MP4. Biomass and Bioenergy 140, 105667. https://doi.org/https://doi.org/10.1016/j.biombioe.2020.105667

Kernan, C., Chow, P.P., Christianson, R.J., Huang, J., 2015. Experimental and Computational Investigation of Biofilm Formation by Rhodopseudomonas palustris

Growth under Two Metabolic Modes. PLoS One 10, e0129354–e0129354. https://doi.org/10.1371/journal.pone.0129354

Kim, M.K., Choi, K.-M., Yin, C.-R., Lee, K.-Y., Im, W.-T., Lim, J.H., Lee, S.-T., 2004. Odorous swine wastewater treatment by purple non-sulfur bacteria, Rhodopseudomonas palustris, isolated from eutrophicated ponds. Biotechnol. Lett. 26, 819–822. https://doi.org/10.1023/b:bile.0000025884.50198.67

Kour D, Rana KL, Yadav N, Yadav AN, Rastegari A, Singh, Negi DP, Singh K, Saxena A: Technologies for Biofuel Production: Current Development, Challenges, and Future Prospects. 2019:1–50.

Larimer, F.W., Chain, P., Hauser, L., Lamerdin, J., Malfatti, S., Do, L., Land, M.L., Pelletier, D.A., Beatty, J.T., Lang, A.S., Tabita, F.R., Gibson, J.L., Hanson, T.E., Bobst, C., Torres Y Torres, J.L., Peres, C., Harrison, F.H., Gibson, J., Harwood, C.S., 2004. Complete genome sequence of the metabolically versatile photosynthetic bacterium Rhodopseudomonas palustris. Nat. Biotechnol. https://doi.org/10.1038/nbt923

Lee, C.-M., Hung, G.-J., Yang, C.-F., 2011. Hydrogen production by Rhodopseudomonas palustris WP 3-5 in a serial photobioreactor fed with hydrogen fermentation effluent. Bioresour. Technol. 102, 8350–8356. https://doi.org/https://doi.org/10.1016/j.biortech.2011.04.072

Lee, C.-M., Yu, K.-M., Chen, P.-C., 2006. Limiting Factors of Photo-Hydrogen Production by Rhodopseudomonas palustris WP3-5. Mod. Multidiscip. Appl. Microbiol., Wiley Online Books. https://doi.org/https://doi.org/10.1002/9783527611904.ch40

Lee, S., Kang, M., Bae, J.-H., Sohn, J.-H. & Sung, B. H. Bacterial Valorization of Lignin: Strains, Enzymes, Conversion Pathways, Biosensors, and Perspectives. *Front. Bioeng. Biotechnol.* **7**, 209 (2019).

Levin, D.B., Pitt, L., Love, M., 2004. Biohydrogen production: prospects and limitations to practical application. Int. J. Hydrogen Energy 29, 173–185. https://doi.org/https://doi.org/10.1016/S0360-3199(03)00094-6

Li, Y.-J., Wang, R., Lin, C.-Y., Chen, S.-H., Chuang, C.-H., Chou, T.-H., Ko, C.-F., Chou, P.-H., Liu, C.-T., Shih, Y., 2021. The degradation mechanisms of

Rhodopseudomonas palustris toward hexabromocyclododecane by time-course transcriptome analysis. Chem. Eng. J. 425, 130489. https://doi.org/https://doi.org/10.1016/j.cej.2021.130489

Liao, Q., Zhong, N.-B., Zhu, X., Chen, R., Wang, Y.-Z., Lee, D.-J., 2013. Enhancement of hydrogen production by adsorption of Rhodoseudomonas palustris CQK 01 on a new support material. Int. J. Hydrogen Energy 38, 15730–15737. https://doi.org/https://doi.org/10.1016/j.ijhydene.2013.04.146

Liu, C.-H., Lee, S.-K., Ou, I.-C., Tsai, K.-J., Lee, Y., Chu, Y.-H., Liao, Y.-T., Liu, C.-T., 2021. Essential factors that affect bioelectricity generation by Rhodopseudomonas palustris strain PS3 in paddy soil microbial fuel cells. Int. J. Energy Res. 45, 2231–2244. https://doi.org/https://doi.org/10.1002/er.5916

Liu, G., Zhou, J., Wang, J., Song, Z., Qv, Y., 2006. Bacterial Decolorization of Azo Dyes by Rhodopseudomonas palustris. World J. Microbiol. Biotechnol. 22, 1069–1074. https://doi.org/10.1007/s11274-005-4857-1

Liu, Y., Ghosh, D., Hallenbeck, P.C., 2015. Biological reformation of ethanol to hydrogen by Rhodopseudomonas palustris CGA009. Bioresour. Technol. 176, 189–195. https://doi.org/https://doi.org/10.1016/j.biortech.2014.11.047

Llorens, I., Untereiner, G., Jaillard, D., Gouget, B., Chapon, V., Carriere, M., 2012. Uranium Interaction with Two Multi-Resistant Environmental Bacteria: Cupriavidus metallidurans CH34 and Rhodopseudomonas palustris. PLoS One 7, e51783.

Lo, K.-J., Lee, S.-K., Liu, C.-T., 2020. Development of a low-cost culture medium for the rapid production of plant growth-promoting Rhodopseudomonas palustris strain PS3. PLoS One 15, e0236739.

Lo, Y.-C., Chen, C.-Y., Lee, C.-M., Chang, J.-S., 2010. Sequential dark-photo fermentation and autotrophic microalgal growth for high-yield and CO. Int. J. Hydrogen Energy 35, 10944–10953. https://doi.org/10.1016/j.ijhydene.2010.07.090

Luo, L., Wang, P., Zhai, Z., Su, P., Tan, X., Zhang, D., Zhang, Z., Liu, Y., 2019. The effects of Rhodopseudomonas palustris PSB06 and CGA009 with different agricultural applications on rice growth and rhizosphere bacterial communities. AMB Express 9, 173. https://doi.org/10.1186/s13568-019-0897-z

Luo, X., Zhang, D., Zhou, X., Du, J., Zhang, S., Liu, Y., 2018. Cloning and

characterization of a pyrethroid pesticide decomposing esterase gene, Est3385, from Rhodopseudomonas palustris PSB-S. Sci. Rep. 8, 7384. https://doi.org/10.1038/s41598-018-25734-9

Ma, Y., Donohue, T.J., Noguera, D.R., 2021. Kinetic modeling of anaerobic degradation of plant-derived aromatic mixtures by Rhodopseudomonas palustris. Biodegradation 32, 179–192. https://doi.org/10.1007/s10532-021-09932-3

Mabutyana, L., Pott, R.W.M., 2021. Photo-fermentative hydrogen production by Rhodopseudomonas palustris CGA009 in the presence of inhibitory compounds. Int. J. Hydrogen Energy. https://doi.org/https://doi.org/10.1016/j.ijhydene.2020.12.189

McCormick, A.J., Bombelli, P., Bradley, R.W., Thorne, R., Wenzel, T., Howe, C.J., 2015. Biophotovoltaics: oxygenic photosynthetic organisms in the world of bioelectrochemical systems. Energy Environ. Sci. 8, 1092–1109. https://doi.org/10.1039/C4EE03875D

McCully, A., McKinlay, J., 2016. Disrupting Calvin cycle phosphoribulokinase activity in Rhodopseudomonas palustris increases the H2 yield and specific production rate proportionately. Int. J. Hydrogen Energy 41. https://doi.org/10.1016/j.ijhydene.2016.01.003

McKinlay, J.B., Oda, Y., Ruhl, M., Posto, A.L., Sauer, U., Harwood, C.S., 2014. Non-growing rhodopseudomonas palustris increases the hydrogen gas yield from acetate by shifting from the glyoxylate shunt to the tricarboxylic acid cycle. J. Biol. Chem. https://doi.org/10.1074/jbc.M113.527515

Morishima, K., Yoshida, M., Furuya, A., Moriuchi, T., Ota, M., Furukawa, Y., 2007. Improving the performance of a direct photosynthetic/metabolic bio-fuel cell (DPBFC) using gene manipulated bacteria. J. Micromechanics Microengineering 17, S274–S279. https://doi.org/10.1088/0960-1317/17/9/s10

Mutharasaiah, K., Govindareddy, V., Chandrakant, K., 2012a. Biodegradation of 2-Chlorophenol by Rhodopseudomonas palustris. Bioremediat. J. 16, 1–8. https://doi.org/10.1080/10889868.2011.628348

Mutharasaiah, K., Govindareddy, V., Karigar, C., 2012b. Biodegradation of 2Chlorophenol by Rhodopseudomonas palustris. Bioremediation J. - BIOREMEDIAT J 16, 1–8. https://doi.org/10.1080/10889868.2011.628348

Muzziotti, D., Adessi, A., Faraloni, C., Torzillo, G., De Philippis, R., 2017. Acclimation strategy of Rhodopseudomonas palustris to high light irradiance. Microbiol. Res. https://doi.org/10.1016/j.micres.2017.01.007

Nagadomi, H., Kitamura, T., Watanabe, M., Sasaki, K., 2000. Simultaneous removal of chemical oxygen demand (COD), phosphate, nitrate and H2S in the synthetic sewage wastewater using porous ceramic immobilized photosynthetic bacteria. Biotechnol. Lett. 22, 1369–1374. https://doi.org/10.1023/A:1005688229783

Navid, A., Jiao, Y., Wong, S.E., Pett-Ridge, J., 2019. System-level analysis of metabolic trade-offs during anaerobic photoheterotrophic growth in Rhodopseudomonas palustris. BMC Bioinformatics 20, 233. https://doi.org/10.1186/s12859-019-2844-z

Oda, Y., Samanta, S.K., Rey, F.E., Wu, L., Liu, X., Yan, T., Zhou, J., Harwood, C.S., 2005. Functional genomic analysis of three nitrogenase isozymes in the photosynthetic bacterium Rhodopseudomonas palustris. J. Bacteriol. 187, 7784–7794. https://doi.org/10.1128/JB.187.22.7784-7794.2005

Oh, Y.-K., Kim, Y.-J., Park, J.-Y., Lee, T.H., Kim, M.-S., Park, S., 2005. Biohydrogen production from carbon monoxide and water byRhodopseudomonas palustris P4. Biotechnol. Bioprocess Eng. 10, 270. https://doi.org/10.1007/BF02932024

Oh, Y.-K., Seol, E.-H., Kim, M.-S., Park, S., 2004. Photoproduction of hydrogen from acetate by a chemoheterotrophic bacterium Rhodopseudomonas palustris P4. Int. J. Hydrogen Energy 29, 1115–1121. https://doi.org/https://doi.org/10.1016/j.ijhydene.2003.11.008

Oh, Y.-K., Seol, E.-H., Lee, E.Y., Park, S., 2002. Fermentative hydrogen production by a new chemoheterotrophic bacterium Rhodopseudomonas Palustris P4. Int. J. Hydrogen Energy 27, 1373–1379. https://doi.org/https://doi.org/10.1016/S0360-3199(02)00100-3

Oshlag, J.Z., Ma, Y., Morse, K., Burger, B.T., Lemke, R.A., Karlen, S.D., Myers, K.S., Donohue, T.J., Noguera, D.R., 2020. Anaerobic Degradation of Syringic Acid by an Adapted Strain of Rhodopseudomonas palustris. Appl. Environ. Microbiol. 86, e01888-19. https://doi.org/10.1128/AEM.01888-19

Otani, S., Nguyen, D.-T., Taguchi, K., 2020. Enhancing the power generation of Rhodopseudomonas palustris-based MFC. Int. J. Appl. Electromagn. Mech. 64,

1261–1268. https://doi.org/10.3233/JAE-209444

Padovani, G., Emiliani, G., Giovanelli, A., Traversi, M.L., Carlozzi, P., 2018. Assessment of glycerol usage by five different purple non-sulfur bacterial strains for bioplastic production. J. Environ. Chem. Eng. 6, 616–622. https://doi.org/https://doi.org/10.1016/j.jece.2017.12.050

Padovani, G., Vaičiulytė, S., Carlozzi, P., 2016. BioH2 photoproduction by means of Rhodopseudomonas palustris sp. cultured in a lab-scale photobioreactor operated in batch, fed-batch and semi-continuous modes. Fuel 166, 203–210. https://doi.org/https://doi.org/10.1016/j.fuel.2015.10.124

Pan, C., Oda, Y., Lankford, P.K., Zhang, B., Samatova, N.F., Pelletier, D.A., Harwood, C.S., Hettich, R.L., 2008. Characterization of Anaerobic Catabolism of p-Coumarate in Rhodopseudomonas palustris by Integrating Transcriptomics and Quantitative Proteomics. Mol. & Cell. Proteomics 7, 938 LP – 948. https://doi.org/10.1074/mcp.M700147-MCP200

Pandey, Ashutosh, Pandey, Archana, Srivastava, P., Pandey, Anjana, 2007. Using reverse micelles as microreactor for hydrogen production by coupled systems of Nostoc/R. palustris and Anabaena/R. palustris. World J. Microbiol. Biotechnol. 23, 269–274. https://doi.org/10.1007/s11274-006-9224-3

Pankan, A.O., Yunus, K., Fisher, A.C., 2020. Mechanistic evaluation of the exoelectrogenic activity of Rhodopseudomonas palustris under different nitrogen regimes. Bioresour. Technol. 300, 122637. https://doi.org/https://doi.org/10.1016/j.biortech.2019.122637

Park, T.-J., Ding, W., Cheng, S., Brar, M.S., Ma, A.P.Y., Tun, H.M., Leung, F.C., 2014. Microbial community in microbial fuel cell (MFC) medium and effluent enriched with purple photosynthetic bacterium (Rhodopseudomonas sp.). AMB Express 4, 22. https://doi.org/10.1186/s13568-014-0022-2

Pechter, K.B., Gallagher, L., Pyles, H., Manoil, C.S., Harwood, C.S., 2015. Essential Genome of the Metabolically Versatile Alphaproteobacterium Rhodopseudomonas palustris. J. Bacteriol. 198, 867–876. https://doi.org/10.1128/JB.00771-15

Phongjarus, N., Suvaphat, C., Srichai, N., Ritchie, R.J., 2018. Photoheterotrophy of

photosynthetic bacteria (Rhodopseudomonas palustris) growing on oil palm and soybean cooking oils. Environ. Technol. Innov. https://doi.org/10.1016/j.eti.2018.03.002

Pintucci, C., Giovannelli, A., Traversi, M.L., Ena, A., Padovani, G., Carlozzi, P., 2013. Fresh olive mill waste deprived of polyphenols as feedstock for hydrogen photo-production by means of Rhodopseudomonas palustris 42OL. Renew. Energy 51, 358–363. https://doi.org/https://doi.org/10.1016/j.renene.2012.09.037

Pintucci, C., Padovani, G., Giovannelli, A., Traversi, M.L., Ena, A., Pushparaj, B., Carlozzi, P., 2015. Hydrogen photo-evolution by Rhodopseudomonas palustris 6A using pre-treated olive mill wastewater and a synthetic medium containing sugars. Energy Convers. Manag. 90, 499–505. https://doi.org/https://doi.org/10.1016/j.enconman.2014.11.045

Piskorska, M., Soule, T., Gosse, J.L., Milliken, C., Flickinger, M.C., Smith, G.W., Yeager, C.M., 2013. Preservation of H2 production activity in nanoporous latex coatings of Rhodopseudomonas palustris CGA009 during dry storage at ambient temperatures. Microb. Biotechnol. 6, 515–525. https://doi.org/https://doi.org/10.1111/1751-7915.12032

Ponnusamy, V.K., Nguyen, D.D., Dharmaraja, J., Shobana, S., Banu, J.R., Saratale, R.G., Chang, S.W., Kumar, G., 2019. A review on lignin structure, pretreatments, fermentation reactions and biorefinery potential. Bioresour. Technol. 271, 462–472. https://doi.org/https://doi.org/10.1016/j.biortech.2018.09.070

Pott, R.W.M., Howe, C.J., Dennis, J.S., 2014. The purification of crude glycerol derived from biodiesel manufacture and its use as a substrate by Rhodopseudomonas palustris to produce hydrogen. Bioresour. Technol. 152, 464–470. https://doi.org/https://doi.org/10.1016/j.biortech.2013.10.094

Qi, X., Bo, Y., Ren, Y., Wang, X., 2018a. The anaerobic biodegradation of poly(lactic) acid textiles in photosynthetic microbial fuel cells: Self-sustained bioelectricity generation. Polym. Degrad. Stab. 148, 42–49. https://doi.org/https://doi.org/10.1016/j.polymdegradstab.2018.01.005

Qi, X., Ren, Y., Wang, X., 2017. New advances in the biodegradation of Poly(lactic) acid. Int. Biodeterior. Biodegradation 117, 215–223.

https://doi.org/https://doi.org/10.1016/j.ibiod.2017.01.010

Qi, X., Tian, E., Ren, Y., Wang, X., 2018b. A weak infrared light strengthens anoxygenic photosynthetic bacteria activated sludge for the anaerobic biodegradation of polylactic acid in microbial fuel cell systems. Polym. Degrad. Stab. 157, 44–52. https://doi.org/https://doi.org/10.1016/j.polymdegradstab.2018.09.024

Qian, E.W., 2013. Pretreatment and Saccharification of Lignocellulosic Biomass, in: Research Approaches to Sustainable Biomass Systems. https://doi.org/10.1016/B978-0-12-404609-2.00007-6

Qin, L., Liu, Q., Meng, Q., Fan, Z., He, J., Liu, T., Shen, C., Zhang, G., 2017. Anoxic oscillating MBR for photosynthetic bacteria harvesting and high salinity wastewater treatment. Bioresour. Technol. 224, 69–77. https://doi.org/https://doi.org/10.1016/j.biortech.2016.10.067

Qing Wang, Lijun Shen, Zhenzhen Zhao, Hai Yan, Qianqian Xu, Chunhua Yin, Xiaolu Liu, H.Z. and Y.L., 2018. Efficient Culture of Rhodopseudomonas palustris Using Landfill Leachate. J. Pure Appl. Microbiol. 12(4), 1679–1686.

Rajesh Banu, J., Kavitha, S., Yukesh Kannah, R., Poornima Devi, T., Gunasekaran, M., Kim, S.-H., Kumar, G., 2019. A review on biopolymer production via lignin valorization. Bioresour. Technol. 290, 121790. https://doi.org/https://doi.org/10.1016/j.biortech.2019.121790

Ranaivoarisoa, T.O., Singh, R., Rengasamy, K., Guzman, M.S., Bose, A., 2019. Towards sustainable bioplastic production using the photoautotrophic bacterium Rhodopseudomonas palustris TIE-1. J. Ind. Microbiol. Biotechnol. https://doi.org/10.1007/s10295-019-02165-7

Rayyan, A., Meyer, T., Kyndt, J., 2018. Draft Whole-Genome Sequence of the Purple Photosynthetic Bacterium Rhodopseudomonas palustris XCP. Microbiol. Resour. Announc. 7, e00855-18. https://doi.org/10.1128/MRA.00855-18

Rengasamy, K., Ranaivoarisoa, T., Bai, W., Bose, A., 2020. Magnetite nanoparticle anchored graphene cathode enhances microbial electrosynthesis of polyhydroxybutyrate by Rhodopseudomonas palustris TIE-1. Nanotechnology 32, 35103. https://doi.org/10.1088/1361-6528/abbe58

Rengasamy, K., Ranaivoarisoa, T., Singh, R., Bose, A., 2018. An insoluble iron complex

coated cathode enhances direct electron uptake by Rhodopseudomonas palustris TIE-1. Bioelectrochemistry 122, 164–173. https://doi.org/https://doi.org/10.1016/j.bioelechem.2018.03.015

Rengasamy, K., Ranaivoarisoa, T.O., Singh, R., Bose, A., 2017. Improving microbial electrosynthesis of polyhydroxybutyrate (PHB) from CO₂ by Rhodopseudomonas palustris TIE-1 using an immobilized iron complex modified cathode. bioRxiv 214577. https://doi.org/10.1101/214577

Rey, F.E., Harwood, C.S., 2010. FixK, a global regulator of microaerobic growth, controls photosynthesis in Rhodopseudomonas palustris. Mol. Microbiol. 75, 1007–1020. https://doi.org/10.1111/j.1365-2958.2009.07037.x

Rey, F.E., Heiniger, E.K., Harwood, C.S., 2007. Redirection of metabolism for biological hydrogen production. Appl. Environ. Microbiol. 73, 1665–1671. https://doi.org/10.1128/AEM.02565-06

Rhee, S.-K., Liu, X., Wu, L., Chong, S.C., Wan, X., Zhou, J., 2004. Detection of genes involved in biodegradation and biotransformation in microbial communities by using 50-mer oligonucleotide microarrays. Appl. Environ. Microbiol. 70, 4303–4317. https://doi.org/10.1128/AEM.70.7.4303-4317.2004

Ross, B.S., Pott, R.W.M., 2021. Hydrogen production by immobilized Rhodopseudomonas palustris in packed or fluidized bed photobioreactor systems. Int. J. Hydrogen Energy 46, 1715–1727. https://doi.org/https://doi.org/10.1016/j.ijhydene.2020.10.061

Rouphael, Y., Colla, G., 2020. Editorial: Biostimulants in Agriculture . Front. Plant Sci..

Rumin, J., Bonnefond, H., Saint-Jean, B., Rouxel, C., Sciandra, A., Bernard, O., Cadoret, J.P., Bougaran, G., 2015. The use of fluorescent Nile red and BODIPY for lipid measurement in microalgae. Biotechnol. Biofuels. https://doi.org/10.1186/s13068-015-0220-4

Sabourin-Provost, G., Hallenbeck, P.C., 2009. High yield conversion of a crude glycerol fraction from biodiesel production to hydrogen by photofermentation. Bioresour. Technol. 100, 3513–3517. https://doi.org/10.1016/j.biortech.2009.03.027

Sakarika, M., Spanoghe, J., Sui, Y., Wambacq, E., Grunert, O., Haesaert, G., Spiller, M.,

Vlaeminck, S.E., 2020. Purple non-sulphur bacteria and plant production: benefits for fertilization, stress resistance and the environment. Microb. Biotechnol. 13, 1336–1365. https://doi.org/https://doi.org/10.1111/1751-7915.13474

Salmon, R.C., Cliff, M.J., Rafferty, J.B., Kelly, D.J., 2013. The CouPSTU and TarPQM Transporters in Rhodopseudomonas palustris: Redundant, Promiscuous Uptake Systems for Lignin-Derived Aromatic Substrates. PLoS One. https://doi.org/10.1371/journal.pone.0059844

Satagopan, S., Chan, S., Perry, L.J., Tabita, F.R., 2014. Structure-Function Studies with the Unique Hexameric Form II Ribulose-1,5-bisphosphate Carboxylase/Oxygenase (Rubisco) from Rhodopseudomonas palustris*,. J. Biol. Chem. 289, 21433–21450. https://doi.org/https://doi.org/10.1074/jbc.M114.578625

Saxena, Divjot KourKusam Lata RanaNeelam YadavAjar Nath Yadav, A.A.R.S.N.S.K., 2019. Technologies for Biofuel Production: Current Development, Challenges, and Future Prospects, in: Prospects of Renewable Bioprocessing in Future Energy Systems. Biofuel and Biorefinery Technologies. Springer, Cham. https://doi.org/https://doi.org/10.1007/978-3-030-14463-0_1

Schaefer, A.L., Greenberg, E.P., Oliver, C.M., Oda, Y., Huang, J.J., Bittan-Banin, G., Peres, C.M., Schmidt, S., Juhaszova, K., Sufrin, J.R., Harwood, C.S., 2008. A new class of homoserine lactone quorum-sensing signals. Nature 454, 595–599. https://doi.org/10.1038/nature07088

Sharma, N., Doerner, K.C., Alok, P.C., Choudhary, M., 2015. Skatole remediation potential of Rhodopseudomonas palustris WKU-KDNS3 isolated from an animal waste lagoon. Lett. Appl. Microbiol. 60, 298–306. https://doi.org/10.1111/lam.12379

Shi, X.-Y., Li, W.-W., Yu, H.-Q., 2014. Optimization of H2 photo-fermentation from benzoate by Rhodopseudomonas palustris using a desirability function approach. Int. J. Hydrogen Energy 39, 4244–4251. https://doi.org/https://doi.org/10.1016/j.ijhydene.2014.01.016

Sogani, M., Pankan, A.O., Dongre, A., Yunus, K., Fisher, A.C., 2021. Augmenting the biodegradation of recalcitrant ethinylestradiol using Rhodopseudomonas palustris in a hybrid photo-assisted microbial fuel cell with enhanced bio-hydrogen production.

J. Hazard. Mater. 408, 124421. https://doi.org/https://doi.org/10.1016/j.jhazmat.2020.124421

Su, H., Cheng, J., Zhou, J., Song, W., Cen, K., 2009a. Combination of dark- and photo-fermentation to enhance hydrogen production and energy conversion efficiency. Int. J. Hydrogen Energy 34, 8846–8853. https://doi.org/https://doi.org/10.1016/j.ijhydene.2009.09.001

Su, H., Cheng, J., Zhou, J., Song, W., Cen, K., 2009b. Improving hydrogen production from cassava starch by combination of dark and photo fermentation. Int. J. Hydrogen Energy 34, 1780–1786. https://doi.org/https://doi.org/10.1016/j.ijhydene.2008.12.045

Su, P., Tan, X., Li, C., Zhang, D., Cheng, J., Zhang, S., Zhou, X., Yan, Q., Peng, J., Zhang, Z., Liu, Y., Lu, X., 2017. Photosynthetic bacterium Rhodopseudomonas palustris GJ-22 induces systemic resistance against viruses. Microb. Biotechnol. 10, 612–624. https://doi.org/https://doi.org/10.1111/1751-7915.12704

Tian, X., Liao, Q., Liu, W., Wang, Y.Z., Zhu, X., Li, J., Wang, H., 2009. Photo-hydrogen production rate of a PVA-boric acid gel granule containing immobilized photosynthetic bacteria cells. Int. J. Hydrogen Energy 34, 4708–4717. https://doi.org/https://doi.org/10.1016/j.ijhydene.2009.03.042

Tian, X., Liao, Q., Zhu, X., Wang, Y., Zhang, P., Li, J., Wang, H., 2010. Characteristics of a biofilm photobioreactor as applied to photo-hydrogen production. Bioresour. Technol. 101, 977–983. https://doi.org/https://doi.org/10.1016/j.biortech.2009.09.007

Tian, Y., Wu, X., Feng, B., Tian, C., Wang, C., Xiao, B., 2017. Nutrient Recovery From Cyanobacteria Biomasses Using Purple Nonsulfur Bacterium Rhodopseudomonas palustris. Polish J. Environ. Stud. 26, 2767–2775. https://doi.org/10.15244/pjoes/70403

Tomei, M.C., Mosca Angelucci, D., Clagnan, E., Brusetti, L., 2021. Anaerobic biodegradation of phenol in wastewater treatment: achievements and limits. Appl. Microbiol. Biotechnol. 105, 2195–2224. https://doi.org/10.1007/s00253-021-11182-5

Touloupakis, E., Poloniataki, E.G., Ghanotakis, D.F., Carlozzi, P., 2021. Production of

Biohydrogen and/or Poly-β-hydroxybutyrate by Rhodopseudomonas sp. Using Various Carbon Sources as Substrate. Appl. Biochem. Biotechnol. 193, 307–318. https://doi.org/10.1007/s12010-020-03428-1

Venkidusamy, K., Megharaj, M., 2016. A Novel Electrophototrophic Bacterium Rhodopseudomonas palustris Strain RP2, Exhibits Hydrocarbonoclastic Potential in Anaerobic Environments . Front. Microbiol. .

Wampler, D.A., Ensign, S.A., 2005. Photoheterotrophic metabolism of acrylamide by a newly isolated strain of Rhodopseudomonas palustris. Appl. Environ. Microbiol. 71, 5850–5857. https://doi.org/10.1128/AEM.71.10.5850-5857.2005

Wang, R., Lin, C.-Y., Chen, S.-H., Lo, K.-J., Liu, C.-T., Chou, T.-H., Shih, Y., 2019. Using high-throughput transcriptome sequencing to investigate the biotransformation mechanism of hexabromocyclododecane with Rhodopseudomonas palustris in water. Sci. Total Environ. 692, 249–258. https://doi.org/https://doi.org/10.1016/j.scitotenv.2019.07.140

Wang, X., Chen, J., Tang, X., Wang, J., Zhu, L., Zhang, W., Wang, H., Li, Y., Zhang, Q., 2019. Biodegradation mechanism of polyesters by hydrolase from Rhodopseudomonas palustris: An in silico approach. Chemosphere 231, 126–133. https://doi.org/https://doi.org/10.1016/j.chemosphere.2019.05.112

Wang, X., Cheng, X., Sun, D., 2008. Autocatalysis in Reactive Black 5 biodecolorization by Rhodopseudomonas palustris W1. Appl. Microbiol. Biotechnol. 80, 907–915. https://doi.org/10.1007/s00253-008-1657-1

WANG, X., CHENG, X., SUN, D., Qi, H., 2008. Biodecolorization and partial mineralization of Reactive Black 5 by a strain of Rhodopseudomonas palustris. J. Environ. Sci. 20, 1218–1225. https://doi.org/https://doi.org/10.1016/S1001-0742(08)62212-3

Wang, X., Feng, Y., Wang, H., Qu, Y., Yu, Y., Ren, N., Li, N., Wang, E., Lee, H., Logan, B.E., 2009. Bioaugmentation for Electricity Generation from Corn Stover Biomass Using Microbial Fuel Cells. Environ. Sci. Technol. 43, 6088–6093. https://doi.org/10.1021/es900391b

Wang, Y.-Z., Liao, Q., Zhu, X., Chen, R., Guo, C.-L., Zhou, J., 2013. Bioconversion characteristics of Rhodopseudomonas palustris CQK 01 entrapped in a

photobioreactor for hydrogen production. Bioresour. Technol. 135, 331–338. https://doi.org/https://doi.org/10.1016/j.biortech.2012.09.105

Wang, Y.-Z., Xie, X.-W., Zhu, X., Liao, Q., Chen, R., Zhao, X., Lee, D.-J., 2012. Hydrogen production by Rhodopseudomonas palustris CQK 01 in a continuous photobioreactor with ultrasonic treatment. Int. J. Hydrogen Energy 37, 15450–15457. https://doi.org/https://doi.org/10.1016/j.ijhydene.2012.02.187

Wang, Y., Tahir, N., Cao, W., Zhang, Q., Lee, D.-J., 2019. Grid columnar flat panel photobioreactor with immobilized photosynthetic bacteria for continuous photofermentative hydrogen production. Bioresour. Technol. 291, 121806. https://doi.org/https://doi.org/10.1016/j.biortech.2019.121806

Wang, Z., Gao, D., Geng, H., Xing, C., 2021. Enhancing Hydrogen Production by Photobiocatalysis through Rhodopseudomonas palustris Coupled with Conjugated Polymers. J. Mater. Chem. A. https://doi.org/10.1039/D1TA01019K

Wong, W.-T., Tseng, C.-H., Hsu, S.-H., Lur, H.-S., Mo, C.-W., Huang, C.-N., Hsu, S.-C., Lee, K.-T., Liu, C.-T., 2014. Promoting effects of a single Rhodopseudomonas palustris inoculant on plant growth by Brassica rapa chinensis under low fertilizer input. Microbes Environ. 29, 303–313. https://doi.org/10.1264/jsme2.me14056

Wu, J., Wang, Y., Lin, X., 2013. Purple Phototrophic Bacterium Enhances Stevioside Yield by Stevia rebaudiana Bertoni via Foliar Spray and Rhizosphere Irrigation. PLoS One 8, e67644.

Wu, P., Chen, Z., Zhang, Y., Wang, Y., Zhu, F., Cao, B., Wu, Y., Li, N., 2019. Rhodopseudomonas palustris wastewater treatment: Cyhalofop-butyl removal, biochemicals production and mathematical model establishment. Bioresour. Technol. 282, 390–397. https://doi.org/https://doi.org/10.1016/j.biortech.2018.11.087

Xiao, L., Zhao, Z., Ma, Z., Chen, J., Song, Z., 2020. Immobilization of Rhodopseudomonas palustris P1 on glass pumice to improve the removal of NH4+-N and NO2−-N from aquaculture pond water. Biotechnol. Appl. Biochem. 67, 323–329. https://doi.org/https://doi.org/10.1002/bab.1863

Xing, D., Zuo, Y., Cheng, S., Regan, J.M., Logan, B.E., 2008. Electricity Generation by Rhodopseudomonas palustris DX-1. Environ. Sci. Technol. 42, 4146–4151.

https://doi.org/10.1021/es800312v

XU, J., FENG, Y., WANG, Y., LIN, X., 2018. Effect of Rhizobacterium Rhodopseudomonas palustris Inoculation on Stevia rebaudiana Plant Growth and Soil Microbial Community. Pedosphere 28, 793–803. https://doi.org/https://doi.org/10.1016/S1002-0160(18)60043-8

Yang, C.-F., Lee, C.-M., 2011. Enhancement of photohydrogen production using phbC deficient mutant Rhodopseudomonas palustris strain M23. Bioresour. Technol. 102, 5418–5424. https://doi.org/https://doi.org/10.1016/j.biortech.2010.09.078

Yin, L., Li, X., Liu, Y., Zhang, D., Zhang, S., Luo, X., 2012. Biodegradation of cypermethrin by rhodopseudomonas palustris GJ-22 isolated from activated sludge. Fresenius Environ. Bull. 21, 397–405.

Yin, Z.P., Shang, Z.W., Wei, C., Ren, J., Song, X.S., 2012. FOLIAR SPRAYS OF PHOTOSYNTHETIC BACTERIA IMPROVE THE GROWTH AND ANTI-OXIDATIVE CAPABILITY ON CHINESE DWARF CHERRY SEEDLINGS. J. Plant Nutr. 35, 840–853. https://doi.org/10.1080/01904167.2012.663439

Zhai, Z., Du, J., Chen, L., Hamid, M.R., Du, X., Kong, X., Cheng, J., Tang, W., Zhang, D., Su, P., Liu, Y., 2019. A genetic tool for production of GFP-expressing Rhodopseudomonas palustris for visualization of bacterial colonization. AMB Express 9, 141. https://doi.org/10.1186/s13568-019-0866-6

Zhang, D., Xiao, N., Mahbubani, K.T., del Rio-Chanona, E.A., Slater, N.K.H., Vassiliadis, V.S., 2015. Bioprocess modelling of biohydrogen production by Rhodopseudomonas palustris: Model development and effects of operating conditions on hydrogen yield and glycerol conversion efficiency. Chem. Eng. Sci. 130, 68–78. https://doi.org/https://doi.org/10.1016/j.ces.2015.02.045

Zhang, S., Luo, X., Cheng, J., Peng, J., Zhang, D., Liu, Y., 2014. Genome Sequence of Pyrethroid-Degrading Bacterium Rhodopseudomonas palustris Strain JSC-3b. Genome Announc. 2. https://doi.org/10.1128/genomeA.01228-13

Zhao, C., Zhang, Y., Chan, Z., Chen, S., Yang, S., 2015. Insights into arsenic multi-operons expression and resistance mechanisms in Rhodopseudomonas palustris CGA009 . Front. Microbiol. .

Zhao, L., Zhao, C., Han, D., Yang, S., Chen, S., Yu, C.-P., 2011. Anaerobic utilization of

phenanthrene by Rhodopseudomonas palustris. Biotechnol. Lett. 33, 2135. https://doi.org/10.1007/s10529-011-0681-x

Zheng, Y., Harwood, C.S., 2019. Influence of Energy and Electron Availability on In Vivo Methane and Hydrogen Production by a Variant Molybdenum Nitrogenase. Appl. Environ. Microbiol. 85, e02671-18. https://doi.org/10.1128/AEM.02671-18

CHAPTER III

3. *Rhodopseudomonas palustris* CGA009 polyhydroxybutyrate production from a lignin aromatic and quantification via flow cytometry

Abstract

Polyhydroxyalkanoates are biopolymers with the potential to replace petroleum-based plastics but are limited by higher productions costs. For the first time, polyhydroxybutyrate (PHB) was produced by the metabolically versatile *Rhodopseudomonas palustris* CGA009 from the lignin breakdown product *p*-coumarate as a renewable carbon source. The PHB titer ranged from 0.08 to 0.41 g/L and yielded a 68.4% carbon conversion efficiency. Quantification of PHB via flow cytometry was conducted with *R. palustris* for the first time, and this study delivers an optimized protocol using either Nile Red or BODIPY 493/503 lipophilic stains. Fluorescence intensity yielded high linear fitness with PHB titers (R^2 = 0.9384 and R^2 = 0.9747 respectively). Unlike previous studies, the use of a permeabilizer yielded high linear fitness for cell counts (R^2 = 0.9383 and R^2 = 0.9955 respectively). This high-throughput quantification of PHB and cell count coupled with PHB production on a lignin aromatic make this study novel.

3.1 Introduction

Polyhydroxyalkonoates (PHAs) are biopolymers produced by microorganisms under certain stress conditions and offer a sustainable alternative to petroleum-based plastics. PHA metabolism has been shown to not only act as a carbon sink for bacteria, but also to provide a pool for reducing redox potential (Higuchi-Takeuchi et al., 2016; Liebergesell et al., 1991). These biopolymers have thermomechanical properties similar to conventional plastics, are biodegradable, and can be produced from a variety of substrates. Polyhydroxybutyrate (PHB) is a short-chain-length PHA that is commonly studied and can be modified to generate various copolymers depending on the metabolism of the bacteria and carbon sources provided for fermentation (Li et al., 2016). Due to its thermomechanical properties, biodegradation, and biocompatibility, PHB has been used in applications ranging from packaging materials to drug delivery systems (Poltronieri and Kumar, 2017). However, widespread use of PHAs is inhibited by high production costs due primarily to the carbon source and extraction methods (Aramvash et al., 2018).

The carbon source for bacterial PHB production accounts for about half of the total production costs (Mozumder et al., 2015). Lignocellulosic biomass is considered to be the most economic carbon source in the world since it is a common agricultural waste and highly renewable (Ponnusamy et al., 2019; Qian, 2013). The production of biopolymers from lignin, such as PHAs, is arguably the most promising route for boosting the valorization of lignin (Rajesh Banu et al., 2019). However, there is still a significant research gap for microbes that are capable of producing high-value byproducts from lignocellulosic biomass. In fact, many bacteria are not capable of catabolizing the complex phenolic structure of lignin due to its recalcitrance. However, *Rhodopseudomonas palustris*

CGA009 (hereafter *R. palustris*) is a purple non-sulfur, gram-negative bacterium that has been shown to grow on lignin breakdown products and lignocellulosic biomass (Austin et al., 2015; Salmon et al., 2013). A particular lignin aromatic, *p*-coumarate, is a major lignin breakdown product that has been highly characterized for *R. palustris* catabolism (Hidetada et al., 2012; Hirakawa et al., 2015). *R. palustris* is one of the most metabolically versatile organisms on the planet (Larimer et al., 2004), and its ability to exploit a wide array of carbon sources in diverse environments could reduce PHB production costs. A variety of *R. palustris* strains have been shown to produce PHB. However, many studies of *R. palustris* involving PHB production have focused on hydrogen gas production (McKinlay et al., 2014; Ranaivoarisoa et al., 2019; Wu et al., 2012). Furthermore, many studies use nitrogen fixation for PHB production by *R. palustris*, which is time consuming and adds to production costs (McKinlay et al., 2014; Ranaivoarisoa et al., 2019; Wu et al., 2012). Although *R. palustris* is known to grow on lignin aromatics and lignocellulosic biomass, PHB production on phenolic lignin breakdown products has yet to be assessed. As mentioned previously, PHA metabolism serves as a redox sink for the bacterium, and since *p*-coumarate has more reducing potential than acetate it was hypothesized in this study that *R. palustris* PHB production would increase using *p*-coumarate as a substrate.

The extraction process also accounts for a large portion of PHB production costs (Aramvash et al., 2018). Extraction and quantification of PHB generally entails depolymerization so that the monomers can subsequently be analyzed with gas chromatography or UV spectrophotometry. This typically involves solvent extraction via acidic methanolysis with chlorinated hydrocarbons, which is time consuming and includes toxic solvents that are nonrecyclable (Anis et al., 2013; Kunasundari and Sudesh, 2011).

For an alternative approach, there have been several studies that show staining bacteria with lipophilic stains followed by flow cytometry analysis yields precise quantification of PHB titers (Kacmar et al., 2006; Karmann et al., 2016; Lagares Jr. and Valverde, 2017; Li and Wilkins, 2020). Recently, Li and Wilkins (2020) developed a flow cytometry protocol for quantifying *Cupriavidus necator* PHB concentrations and cell counts for cultures that were grown on alkaline pretreated liquor from corn stover and stained with Nile Red (9-diethylamino-5-benzo[a]phenoxazinone). While Nile Red fluorescence had a good linear fitness for PHB concentrations ($R^2 = 0.9939$), the protocol showed less linear fitness for cell counts ($R^2 = 0.8614$). Nile Red is a lipophilic fluorescent dye that has a high affinity for lipids, an excitation wavelength of over 528 nm, emission wavelengths between 570-630 nm, has been used in a variety of organisms from yeasts to animal cells, and can be used with cells expressing green fluorescent proteins (Wang et al., 2018). A possible explanation for the lower fitness for cell count correlation could be that Nile Red has a higher sensitivity to polarity, large spectrums for adsorption and emission, low relative fluorescent stability, and limited permeability capacity compared to other fluorescent dyes (Wang et al., 2018). Although studies have shown Nile Red to be ideal for evaluating some lipids, its efficiency varies across species and experimental parameters. BODIPY (a boron dipyrromethene dye) is a relatively newer lipophilic stain that also has a high specificity for lipids, but does not have some of the drawbacks of Nile Red. Unlike Nile Red, BODIPY is not sensitive to changes in polarity or pH, has better photochemical stability, lower background signal, and a narrower emission spectrum (Wang et al., 2018). Compared to Nile Red that emits red fluorescence, BODIPY emits green fluorescence in the 510-540 nm range and can thus be used with cells expressing red fluorescent proteins.

Several studies have shown BODIPY to be a better fluorescent marker for lipids than Nile Red (Wang et al., 2018). Ultimately, factors such as spectral properties, incubation periods, and recalcitrance of cells can be an issue with lipophilic stains and flow cytometry analysis. For bacteria with many pigments such as *R. palustris*, the various pigments can absorb light at different wavelengths (Muzziotti et al., 2017). It is therefore essential to develop high-throughput quantification methods across different PHB-producing strains on various carbons sources. To the best of the author's knowledge, a flow cytometry method for PHB quantification from *R. palustris* has never been reported for Nile Red or BODIPY.

Thus, this study aims to i) apply flow cytometry for quantification of PHB in *R. palustris* for the first time, ii) optimize a flow cytometry method for accurate correlations of *both* PHB titers and cell counts using Nile Red and BODIPY 493/503 stains, and iii) produce PHB from *R. palustris* on the lignin aromatic *p*-coumarate for the first time. This approach addresses the two leading causes of increased PHB production costs (carbon and quantification), is the first reported analysis for *R. palustris* PHB production on the lignin aromatic *p*-coumarate, is the first reported *R. palustris* PHB quantification with flow cytometry, and delivers a multi-pronged optimization protocol for flow cytometry analysis.

3.2 Materials and Methods

3.2.1 Bacterial strains and culture conditions

R. palustris was obtained from the American Type Culture Collection (ATCC) and cells were stored at -80°C in 20% glycerol until ready for further processing. Cells were taken from -80°C and streaked onto agar plates. For seed culture preparation, cells were inoculated into 50 mL of prepared media in 250 mL flasks. Seed culture media was

photosynthetic mineral medium (PM) containing 10mM sodium bicarbonate, 15.2mM ammonium sulfate, 0.1457mM thiosulfate, and 50mM of both monopotassium phosphate and sodium phosphate dibasic (Gibson et al., 1990). Sodium acetate (20mM) was also added for seed cultures. Cultures were grown aerobically in the dark in an AlgaeTron AG 230 (Photon Systems Instruments™) at 30°C with continuous shaking at 275 rpm with an Innova® 2000 (New Brunswick™). Cell growth was monitored by optical density at 660nm with a Genesys 10S UV-VIS spectrophotometer (Thermo Scientific™).

3.2.2 Growth curves and PHB production

Cultures were diluted to an optical density of 0.2 for all experiments. *R. palustris* was grown anaerobically inside 14 mL Falcon™ Round-Bottom Polystyrene Tubes, which were completely filled and sealed to the second stop. Samples were grown at 30°C with 100 µE white light using an AlgaeTron AG 230 (Photon Systems Instruments™). The media used was the same PM used for seed cultures but with either 10mM sodium acetate or 1mM *p*-coumarate substituted for 20mM sodium acetate. Cell growth was monitored by optical density at 660nm with a Genesys 10S UV-VIS spectrophotometer (Thermo Scientific™). To determine growth parameters, growth data were fitted to the modified logarithmic growth equation in Eq. 1 (Zwietering et al., 1990).

$$y = \frac{A}{\{1+\exp\left[\frac{4\mu}{A}(\lambda - t)+2\right]\}} \quad (1)$$

Where µ is the maximum growth rate, A is the maximum optical density, and λ is the lag time.

Cultures were nitrogen starved at mid-exponential growth (Figure 1) on either 10mM sodium acetate or 1mM *p*-coumarate in the anaerobic conditions described previously. Each culture tube was centrifuged at 3800 rpm for 30 minutes to generate a pellet, the supernatant was discarded, and the pellet was resuspended in PM that did not contain ammonium sulfate as a nitrogen source. Either 10mM sodium acetate or 1mM *p*-coumarate was added. Culture tubes were completely filled and sealed at the second stop.

3.2.3 PHB quantification via gas-chromatography mass spectrometry (GC-MS)

PHB extraction and quantification was conducted by an adapted protocol used previously (Juengert et al., 2018; Li and Wilkins, 2020). Each 14 mL culture tube was centrifuged to obtain a pellet, washed twice with 0.89% NaCl, and frozen at -80°C until ready for processing. External standards were created from serial dilutions of sodium 3-hydroxybutyrate (Sigma-Aldrich™). Cell pellets and standards were vortexed with 1 mL acidic methanol (15% H_2SO_4) and 1 mL chloroform, and methanolized at 105°C for 2.5 hours. Samples were allowed to come to room temperature, and 1 mL deionized water (ELGA PURELAB® flex 1 and 2 Water Systems, 18.2 MΩ*cm) was added and then vortexed. Once phase separation was complete, the methyl-ester derivatives were extracted from the lower organic phase with a Pasteur pipette. At least 200 µL was extracted into GC-MS vial inserts. GC-MS operating and processing parameters were the same as outlined in (Li and Wilkins, 2020), including software analysis.

3.2.4 Permeability and stain volume assay

In order to decipher the ideal combination of permeabilizer and stain volume for flow cytometry analysis, a 96-well plate assay was developed. It has been shown that

ethylenediaminetetraacetic acid (EDTA) and polyethylenimine (PEI) are efficient permeabilizers for other gram-negative bacteria, and thus they were chosen for the assay on *R. palustris* (Alakomi et al., 2006). To compare staining efficiency, solutions of either 10mM PBS, 40% ethanol + PBS, 50% ethanol + PBS, 1mM EDTA + PBS, 2mM EDTA + PBS, 1mM PEI + PBS, and 2mM PEI + PBS were assessed. PBS concentration was 10mM for all conditions. To decipher the optimal volume of stain, each solution was stained with either 3 µL, 6 µL, or 9 µL Nile Red or BODIPY 493/503. All conditions were run using live cells from the maximum PHB production on *p*-coumarate (approx. 0.41 g/L) to ensure the parameters would be sufficient for staining the largest titer. All conditions were conducted with biological duplicates. Both stains were created with equal concentrations of 1 mg stain per mL dimethyl sulfoxide (DMSO).

Samples were loaded into a 96-well plate with a E1-ClipTip™ Electronic Multichannel Pipette for refined accuracy (Thermo Scientific™). Precisely 100 µL of live cell cultures that had been grown on 1mM *p*-coumarate and nitrogen starved for seven days were placed into each well. The plate was centrifuged at 4200 rpm for 30 minutes to generate pellets, and the pellets were washed with 1mM PBS before proceeding with the permeability assay. After cells were washed, the pellets were resuspended with the multichannel pipette in the corresponding permeabilizers described previously. Samples were incubated with the permeabilizer for 15 minutes, and the corresponding amount of the required stain was placed into the sample. The samples were incubated in the dark for another 15 minutes with the stain and then centrifuged to generate pellets in each well. Samples were washed twice with 10mM PBS and resuspended in precisely 100 µL of 10mM PBS. The 100 µL of each sample was diluted in 1 mL 10mM PBS inside 5 mL BD

Falcon™ Round-Bottom Tubes for analysis via flow cytometry. All samples were run in a FACS Aria II flow cytometer (BD Biosciences, San Jose, CA) with a 488 nm wavelength laser. BODIPY signal was detected using a 530/30 bandpass filter, while Nile Red was detected with a 610/20 bandpass filter. Samples were analyzed with BD FACSDiva 8.0.1 software.

3.2.5 Analysis of live and frozen samples

Once the ideal permeability condition of 50% ethanol/PBS and 3 µL of either stain was established from the permeability assay, this combination of parameters was used to compare the stain efficiency of live and frozen samples. The remaining amount of the same live cell cultures that were used for the permeability assay that had not been processed were saved as pellets in -80°C. Samples were allowed to thaw for 10 minutes before processing and were run with at least two biological duplicates for each condition. Precisely 100 µL of thawed cell culture in 10mM PBS was centrifuged in an Eppendorf tube at 17,000 rpm for 4 minutes and resuspended in 50% ethanol/PBS solution for 15 minutes. Either 3 µL of Nile Red or BODIPY stains was mixed into the sample by pipetting and incubated for another 15 minutes in the dark. Samples were washed twice with 10mM PBS, resuspended in exactly 100 µL 10mM PBS, and transferred to 5 mL BD Falcon™ Round-Bottom Tubes that contained 1 mL 10mM PBS. The samples were immediately analyzed with the same flow cytometry parameters described in Section 3.2.4.

3.2.6. PHB and cell count analysis

Previous analyses revealed that 50% ethanol/PBS with either 3 µL of Nile Red or BODIPY stains was ideal for staining efficiency, and that frozen cells still yield high stain

efficiency similar to that of live cells. Thus, flow cytometry was conducted with frozen PHB samples across a range of concentrations (approximately 0.001 – 0.41 g/L) on cultures grown from 10mM sodium acetate and 1mM *p*-coumarate. All conditions were run with a minimum of biological duplicates, with the same processing procedures outlined in Section 3.2.5. To compare cell counts and decipher if this staining method is efficient for cell number calculations, 25 µL of 5 µm AccuCount particles (ACFP-50–5, Spherotech Inc, IL, USA) of known number was injected into each sample before flow cytometry analysis. Particles were excited with a 561 nm laser and detected with a 780/60 bandpass filter during flow cytometry. Two unstained samples in PBS and two unstained samples in PBS + AccuCount particles were used as controls. The signals of these controls were removed to determine the regions of bacterial cells and stained cells (also known as gates). Cell number was calculated with Eq. 2:

$$Stained\ cell\ \#\ =\ (\#\ stained\ events/\#\ events\ of\ particles) \qquad (2)$$

$$*\ (\#\ particles\ added\ by\ volume/initial\ volume\ of\ culture\ sample)$$

The initial volume of culture sample was 100 µL, and the number of particles added by volume is supplied by the manufacturer and specific for each solution of AccuCount particles.

3.2.7 Fluorescence microscopy

After the permeability assay, fluorescence microscopy was conducted to image PHB-producing cells stained with either Nile Red or BODIPY. The optimal combination of permeabilizer and stain volume was 50% ethanol and 3 µL of stain for both Nile Red and BODIPY. Thus, 100 µL of live cells that were grown anaerobically on 1mM *p*-

coumarate and nitrogen starved were subjected to these conditions. Cell cultures were centrifuged at 17,000 rpm in microcentrifuge tubes for 4 minutes and washed twice with 10mM PBS. The cell pellet was then resuspended in 100 µL of 50% ethanol/PBS solution, and incubated for 15 minutes. Either 3 µL of Nile Red or BODIPY was placed into the sample, mixed by pipetting, followed by another 15 minutes of incubation in the dark. Cell cultures were then washed twice with 10mM PBS. The washed cells were resuspended in 100 µL of 10mM PBS for imaging by a Nikon A1R confocal system (Thermo Scientific™). Nile red stained cells were subjected to a red fluorescent protein channel, while BODIPY stained cells were subjected to a green fluorescent protein channel. Each sample was subjected to a 100x lens with an additional 1.5x optical magnification set on the scope.

3.2.8 Statistical Analyses

Growth curves and GC-MS data represent the averages of biological triplicate data points (Figure 3.2). All error bars represent the calculated standard deviation from raw data based on the entire population. All flow cytometry experiments were run with biological duplicates (Figures 3.3 - 3.5). One-way Analyses of Variance (ANOVAs) were conducted for both Nile Red and BODIPY data to compare differences in 40% and 50% ethanol solution, 3 µL and 9 µL stain volumes in the 50% ethanol/PBS solution data, and live vs. frozen stain efficiency ($p < 0.05$).

3.3. Results and discussion

3.3.1 Growth curves and PHB production results

It was hypothesized that nitrogen starvation would encourage PHB production since this has been shown with *R. palustris* previously (McKinlay et al., 2014).

Furthermore, *R. palustris* was intentionally not subjected to nitrogen fixation to decipher PHB yields without having to incur that processing burden or increase in production cost. The anaerobic growth curve and growth constants for both 10mM sodium acetate and 1mM *p*-coumarate are shown in Figure 3.1. Cells grown on 10mM sodium acetate produced a PHB titer from 0.001-0.06 g/L over a five-day period (data not shown). The PHB production from 1mM *p*-coumarate with CO_2 fixation from 10mM sodium bicarbonate reached a maximum titer of approximately 0.41 g/L (or 3.25mM sodium 3-hydroxybutyrate) at six days of nitrogen starvation (Figure 3.1). Using Eq. 3 below for the conversion of 1mM *p*-coumarate and 10mM sodium bicarbonate to 3.25mM 3-hydroxybutyrate, this equates to approximately 68.4% carbon conversion efficiency.

$$\frac{0.013\ moles\ carbon\ produced\ in\ PHB}{0.019\ moles\ carbon\ invested}\ x\ 100 = 68.4\%\ carbon\ conversion \qquad (3)$$

Cells produced PHB without nitrogen fixation, which simplifies processing and could reduce production costs. Maximum production capacity could be due to a number of factors such as the amount of carbon source, the type of nutrient deprivation (i.e. nitrogen starvation), and fermentation conditions. Future efforts could focus on further increasing the carbon to nitrogen ratio, manipulating the size or quantity of the granules inside the cytoplasm via a synthetic biology approach, and engineering an optimized fermentation strategy to increase titer.

3.3.2 Permeability and stain volume assay results

It was hypothesized that incorporating a permeabilizer into the experimental workflow would increase staining efficiencies, thus optimizing PHB titer and cell count predictions using flow cytometry. Furthermore, it is likely that an efficient permeabilizer would reduce the amount of stain required, resulting in less washing and a reduction in false positives. Developing a method using a permeabilizer could also reduce the amount of time necessary for staining, which has been previously performed with a 30-minute incubation period (Li and Wilkins, 2020). Results of the permeability assay and stain volume analysis are depicted in Figure 3.2. Ethanol and PEI were the most efficient permeabilizers for staining *R. palustris* for both Nile Red and BODIPY. Since ethanol is far more common than PEI generally, it was chosen as the permeabilizer for further testing. A one-way ANOVA was conducted to decipher if the values for 40% and 50% ethanol solutions were statistically different from one another for Nile Red and BODIPY ($p < 0.05$). No significant difference was observed between 40% and 50% data. Since data for the 40% solution showed larger standard deviations, the 50% ethanol solution was chosen as the permeabilizer for further PHB analysis. Furthermore, a one-way ANOVA was conducted to evaluate differences in staining efficiencies for 3 µL and 9 µL in 50% ethanol solution. No significant difference was observed between the amounts of stain for either dye, so 3 µL was used for further testing. A Tukey's Honestly Significant Difference (HSD) was conducted for conditions in which an ANOVA yielded significant results, and significance is denoted by different letters in Figure 3.2 (where $\alpha = 0.05$). Overall, the 50% ethanol solution with 3 µL of either stain was chosen as the ideal parameters for future analysis. Ultimately, the permeability method developed here helps increase staining efficiency

compared to samples with no permeabilizer, optimizes efficiency with only a 15-minute stain incubation, and helps reduce the number of washes and false positives by limiting the amount of stain required.

3.3.3 Analysis of live and frozen samples results

The results of live and frozen stain efficiencies are depicted in Figure 3.3. Frozen cells yielded similar staining efficiencies as live cells, with no confirmed statistical significance based on a one-way ANOVA ($p > 0.05$). However, frozen cells produced higher standard deviations. Some recommended remedies for this are to freeze the pellets in new vials after washing them to ensure there is no media present and to vortex the samples after adding the stains to ensure even staining. Since frozen samples still provided high staining efficiencies, subsequent cultures were nitrogen starved, pelleted after each day of nitrogen starvation, and stored in -80°C until ready for processing with flow cytometry. Nitrogen starved samples were saved over a seven-day period from both 10mM sodium acetate and 1mM *p*-coumarate to assess a range of PHB concentrations (0.001 – 0.41 g/L).

3.3.4 PHB and cell count analysis results

The linear regressions for PHB concentration and cell count predictions are shown in Figure 3.4. Linear models for PHB concentration and fluorescence intensity for both Nile Red and BODIPY yielded strong fitness ($R^2 = 0.9495$ and $R^2 = 0.9928$ respectively). Both stains yielded good fitness for cell count predictions as well ($R^2 = 0.9383$ and $R^2 = 0.9967$ respectively). It is notable that BODIPY was a better fit than Nile Red for both PHB concentration and cell count. This is in agreement with other studies that show BODIPY

has a very high affinity for PHA granules (Rumin et al., 2015). Nile Red also has spectral properties that are very sensitive to polarity in the surrounding environment, which could contribute to the decrease in fitness as compared to BODIPY (Rumin et al., 2015). Adding ethanol as the permeabilizer would decrease the polarity, which could increase the overall absorption efficiency of Nile Red compared to other studies. *R. palustris* has a high pigment concentration, which could be yet another factor attributing to the variation in Nile Red staining. *R. palustris* can typically be found as a clump of rod-shaped bacteria, and it is hypothesized that the permeabilizer helped break up these clumps and make the cells more ideal for flow cytometry. This could be a factor for why Nile Red cell count predictions are a good fit for this optimized method compared to a previous study in which it was not (Li and Wilkins, 2020). Permeation of BODIPY is also faster than that of Nile Red typically, and thus it might be beneficial to use a slightly longer incubation time for Nile Red (Wang et al., 2018).

Unlike previously reported methods, this protocol is accurate for cell count and enables estimations of PHB production efficiency on a per cell basis. Moreover, this study shows that frozen cells can be used with this protocol, enabling more flexible analyses over time. Compared to the conventional PHB quantification method with methanolysis and GC-MS analysis that takes hours to perform and requires toxic chemicals, the method delivered here can be conducted in 30 minutes without organic solvents. Additionally, PHB is not depolymerized in the process, providing more flexibility for analysis or extraction. Since Nile Red and BODIPY can be used concurrently with cells expressing green and red fluorescent proteins respectively, this method also provides flexibility for future synthetic biology experiments. If cells expressing red or green fluorescent proteins is not an issue, it

is recommended that BODIPY be used since it showed higher linear fitness than Nile Red for both PHB concentration and cell count linear regressions. Ultimately, producing PHB from such a metabolically versatile organism, using a renewable and cheap carbon source, and developing a quick and reliable quantification method helps promote the valorization of PHB. Our future efforts with *R. palustris* will focus on optimizing PHB production from *p*-coumarate and lignocellulosic biomass, analyzing PHB granules with transmission electron microscopy, engineering the overproduction of PHB, and upscaling fermentation.

3.3.5 Fluorescence microscopy results

Fluorescent microscopy was used to image *R. palustris* Nile Red and BODIPY stained cells that had been subjected to nitrogen starvation (Figure 3.5). As expected, cells showed rod shapes with both stains. PHB granules are visible with a transmitted light image overlaid onto the fluorescent image, and the majority of cells show polarity to the granules. Variations in brightness are thought to be due to either different sizes of a single PHB granule inside each cell or several PHB granules within the cytoplasm, such that these would have picked up more stain and appear brighter. Variations would cause Nile Red to appear brighter red while BODIPY would be brighter green. Other imaging techniques, such as transmission electron microscopy, will be employed in the future to analyze the shape, polarity, number, and other factors of the PHB granules when *R. palustris* is grown on lignocellulosic biomass.

3.4. Conclusions

This study demonstrates for the first time that *R. palustris* produces PHB on the lignin aromatic *p*-coumarate and delivers an optimized process for quantifying both PHB

concentration and cell count via flow cytometry. *R. palustris* produced approximately 0.41 g/L on 1mM *p*-coumarate after six days of nitrogen starvation, resulting in a 68.4% carbon conversion efficiency. The protocol created here is a multi-pronged optimization that allows for a quick and accurate assessment of both *R. palustris* PHB titer and cell concentrations using either Nile Red or BODIPY coupled with flow cytometry analysis.

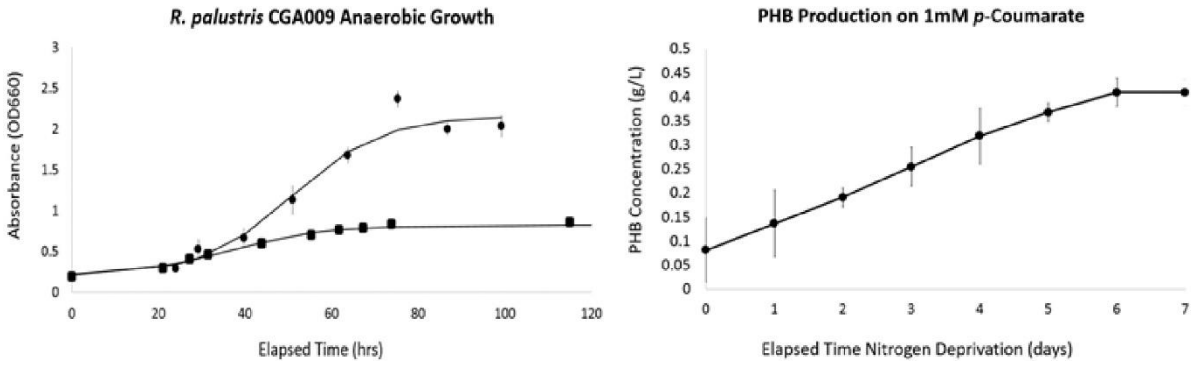

Fig. 3.1. (A) *R. palustris* anaerobic growth on 10 mM sodium acetate and 1 mM *p*-coumarate. Data have been fitted to a logarithmic growth model as described in Section 3.2.2. (B) *R. palustris* PHB production on 1 mM *p*-coumarate from nitrogen starved cells at mid-exponential growth. All data points represent averages of biological triplicates and error bars are the calculated standard deviation of the population.

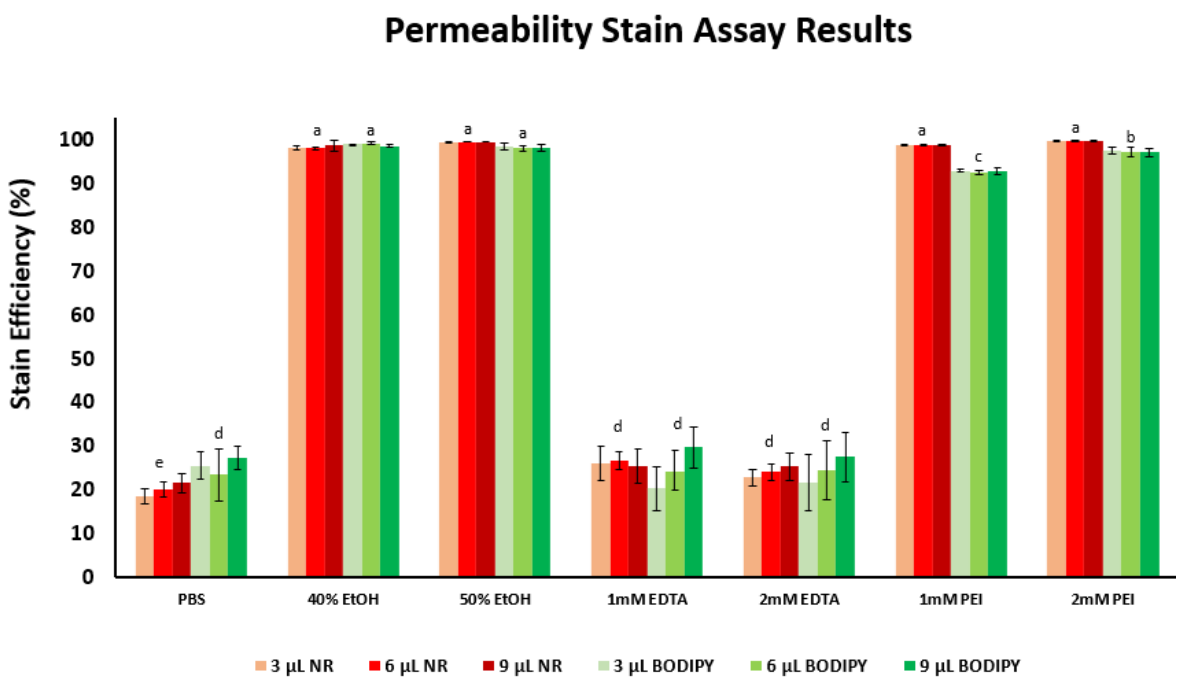

Fig. 3.2. Permeability stain assay results for Nile Red and BODIPY with *R. palustris*. Values are averages of the percent of staining from flow cytometry data using biological duplicates. Error bars are the calculated standard deviations based on the population. An ANOVA was conducted to decipher if there was overall statistical significance, followed by a post-hoc Tukey's HSD analysis ($\alpha = 0.05$). Nile Red or BODIPY groups connected by different letters are significantly different.

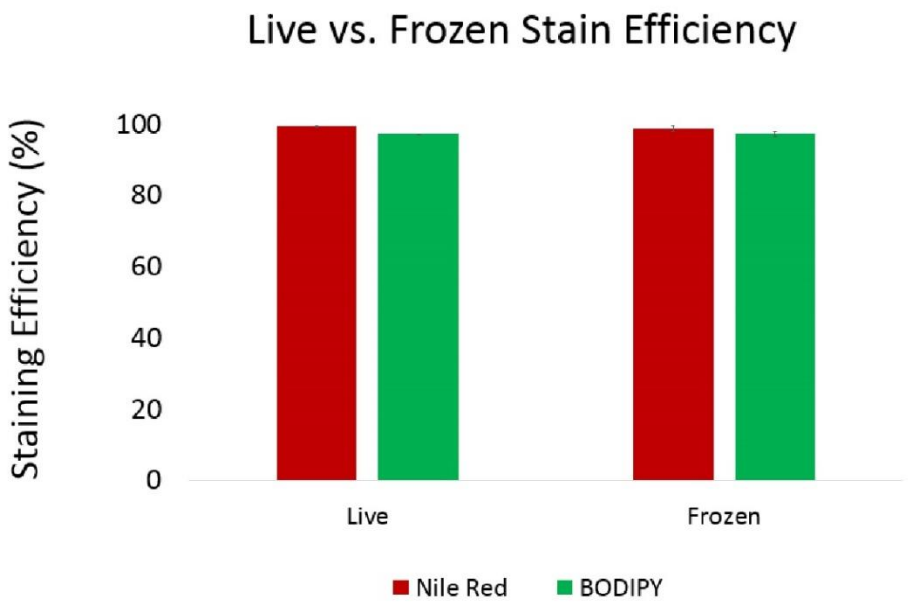

Fig. 3.3. Staining efficiency comparison of *R. palustris* live and frozen cells. Data represent averages of biological duplicates using the same cultures for both live and frozen cells. Error bars are the calculated standard deviation based on the entire population. There was no statistical difference in staining efficiency between live versus frozen samples for either Nile Red or BODOIPY stains ($\alpha = 0.05$).

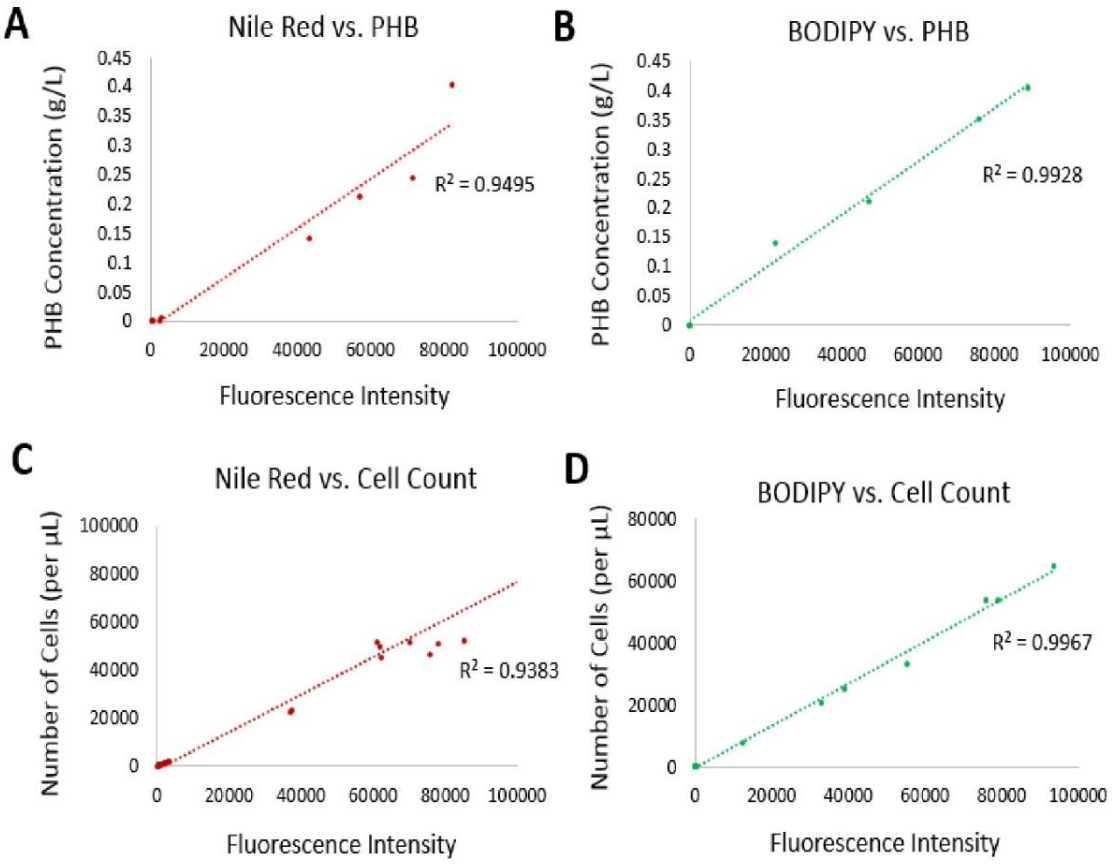

Fig. 3.4. Fluorescence intensity of (A) Nile Red and (B) BODIPY stained cells compared to PHB production. (C) Nile Red and (D) BODIPY stained cell counts compared to the calculated cell counts per µL of sample.

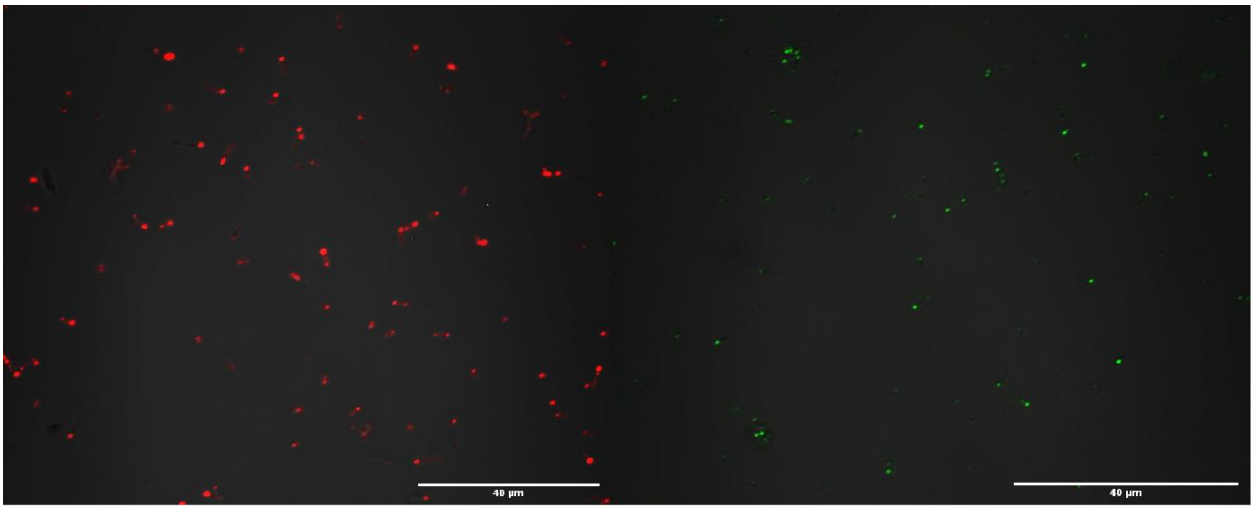

Fig. 3.5. Nile Red (A) and BODIPY (B) stained *R. palustris* cells under fluorescence microscopy. Cells were grown on *p*-coumarate, nitrogen starved, and contain PHB granules. For interpretation of the references to colors in this figure, the reader is referred to the web version of this article.

3.5 References

Alakomi, H.L., Paananen, A., Suihko, M.L., Helander, I.M., Saarela, M., 2006. Weakening effect of cell permeabilizers on gram-negative bacteria causing biodeterioration. Appl. Environ. Microbiol. https://doi.org/10.1128/AEM.00142-06

Anis, S.N.S., Iqbal, N.M., Kumar, S., Al-Ashraf, A., 2013. Increased recovery and improved purity of PHA from recombinant Cupriavidus necator. Bioengineered. https://doi.org/10.4161/bioe.22350

Aramvash, A., Moazzeni Zavareh, F., Gholami Banadkuki, N., 2018. Comparison of different solvents for extraction of polyhydroxybutyrate from Cupriavidus necator. Eng. Life Sci. https://doi.org/10.1002/elsc.201700102

Austin, S., Kontur, W.S., Ulbrich, A., Oshlag, J.Z., Zhang, W., Higbee, A., Zhang, Y., Coon, J.J., Hodge, D.B., Donohue, T.J., Noguera, D.R., 2015. Metabolism of Multiple Aromatic Compounds in Corn Stover Hydrolysate by Rhodopseudomonas palustris. Environ. Sci. Technol. https://doi.org/10.1021/acs.est.5b02062

Gibson, J., Geissler, J.F., Harwood, C.S., 1990. Benzoate-CoA ligase from Rhodopseudomonas palustris. Methods Enzymol. https://doi.org/10.1016/0076-6879(90)88028-9

Hidetada, H., L., S.A., Peter, G.E., S., H.C., 2012. Anaerobic p-Coumarate Degradation by Rhodopseudomonas palustris and Identification of CouR, a MarR Repressor Protein That Binds p-Coumaroyl Coenzyme A. J. Bacteriol. 194, 1960–1967. https://doi.org/10.1128/JB.06817-11

Higuchi-Takeuchi, M., Morisaki, K., Toyooka, K., Numata, K., 2016. Synthesis of High-Molecular-Weight Polyhydroxyalkanoates by Marine Photosynthetic Purple Bacteria. PLoS One 11, e0160981.

Hirakawa, H., Hirakawa, Y., Greenberg, E.P., Harwood, C.S., 2015. BadR and BadM Proteins Transcriptionally Regulate Two Operons Needed for Anaerobic Benzoate Degradation by Rhodopseudomonas palustris. Appl. Environ. Microbiol. 81, 4253–4262. https://doi.org/10.1128/AEM.00377-15

Juengert, J., Bresan, S., Jendrossek, D., 2018. Determination of Polyhydroxybutyrate (PHB) Content in Ralstonia eutropha Using Gas Chromatography and Nile Red Staining. BIO-PROTOCOL 8. https://doi.org/10.21769/BioProtoc.2748

Kacmar, J., Carlson, R., Balogh, S.J., Srienc, F., 2006. Staining and quantification of poly-3-hydroxybutyrate in Saccharomyces cerevisiae and Cupriavidus necator cell populations using automated flow cytometry. Cytometry. A 69, 27–35. https://doi.org/10.1002/cyto.a.20197

Karmann, S., Follonier, S., Bassas-Galia, M., Panke, S., Zinn, M., 2016. Robust at-line quantification of poly(3-hydroxyalkanoate) biosynthesis by flow cytometry using a BODIPY 493/503-SYTO 62 double-staining. J. Microbiol. Methods. https://doi.org/10.1016/j.mimet.2016.10.003

Kunasundari, B., Sudesh, K., 2011. Isolation and recovery of microbial polyhydroxyalkanoates. Express Polym. Lett. https://doi.org/10.3144/expresspolymlett.2011.60

Lagares Jr., A., Valverde, C., 2017. Quantification of Bacterial Polyhydroxybutyrate

Content by Flow Cytometry. BIO-PROTOCOL. https://doi.org/10.21769/bioprotoc.2638

Larimer, F.W., Chain, P., Hauser, L., Lamerdin, J., Malfatti, S., Do, L., Land, M.L., Pelletier, D.A., Beatty, J.T., Lang, A.S., Tabita, F.R., Gibson, J.L., Hanson, T.E., Bobst, C., Torres Y Torres, J.L., Peres, C., Harrison, F.H., Gibson, J., Harwood, C.S., 2004. Complete genome sequence of the metabolically versatile photosynthetic bacterium Rhodopseudomonas palustris. Nat. Biotechnol. https://doi.org/10.1038/nbt923

Li, M., Wilkins, M., 2020. Flow cytometry for quantitation of polyhydroxybutyrate production by Cupriavidus necator using alkaline pretreated liquor from corn stover. Bioresour. Technol. https://doi.org/10.1016/j.biortech.2019.122254

Li, Z., Yang, J., Loh, X.J., 2016. Polyhydroxyalkanoates: Opening doors for a sustainable future. NPG Asia Mater. https://doi.org/10.1038/am.2016.48

Liebergesell, M., Hustede, E., Timm, A., Steinbüchel, A., Fuller, R.C., Lenz, R.W., Schlegel, H.G., 1991. Formation of poly(3-hydroxyalkanoates) by phototrophic and chemolithotrophic bacteria. Arch. Microbiol. 155, 415–421. https://doi.org/10.1007/BF00244955

McKinlay, J.B., Oda, Y., Ruhl, M., Posto, A.L., Sauer, U., Harwood, C.S., 2014. Non-growing rhodopseudomonas palustris increases the hydrogen gas yield from acetate by shifting from the glyoxylate shunt to the tricarboxylic acid cycle. J. Biol. Chem. https://doi.org/10.1074/jbc.M113.527515

Mozumder, M.S.I., Garcia-Gonzalez, L., De Wever, H., Volcke, E.I.P., 2015. Effect of

sodium accumulation on heterotrophic growth and polyhydroxybutyrate (PHB) production by Cupriavidus necator. Bioresour. Technol. https://doi.org/10.1016/j.biortech.2015.04.110

Muzziotti, D., Adessi, A., Faraloni, C., Torzillo, G., De Philippis, R., 2017. Acclimation strategy of Rhodopseudomonas palustris to high light irradiance. Microbiol. Res. https://doi.org/10.1016/j.micres.2017.01.007

Poltronieri, P., Kumar, P., 2017. Polyhydroxyalcanoates (PHAs) in Industrial Applications, in: Handbook of Ecomaterials. https://doi.org/10.1007/978-3-319-48281-1_70-1

Ponnusamy, V.K., Nguyen, D.D., Dharmaraja, J., Shobana, S., Banu, J.R., Saratale, R.G., Chang, S.W., Kumar, G., 2019. A review on lignin structure, pretreatments, fermentation reactions and biorefinery potential. Bioresour. Technol. 271, 462–472. https://doi.org/https://doi.org/10.1016/j.biortech.2018.09.070

Qian, E.W., 2013. Pretreatment and Saccharification of Lignocellulosic Biomass, in: Research Approaches to Sustainable Biomass Systems. https://doi.org/10.1016/B978-0-12-404609-2.00007-6

Rajesh Banu, J., Kavitha, S., Yukesh Kannah, R., Poornima Devi, T., Gunasekaran, M., Kim, S.-H., Kumar, G., 2019. A review on biopolymer production via lignin valorization. Bioresour. Technol. 290, 121790. https://doi.org/https://doi.org/10.1016/j.biortech.2019.121790

Ranaivoarisoa, T.O., Singh, R., Rengasamy, K., Guzman, M.S., Bose, A., 2019. Towards sustainable bioplastic production using the photoautotrophic bacterium

Rhodopseudomonas palustris TIE-1. J. Ind. Microbiol. Biotechnol. https://doi.org/10.1007/s10295-019-02165-7

Rumin, J., Bonnefond, H., Saint-Jean, B., Rouxel, C., Sciandra, A., Bernard, O., Cadoret, J.P., Bougaran, G., 2015. The use of fluorescent Nile red and BODIPY for lipid measurement in microalgae. Biotechnol. Biofuels. https://doi.org/10.1186/s13068-015-0220-4

Salmon, R.C., Cliff, M.J., Rafferty, J.B., Kelly, D.J., 2013. The CouPSTU and TarPQM Transporters in Rhodopseudomonas palustris: Redundant, Promiscuous Uptake Systems for Lignin-Derived Aromatic Substrates. PLoS One. https://doi.org/10.1371/journal.pone.0059844

Wang, J., Guo, X., Li, L., Qiu, H., Zhang, Z., Wang, Y., Sun, G., 2018. Application of the fluorescent dye BODIPY in the study of lipid dynamics of the rice blast fungus magnaporthe oryzae. Molecules. https://doi.org/10.3390/molecules23071594

Wu, S.C., Liou, S.Z., Lee, C.M., 2012. Correlation between bio-hydrogen production and polyhydroxybutyrate (PHB) synthesis by Rhodopseudomonas palustris WP3-5. Bioresour. Technol. https://doi.org/10.1016/j.biortech.2012.01.090

Zwietering, M.H., Jongenburger, I., Rombouts, F.M., van 't Riet, K., 1990. Modeling of the bacterial growth curve. Appl. Environ. Microbiol. 56, 1875–1881.

CHAPTER IV

4. Synergistic Experimental and Computational Approach Identifies Novel Strategies for Polyhydroxybutyrate Overproduction

Portions of this material have been prepared by two co-first authors with equal contribution. Brandi Brown conducted bulk of the experimental workflow while Adil Alsiyabi conducted the metabolic modelling, flux balance analysis, and Pulse Amplitude Modulation fluorometry. Both authors contributed to experimental design and peer-reviewed communication.

Abstract

Polyhydroxybutyrate (PHB) is a sustainable bioplastic produced by bacteria that is a potential replacement for conventional plastics. This study delivers an integrated experimental and computational modeling approach to decipher metabolic factors controlling PHB production and offers engineering design strategies to boost production. In the metabolically robust *Rhodopseudomonas palustris* CGA009, PHB production significantly increased when grown on the carbon- and electron-rich lignin breakdown product *p*-coumarate ($C_9H_8O_3$) compared to virtually no PHB titer from acetate ($C_2H_3NaO_2$). The maximum yield did not improve further when grown on coniferyl alcohol ($C_{10}H_{12}O_3$), but comparison of the PHB profiles showed that coniferyl alcohol's higher carbon content resulted in a higher rate of PHB production. Combined experimental results revealed that cytoplasmic space may be a limiting factor for maximum PHB titer. In order to obtain a systems-level understanding of factors driving PHB yield, a model-driven investigation was performed. The model yielded several engineering design strategies including utilizing reduced, high molecular weight substrates that bypass the thiolase reaction (*phaA*). Based on these strategies, utilization of butyrate was predicted and

subsequently validated to produce PHB. Model analysis also explained why nitrogen starvation was not essential for PHB production and revealed that renewable and abundant lignin aromatics are ideal candidates for PHB production. Most importantly, the generality of the derived design rules allows them to be applied to any PHB-producing microbe with similar metabolic features.

4.1. Introduction

Due to the global plastic waste crisis, there has been extensive research on polyhydroxyalkanoates (PHAs) as potential replacements for petroleum-derived plastics. PHAs are biopolymers produced by bacteria that have similar thermomechanical properties as conventional plastics, but are also biodegradable, have shown biocompatibility in therapeutics, and can be produced from a wide array of sustainable carbon sources (Brown et al., 2020; Medeiros Garcia Alcântara et al., 2020). These bioplastics are generally produced by microbes under stressful conditions (e.g. nutrient starvation) and stored as granules inside the cytoplasm for carbon balance, stress mitigation, and as a redox sink (Kleiner et al., 2012). PHAs are considered to be the largest group of natural polyesters with over 150 monomers reported, and offer a unique platform for easily manipulating the thermomechanical properties of the bioplastic produced (Li et al., 2016). Due to these characteristics, PHAs have been used in a wide array of applications ranging from medical implants to biodegradable packaging (Chen, 2009; Chen and Zhang, 2018; Medeiros Garcia Alcântara et al., 2020). However, the widespread adoption of PHAs is hampered by high production costs, which is largely attributed to feedstock costs (Chen et al., 2020). Therefore, engineering a microbe that can overproduce the most common form of PHA, called poly-3-hydroxybutyrate (PHB), from inexpensive renewable feedstocks is needed.

However, choosing a successful engineering strategy to maximize PHB production is difficult due to the complexity in metabolism across PHB-producing bacteria (Lopar et al., 2013). The PHB synthesis pathway (Fig. 4.1) has been investigated extensively in multiple organisms (Chen and Jiang, 2017; Chen, 2009; Kocharin et al., 2012; Leaf and Srienc, 1998; Ranaivoarisoa et al., 2019; Sekar and Tyo, 2015; Tyo et al., 2010; Uchino et al., 2007; Van Wegen et al., 2001) but different studies primarily point to three different bottlenecks that constrict the rate through the pathway (Chen and Jiang, 2017; Kocharin et al., 2012; Leaf and Srienc, 1998; Ranaivoarisoa et al., 2019; Sekar and Tyo, 2015; Tyo et al., 2010; Uchino et al., 2007; Van Wegen et al., 2001). First, a number of studies have indicated that the rate of PHB synthesis is dependent on the acetyl-CoA pool size or the acetyl-CoA/CoA ratio (Kocharin et al., 2012; Van Wegen et al., 2001). Since acetyl-CoA is the first substrate in the pathway, it is intuitive to postulate that increasing its intracellular concentration will lead to an increase in the rate of PHB synthesis. Indeed, this has been shown in *Saccharomyces cerevisiae* (Kocharin et al., 2012). Furthermore, the first reaction in the PHB pathway is involves thiolase (*phaA*), which is thermodynamically unfavorable in the forward direction ($\Delta G'^{\circ} = 26\ kJ/mol$). This means that the ratio of reactants to products should be high in order for this reaction to proceed. This hypothesis is related to the pathway's role as a carbon sink, as any increase in the production of the central metabolite (i.e., acetate) will be funneled towards PHB for storage (James B McKinlay et al., 2014). Second, other studies have reported that the rate of PHB synthesis is correlated to the redox state of NADPH ([NADPH]/[$NADP^+$]) (Centeno-Leija et al., 2014; Chohan and Copeland, 1998; Lee et al., 1996; Sacomboio et al., 2017). This observation can be connected to the pathway's role as an electron sink (James B McKinlay et al., 2014).

Furthermore, an increase in the NADPH to $NADP^+$ ratio increases the thermodynamic driving force of the second reaction in the pathway (*phaB*). Third, a study investigating the effect of overexpressing different enzymes in the pathway found that the expression of *phaB* was the limiting factor in PHB synthesis (Tyo et al., 2010). This result is consistent with a number of previous kinetic analyses which revealed that the catalytic efficiency of the reductase reaction (*phaB)* was substantially lower than that of other reactions in the pathway (Sim et al., 1997; Wang and Lee, 1997). Interestingly, this study also shows that an increase in the expression of the thiolase (*phaA*) actually leads to a slight decrease in PHB production, which further points to the thermodynamic driving force favoring the reverse direction of the reaction (Tyo et al., 2010).

Based on these findings, it is apparent that the overall rate through the pathway is highly dependent on metabolic factors, such as the relative abundance of the participating metabolites and cofactors. Furthermore, due to the inherently high connectivity of the participating metabolites, their condition-specific availability is reliant on their overall generation and consumption rates from a number of different pathways. It is therefore vital to make use of a systems-wide framework such as genome-scale metabolic models (GSMMs) that can account for changes that occur in all parts of the metabolic network. These models translate the repertoire of all known metabolic functionalities performed by an organism into a mathematical representation which can then be used to infer the activity throughout the metabolic network (Fondi and Liò, 2015; Islam and Saha, 2018; Saha et al., 2014). With the aid of methods such as Flux Balance Analysis (FBA) (Orth et al., 2010), GSMMs have been successful in accurately predicting how metabolism changes under different genetic and environmental perturbations, as well as generating testable

hypotheses on what drives such changes. Thus far, GSMMs of several PHB producing bacteria have been constructed (Bordel et al., 2019b, 2019a; Park et al., 2011; Tajparast and Frigon, 2018; Tyo et al., 2010). These models were mainly used to explain observed behavior (e.g., storage metabolism under feast-famine cycles) in the specific organism of interest, and accordingly only considered a subset of the possible metabolic states. Therefore, a holistic understanding of how the PHB pathway interacts with the rest of the metabolic network is crucial for obtaining a set of generalized design strategies to increase PHB productivity.

The metabolically diverse *Rhodopseudomonas palustris* CGA009 (hereafter *R. palustris*) is an ideal candidate for deciphering key engineering design strategies for PHB production using a GSMM. *R. palustris* can utilize a wide variety of carbon sources in both aerobic and anerobic conditions, including over two dozen aromatic compounds derived from lignin (Austin et al., 2015; Harwood and Gibson, 1988), an underutilized abundant raw material that would be toxic to many microbes used in industrial bioprocessing (Lee et al., 2019). Of note, *R. palustris* is renowned for its metabolism of the lignin breakdown product (LBP) *p*-coumarate, as well as its ability to perform anoxic photosynthesis and fix CO_2 (Larimer et al., 2004). During anaerobic growth, *R. palustris* utilizes the Calvin Benson Bassham (CBB) cycle as an electron sink (McKinlay and Harwood, 2010). This allows a direct comparison between the redox state of the cell and the rate of CO_2 fixation (McKinlay and Harwood, 2010; James B McKinlay and Harwood, 2011). This feature of the bacterium's metabolism is especially pronounced under conditions where other electron consuming routes (e.g., N_2 fixation and biomass production) are halted, as is the case during nitrogen starvation (James B. McKinlay et al., 2014). The ability of *R. palustris*

to utilize substrates of varying properties (Larimer et al., 2004; James B. McKinlay and Harwood, 2011), the limited metabolic routes it can operate to maintain redox balance (James B. McKinlay et al., 2014), and its constant expression of *pha* genes across different conditions (James B. McKinlay et al., 2014; Ranaivoarisoa et al., 2019) make it an ideal candidate for probing the metabolic elements that control PHB production.

This study delivers an integrated experimental and computational modeling approach to decipher metabolic factors controlling PHB production and offers engineering design strategies to boost production. In the metabolically robust *R. palustris*, PHB production significantly increased when grown on the carbon- and electron-rich lignin breakdown product (LBP) *p*-coumarate ($C_9H_8O_3$) compared to virtually no PHB titer from acetate ($C_2H_4O_2$). The maximum PHB titer did not improve when grown on the LBP coniferyl alcohol ($C_{10}H_{12}O_3$), but comparison of the PHB profiles showed that coniferyl alcohol's higher carbon content resulted in a higher rate of PHB production. Combined experimental results revealed that cytoplasmic space may be a limiting factor for maximum PHB titer. This study also reveals that *R. palustris* can create a copolymer called poly-3-hydroxybutyrate-co-hydroxyvalerate (PHBV) (Fig. 4.2), which boosts the thermomechanical properties compared to PHB alone. It was unclear why the LBPs yielded more PHB production compared to virtually no titer from acetate. Furthermore, measurements prior to nitrogen starvation revealed the presence of PHB, which indicated that PHB production was not strictly a stress response. H_2 production measurements were also conducted to qualitatively assess electron secretion. These observations along with previously described data on PHB production (Brown et al., 2020) lead to the hypothesis that the rate of PHB production was mainly controlled by metabolic factors, especially

since expression of *pha* genes has been reported to remain constant under different conditions (James B. McKinlay et al., 2014; Ranaivoarisoa et al., 2019). To examine this hypothesis, a thermo-kinetic analysis of the PHB pathway was conducted to determine the specific metabolic factors controlling pathway activity. This analysis revealed a significant thermodynamic bottleneck associated with the thiolase reaction (*phaA)* and a high dependence of the reductase reaction (*phaB)* on the NADP(H) redox state. Based on this analysis, butyrate ($C_4H_8O_2$) was identified as a potential substrate for PHB production due to its ability to bypass the *phaA* reaction and its high electron content.

To combine the study's findings within the context of whole-cell metabolism, a recently constructed GSMM of *R. palustris, iRpa940* (Alsiyabi et al., 2019), was used to compare growth simulations on substrates with annotated breakdown pathways. Figure 4.3 shows the general workflow followed in this study. *iRpa940* was chosen due to its ability to simulate growth under different conditions, including an array of organic acids (i.e., acetate, butyrate, fumarate, and succinate) and LBPs and very high correlation of model-predicted fluxes with experimental flux measurements. The model was also used to capture the observed complex trade-offs between different metabolic modules required for *R. palustris* to maintain optimum redox balance. Hence, the GSMM was applied to uncover possible causes for these experimental findings and to offer engineering design strategies that optimize PHB production. Four major findings from the GSMM include (i) a very high AcCoA/CoA ratio is required to drive the thiolase reaction (*phaA*), (ii) substrates with high carbon uptake rates accumulate higher amounts of acyl-CoA, (iii) the rate through reductase (*phaB)* is linearly dependent on the NADPH/NADP ratio, and (iv) *phaB* will likely be rate-limiting even under optimal metabolic conditions due to the very low

catalytic efficiency. These findings suggest novel engineering design strategies to optimize PHB production including choosing substrates that bypass the thiolase reaction (e.g. *p*-coumarate), utilizing high molecular weight substrates for high carbon uptake rates, and using highly reduced substrates. Furthermore, this study shows that renewable and abundant LBPs are ideal candidates for PHB production. Ultimately, this study showcases how an integrated approach utilizing GSMMs can help identify key factors associated with a bioconversion that would have otherwise not been recognizable. The engineering design strategies derived from this integrated approach could be applied to other bacteria with similar metabolic features, advancing the replacement of petroleum-derived plastics with sustainable biopolymers.

4.2. Materials and Methods

4.2.1 Growth curves and PHBV production

R. palustris seed culture preparation, growth curves, and PHB production were performed as described (Brown et al., 2020). Briefly, seed cultures were diluted to an optical density (OD) (660 nm) of 0.2 and grown anaerobically at 30°C with 100 µE white light in the same media as the seed cultures but with different carbon sources. Instead of the 20mM sodium acetate used for seed cultures, either 10mM sodium acetate, 5mM sodium butyrate, 1mM *p*-coumarate, or 1mM coniferyl alcohol were supplied. All substrates were supplemented with 10mM sodium bicarbonate unless specified otherwise, and this carbon content was factored into the analyses. Growth data were fitted to a modified logarithmic growth model as described previously (Brown et al, 2020).

Once growth parameters were determined from the growth models (Fig. 4.4A), cultures were grown to mid-exponential phase in the respective conditions (except when specified otherwise) and subsequently nitrogen starved as described previously (Brown et al., 2020). Briefly, for nitrogen starvation the anaerobic vials were centrifuged to generate a pellet, the supernatant was discarded, and the pellet was resuspended in media with the desired carbon sources without ammonium sulfate as a nitrogen source. For phosphorus starvation regarding the starvation analysis (Fig. 4.4B), the same methods were applied but instead of removing nitrogen from the media phosphorous was omitted.

4.2.2 PHBV quantification via gas-chromatography mass spectrometry (GC-MS)

PHBV extraction and quantification was conducted as described previously (Brown et al., 2020). A triplicate of anaerobic culture vials was harvested from each condition for analysis at the desired growth phase (i.e., mid-exponential or stationary phase) and after each day of nitrogen starvation. Each vial was subjected to acidic methanolysis, and PHBV was quantified with conventional GC-MS as described (Brown et al., 2020). External standards were created from serial dilutions of sodium 3-hydroxybutyrate or (−)-Methyl (R)-3-hydroxyvalerate (Sigma-Aldrich™).

4.2.3 Hydrogen quantification via gas chromatography-thermal conductivity detector (GC-TCD)

Samples were nitrogen-starved as described above. Precisely 3 mL of the nitrogen-starved culture was placed into a 10 mL air-tight glass vial with 18 mm headspace (Thermo Scientific®). The glass vials were immediately closed with air-tight magnetic screw caps that contained self-sealing septa (Thermo Scientific®). The vials were flushed with argon for 30 mins by piercing the septum with a needle attached to the argon tank and another

needle for outlet gas. Once the samples were purged with argon, they were placed into the lighted growth chamber until testing, using the same light intensity, temperature, and shaking as described above. Hydrogen quantification was conducted by drawing 500 µL of gas from the headspace into an airtight, fixed needle syringe (Thermo Scientific®) and manually injected into the thermal conductivity detector (TCD) (Thermo Scientific Trace 1300) of the gas chromatograph. The characterization methods were the same as described, including the carrier gas, column, and GC parameters (Tiryaki and Irmak, 2020). A gas mixture of known composition was used as a standard, and had the same composition as described (Tiryaki and Irmak, 2020).

4.2.4 Transmission Electron Microscopy (TEM)

To visualize the PHB/V granule(s) inside the cell, samples from 10mM acetate, 1mM *p*-coumarate, and 1mM coniferyl alcohol after five days of nitrogen starvation were subjected to TEM. The bacteria were fixed in 2% glutaraldehyde and 1.5% paraformaldehyde in 100mM sodium cacodylate buffer for > 1 hour at room temperature and then 4°C overnight per established procedures (Graham and Orenstein, 2007). The samples were washed in sodium cacodylate buffer three times (10 min each) and post-fixed in 1% osmium tetroxide in deionized water at room temperature for one hour. After washing in water twice, the samples were dehydrated through an ethanol series and embedded in Spurr medium using a conventional TEM processing protocol. Ultrathin sections were cut using a Leica UC7 ultramicrotome and stained with 1% uranyl acid and 1% lead citrate. Images were collected using a Hitachi H7500 TEM at the Microscopy Core Research Facility of the Center for Biotechnology, University of Nebraska-Lincoln.

4.2.5 Pulse Amplitude Modulation (PAM) Fluorometry

PAM fluorometry was conducted using the LI-6800 Portable Photosynthesis System, Software Version 1.4. LI-COR, Inc. to determine the photosynthetic yield (Φ_{PSII}) following previously established procedures (Phongjarus et al., 2018; Ritchie, 2013, 2008; Ritchie and Larkum, 2012; Ritchie and Mekjinda, 2015). Briefly, anaerobically growing cells were centrifuged during the mid-exponential phase and re-suspended in 400 µL of PM media (with no carbon source) (Kim and Harwood, 1991). Precisely 250 µL of cell suspension was then uniformly pipetted onto a Whatman® glass fiber disk and air-dried for 20 minutes at room temperature. Next, the fiber disks were dark-adapted in an opaque container for 10-30 minutes and subsequently placed in the chamber of the LI-6800's multiphase flash fluorometer. Both the measuring and actinic light sources were set to ~465 nm (blue light) (Ritchie, 2013). After setting the irradiance, the cells require approximately 15 minutes to reach a new steady-state (characterized by constant fluorescence), at which time a saturating light pulse is introduced to measure Φ_{PSII} (Maxwell and Johnson, 2000). Since the electron transport rate (ETR) is proportional to Φ_{PSII} (Maxwell and Johnson, 2000; Phongjarus et al., 2018) the relative photosynthetic rates during growth on any two conditions can be inferred from the relative photosynthetic yields (see Eqn. 3).

4.2.6 Thermo-kinetic Analysis

The rate law of a bi-molecular reaction can be re-written into the separable form below, as derived (Noor et al., 2013a):

$$v = Ek_{cat}^{+}\left(\frac{s/K_s}{1 + s/K_s + p/K_p}\right)\left(1 - e^{\Delta_r G'/RT}\right) \quad (1)$$

Where the first factor refers to the enzyme's catalytic capacity (V^{max}) and is a product of the enzyme concentration (E) and the maximal catalytic efficiency of the reaction in the forward direction (k_{cat}^{+}). The second term refers to the fractional substrate saturation (κ) and is a function of the substrate (s) and product (p) concentrations and their associated Michaelis constants K_s and K_p. The third factor denotes the thermodynamic driving force (γ) and is mainly a function of the Gibbs free energy of a reaction ($\Delta_r G'$), which can be calculated from the standard Gibbs free energy ($\Delta_r G'^o$) and the metabolite concentrations (or product to substrate ratios) (Noor et al., 2013a):

$$\Delta_r G' = \Delta_r G'^o + RTln\left(\frac{p}{s}\right) \quad (2)$$

The $\Delta_r G'^o$ values of the thiolase (*phaA*) and reductase (*phaB*) reactions were calculated using the component contribution method (Noor et al., 2013b). For thiolase, the acetoacetyl-concentration was set to the minimum physiological concentration of 1 µM (Noor et al., 2013b) and the acetyl-CoA:CoA ratio was sampled to determine its effect on γ. For reductase, simulations were conducted using 3-hydroxybutyryl-CoA concentrations of 30 µM and 300 µM to capture the range of reported concentrations (Leaf and Srienc, 1998). The NADPH:NADP ratio was sampled to determine its effect on γ.

Michaelis constants (K_s and K_p) used during simulation were reported for the soil bacterium *Cupriavidus necator* (Leaf and Srienc, 1998) as no values have been reported for *R. palustris*. Due to the high homology of both *phaA* and *phaB* (E value < 10^{-80}) between the two organisms, the substrate saturation effects were assumed to be similar. Tables 4.1 and 4.2 contain the parameters used in this analysis and the references they were obtained from.

4.2.7 GSMM Simulations

Growth simulations under different environmental conditions were performed through parsimonious Flux Balance Analysis as in (Lewis et al., 2010). The rate through the photosynthetic electron transport reaction PSII (light-induced reduction of quinol) was fixed based on previous analysis for growth on acetate and butyrate (Alsiyabi et al., 2019). The rate of this reaction during growth simulations on *p*-coumarate was calculated based on the relative photosynthetic yield (Φ_{PSII}) between *p*-coumarate and acetate:

$$v_{PSII}^{pC} = v_{PSII}^{ace} \frac{\Phi_{PSII}^{\mathrm{pC}}}{\Phi_{PSII}^{\mathrm{ace}}} \quad (3)$$

Where "pC" and "ace" refer to *p*-coumarate and acetate, respectively.

Finally, the generation rate of a metabolite *k* (e.g., acetyl-CoA) was calculated using Eq. 4 below:

$$genRate_k = \sum_{j \in J} v_j \;\; \forall\, j \in J \;\; s.t.\; S_{kj} > 0 \quad (4)$$

4.2.8 Statistical Methods

Independent, two-tailed *t* tests were conducted to identify statistically significant differences in maximum ODs between the substrates. Similarly, *t* tests were conducted to compare maximum PHB titers between *p*-coumarate, coniferyl alcohol, and butyrate at 5 days of nitrogen starvation (acetate was not included since it yielded no PHB titer). Paired, one-tailed t-tests were conducted to determine the time of maximum PHB production from *p*-coumarate, coniferyl alcohol, and butyrate. For example, a paired *t* test was conducted between days 4, 5, and 6 of nitrogen starvation on *p*-coumarate to decipher the time of

maximum PHB production. All *t* tests were conducted with a 95% confidence level (α = 0.05).

4.3. Results and Discussion

4.3.1 Disparities in PHB/V titers from cells grown on various carbon sources

In our previous study, *R. palustris* was shown to grow on *p*-coumarate and produce PHB to a much higher titer than on acetate (Brown et al., 2020). It was unclear as to why more PHB production was observed from the LBP *p*-coumarate compared to virtually no PHB production from acetate. In this study, PHB production was produced from *R. palustris* on the LBP coniferyl alcohol ($C_{10}H_{12}O_3$) for the first time, which has higher carbon content than *p*-coumarate. *R. palustris* was indeed able to grow on the LBP coniferyl alcohol (Fig. 4.4A) and reached a significantly higher maximum OD (3.22) compared to *p*-coumarate (2.17) or acetate (0.87). A higher maximum OD suggests more CO_2 is being utilized during the degradation of the LBPs compared to the other carbon sources (James B McKinlay and Harwood, 2011; McKinlay and Harwood, 2010). Furthermore, the increased growth rates of the LBPs signify faster carbon uptake rates. Before proceeding with PHB analysis between the carbon sources, a starvation analysis was conducted to quantify if nitrogen or phosphorous limitation yields more PHB since this has been shown previously to boost production (Wen et al., 2010). Starvation analysis was conducted on *p*-coumarate and employed either nitrogen, phosphorus, or both nitrogen and phosphorous starvation conditions. Nitrogen starvation yielded a significantly higher PHB titer, and thus it was used to compare PHB production across the substrates (Fig. 4.4B). A subsequent analysis was conducted to quantify PHB production on *p*-coumarate without nitrogen starving the cells (Fig. 4.4E). PHB production peaked at approximately

10 days past stationary phase with a similar maximum titer as that of the nitrogen-starved cells (0.41 g/L).

Despite the higher growth rate on coniferyl alcohol, the maximum PHB titer (0.41 g/L) did not improve. The carbon conversion efficiency for the maximum PHB titer on each substrate is summarized in Table 4.3. Comparison of the PHB profiles showed that coniferyl alcohol's higher carbon content resulted in a higher rate of PHB production without changing the final titer.

Combined experimental results from growth rates (Fig. 4.4A), PHB production (Fig. 4.4C), H_2 production (Fig. 4.4F), and transmission electron microscopy (Fig. 4.5) revealed that cytoplasmic space may be a limiting factor for maximum PHB titer. Transmission electron microscopy was conducted to image granules inside of the cells on the LBPs vs. acetate, and revealed stark discrepancies between the LBPs and acetate as expected based on the measured titers (Fig. 4.5). Virtually no granules were present inside cells grown on acetate, whereas there was an abundance of cells that contained one large granule when grown on the LBPs. Of note, one large granule is produced in the cells utilizing the LBPs, which indicated cytoplasmic space might be a major limiting factor for the maximum PHB titer as shown in *Halomonas bluephagenesis* (Shen et al., 2019).

This study also reveals that *R. palustris* can create a copolymer called poly-3-hydroxybutyrate-co-hydroxyvalerate (PHBV) (Fig. 4.2), which boosts the thermomechanical properties compared to PHB alone. The LBPs and butyrate all fostered a 3-hydroxyvalerate (3HV) component that creates the copolymer PHBV (Fig 4.4D), with *p*-coumarate yielded the highest 3HV titer of approximately 0.04 g/L.

4.3.2 Tradeoffs between PHB and H_2 production

H_2 production measurements were also conducted to qualitatively assess electron secretion (Fig. 4.4F). H_2 production significantly increases at approximately five days of nitrogen starvation, which is when PHB production peaks. These observations along with previously described data on PHB production (Brown et al., 2020) lead to the hypothesis that the rate of PHB production was mainly controlled by metabolic factors, especially since expression of *pha* genes has been reported to remain constant under different conditions (James B. McKinlay et al., 2014; Ranaivoarisoa et al., 2019).

4.3.3 The need for metabolic modelling

It was still unclear why the LBPs yielded more PHB production compared to virtually no titer from acetate. Furthermore, measurements prior to nitrogen starvation revealed the presence of PHB, which indicated that PHB production was not strictly a stress response (Fig. 4.4C, E). The GSMM was next employed to investigate the potential mechanisms behind these findings and identify specific design strategies that can be implemented to optimize PHB production. Due to the lack of kinetic parameters and concentration ranges for PHBV-producing reactions and their corresponding metabolites, the model was strictly used to investigate PHB production. However, since both monomer products (3-hydroxybutyrate and 3-hydroxyvalerate) are produced by the same enzymes, it is likely that the identified design strategies are applicable to both products. Furthermore, coniferyl alcohol is not included in the GSMM analysis because its degradation pathway is not yet known, which we aim to illuminate through an ongoing transcriptomics analysis.

4.3.4 Computational analysis of PHB production

Computational methods were employed to investigate the observed experimental findings. The main question that the GSMM intended to address was what underlying factors cause the observed disparity in PHB production between the tested carbon sources. More importantly, can a set of generalized design strategies for PHB overproduction be deduced by incorporating the observed experimental findings into a whole-cell metabolic modeling framework? To guide the analysis of the GSMM, a detailed thermokinetic study of the pathway was conducted to determine how the overall production rate of PHB is affected by the cell's metabolic state. The goal of this analysis was to identify the different metabolic factors (e.g., NADPH redox state) governing the activity of the PHB pathway. Growth simulations facilitated by the GSMM can then be used to determine how consumption of each substrate affects the identified factors and therefore the rate of PHB synthesis.

4.3.4.1 Thermokinetic analysis of the PHB pathway

The rate of an unregulated enzymatic reaction that follows Michaelis-Menten kinetics can be broken down into a product of three main constituents: (i) the enzyme's catalytic capacity (V^{max}), (ii) the reaction's thermodynamic driving force (γ), and (iii) enzyme substrate saturation (κ) (Noor et al., 2013a).

This can be expressed mathematically as shown in Eq. 5:

$$v = V^{max} * \gamma * \kappa \tag{5}$$

where, the maximal rate of the reaction is determined by its catalytic efficiency and enzyme concentration ($V^{max} = [E]k_{cat}$). The thermodynamic driving force can take on values of

0 to 1 when the reaction is in the forward direction and -1 to 0 when the reaction is going in the reverse direction. Moreover, the enzyme saturation factor has a range of 0 to 1. Since the rate law, written in this form, is separable, the effect of each factor on the overall rate can be analyzed individually (Noor et al., 2013a). Starting with the first reaction in the pathway (*phaA*), it was found that this reaction is significantly constrained thermodynamically (Fig. 4.6A). As described previously, the rate of the reaction was highly dependent on the acetyl-CoA/CoA ratio (Kocharin et al., 2012; Van Wegen et al., 2001). Surprisingly, the reaction was found to be infeasible under a ratio 12, which is relatively high compared to ratios observed in most bacteria (<5) (Bennett et al., 2009; Chohnan et al., 1998; Gameiro et al., 2016; Park et al., 2016; Thauer et al., 1977). This means that a significant accumulation of acetyl-CoA is required for thiolase (*phaA*) to become thermodynamically viable and start forming acetoacetyl-CoA. This limitation is likely a major contributor to why no PHB was observed during growth on acetate, even after nitrogen starvation. On the other hand, the breakdown pathways of the other carbon substrates produced acetoacetyl-CoA as an intermediary metabolite (Fig. 4.7), therefore bypassing this thermodynamic obstacle. Moreover, changes to this ratio displayed a minimal effect on κ (Fig. 4.6A), meaning that during any given condition, the rate of the reaction, relative to Vmax, can be estimated solely based on γ (Fig. 4.6B). Due to the high thermodynamic burden of the *phaA* reaction, substrates that breakdown into acetoacetyl-CoA as an intermediary metabolite could help maximize PHB production.

Interestingly, an opposite conclusion was reached during analysis of the reaction through acetoacetyl-CoA reductase (*phaB*). Although both factors (γ and κ) contributed to the overall rate, substrate saturation was significantly more limiting (Fig. 4.6C). An

increase in the NADPH/NADP ratio reduces the bottleneck through this reaction by increasing both the thermodynamic driving force and substrate saturation. Furthermore, the concentration of the main reaction product (3-hydroxybutyryl-CoA) has a pronounced effect on substrate saturation. The solid and dotted lines in Fig. 4.6C correspond to the minimum and maximum 3-hydroxybutyryl-CoA concentrations reported in literature (Leaf and Srienc, 1998; Van Wegen et al., 2001). The combined effect of both factors on the overall flux through the reaction is shown in Fig. 4.6D. Although the reaction is viable under different biologically relevant NADPH:NADP ratios, flux through *phaB* is significantly hindered during high NADP(H) oxidation states (i.e., low NADPH:NADP ratios) due to the enzyme being sub-saturated ($\kappa << 1$). Finally, reports from previous kinetic studies had identified that *phaB*'s kinetic capacity (V^{max}) was notably lower than that of *phaA* and *phaC* (Sim et al., 1997; Wang and Lee, 1997), meaning that for steady-state PHB accumulation to occur, a relatively higher expression rate of this enzyme is required for the fluxes to be balanced. The implications of this difference in catalytic efficiency are discussed in the Supplementary Methods. Therefore, even under optimal metabolic conditions (high NADPH:NADP ratio), the catalytic inefficiency of the reductase enzyme (*phaB)* may limit the overall rate of the PHB pathway.

4.3.4.2 Genome-scale prediction of metabolic activity through fluorometry and *iRpa940*

To investigate the cause of the disparities between PHB production during growth on *p*-coumarate compared to that on butyrate, *iRpa940* model was employed to explore differences in the generation of both carbon and electron sources. It had been previously observed that the activity of *R. palustris'* metabolic network during anaerobic growth

conditions can be predicted accurately if the rate of photosynthesis, or the electron transport rate (ETR), was known *a priori* (Alsiyabi et al., 2019). When ^{13}C metabolic flux analysis (MFA) measurements are available, the ETR can be determined by fitting pFBA-generated flux predictions to those measured through MFA (Alsiyabi et al., 2019). The ETR values during growth on acetate and butyrate were available *a priori* (Alsiyabi et al., 2019). However, due to the absence of MFA measurements during growth on *p*-coumarate, pulse amplitude modulation (PAM) fluorometry was conducted to determine the relative ETR through cells growing on *p*-coumarate compared to those growing on acetate. First, ETR values predicted through MFA measurements (Alsiyabi et al., 2019) during growth on acetate and butyrate were validated. Based on the MFA measurements, the model had predicted that the ETR, and therefore the photosynthetic yield, was similar during growth on these two substrates (Alsiyabi et al., 2019). Fluorometry measurements show that the photosynthetic yields are indeed similar (Fig. 4.8). These results gave confidence in the validity of subsequent model predictions. Next, PAM fluorometry was used to measure the photosynthetic yield during growth on *p*-coumarate. Interestingly, the ETR was found to be significantly higher during growth on *p*-coumarate compared to growth on acetate and butyrate (Fig. 4.8). These measurements provided the parameters required for the GSMM to simulate anaerobic growth on each of the carbon sources. Figs. 4.9 - 4.11 show the metabolic activity through the central metabolism during growth on the three substrates. Next, these predictions were used to compare how the generation rates of different metabolites participating in PHB synthesis varied between carbon sources.

4.3.4.3 PHB synthesis within the context of metabolism

First, the overall generation rate of NAD(P)H was determined during growth on each carbon source based on the model-generated growth predictions. The rationale behind this analysis was that a higher generation rate of reducing power results in a more reduced state and a higher driving force through the reductase (*phaB*). It has also been reported that *R. palustris'* metabolism is constrained by its inability to oxidize cofactors through the electron transport chain due to the lack of a terminal electron acceptor (James B McKinlay and Harwood, 2011; McKinlay and Harwood, 2010), which forces it to utilize other routes such as carbon fixation, nitrogen fixation or PHB synthesis to accomplish this (McKinlay, 2014; James B McKinlay and Harwood, 2011). The rate at which cofactors are oxidized needs to be equivalent to the rate of reduction to avoid the accumulation of electrons. As can be seen from Fig. 4.12, growth on butyrate and *p*-coumarate generate approximately 40% and 95% more reducing equivalents compared to acetate, respectively. Since reduced cofactors (NAD(P)H) are generated during substrate breakdown, the differences in generation rates (Fig. 4.12) correspond to differences in substrate oxidation states, uptake rates, and breakdown pathways (Fig. 4.7). Furthermore, since both of these substrates (butyrate and *p*-coumarate), generate acetoacetyl-CoA during their breakdown, the redox state of their respective NADP(H) pool can be considered the rate-limiting factor for PHB production. It is noted that since both nitrogen fixation and biomass production are major electron sinks, this effect becomes more pronounced during nitrogen-starvation when both of these processes are halted. Results from this analysis indicate that the higher rate of NAD(P)H generation likely leads to a significantly more reduced intracellular state. In the closely related strain *R. palustris* TIE1, the measured NADPH:NADP ratio during

anaerobic growth on butyrate was approximately 2 (Guzman et al., 2019). Therefore, as indicated by the thermo-kinetic analysis, a higher ratio during growth on *p*-coumarate will lead to a higher rate through the reductase reaction (*phaB)* in the PHB pathway.

During anaerobic growth conditions in which a reduced nitrogen source (e.g. ammonia) is present and hence nitrogen fixation is downregulated?, *R. palustris* utilizes CO_2 fixation through the Calvin Cycle as its primary electron sink (James B McKinlay and Harwood, 2011; McKinlay and Harwood, 2010). Therefore, the rate of carbon fixation was expected to show a similar trend to that of NAD(P)H generation (McKinlay and Harwood, 2010). Indeed, as shown on Fig. 4.13, the relative rate of carbon fixation is proportional to the rate of reducing cofactors. Relative rates were calculated by normalizing the predicted CO_2 fixation rates by the rate predicted during growth on acetate. The predicted rates during growth on each carbon source are shown on the metabolic maps in Figs. 4.9 - 4.11. Due to the high NAD(P)H generation rate during growth on *p*-coumarate, the model predicts a 3-fold increase in carbon fixation compared to growth on acetate (Fig. 4.4). However, due to known inefficiency of the carbon fixing enzyme Ribulose-1,5-bisphosphate carboxylase-oxygenase (RuBisCO) (Cummins et al., 2018), it is plausible to postulate that kinetics of the RuBisCO enzyme do not permit such a high rate. Therefore, the cell would be required to store the remaining excess electrons in PHB, which is the only alternative electron sink under such conditions. It is also noted that model predictions indicate that both NAD(P)H generation and carbon fixation rates increase with increasing ETR during growth on any of the three substrates.

Finally, the model was used to investigate how utilization of each of the carbon substrates affected the rate of acetyl-CoA and acetoacetyl-CoA generation (Fig. 4.14). As

previously described, although acetyl-CoA is considered to be the first metabolite in the PHB synthesis pathway, its conversion to acetoacetyl-CoA is thermodynamically very unfavorable. It was therefore hypothesized that exploring the rate of acetoacetyl-CoA generation may give a better indication of PHB production. Growth simulations on acetate showed that all of the consumed substrate was converted into acetyl-CoA before entering the central metabolic pathways through the TCA cycle. Since acetate assimilation into central metabolism does not produce acetoacetyl-CoA, model predictions indicate that only a small fraction of the starting carbon gets converted to this metabolite, while the majority is used to synthesize other biomass precursors and constituents. Conversely, consumption of butyrate mandates that all of the starting substrate goes through acetoacetyl-CoA before entering central metabolism. In fact, butyrate's breakdown pathway also goes through 3-hydroxybutyrate CoA (Fig. 4.7), which is the monomer form of PHB. Furthermore, due to the constitutive nature of the genes involved in PHB synthesis, generation of acetoacetyl-CoA during assimilation of the carbon source into central metabolism is expected to result in PHB production even under conditions when carbon or electron storage is not required (James B. McKinlay et al., 2014; Ranaivoarisoa et al., 2019). As shown in Fig. 4.4C, PHB production is observed in cells growing even prior to nitrogen starvation (day 0). Finally, growth on *p*-coumarate results in relatively high generation rates of both acetyl- and acetoacetyl-CoA. Model analysis reveals that based on the measured growth rates, and the rate of carbon uptake is 4.5-fold higher during growth on *p*-coumarate compared to acetate. Therefore, this analysis reveals that the basis behind the highly observed PHB production rate on *p*-coumarate is likely due to both an excess of carbon and electrons. It is likely that due to the large size of *p*-coumarate (and LBPs in general), the rate at which central

metabolites are generated is too high to enter central metabolism, which is why PHB production can be observed even during exponential growth. Similar behavior has been observed in *E. coli* under high carbon uptake rates and has been referred to as Janusian growth (O'Brien et al., 2013).

4.3.5 General design strategies for PHB production

These findings can be generalized into a set of design strategies for optimal PHB production. Due to the constitutive expression of the metabolic *pha* genes in *R. palustris*, changes in the intracellular metabolic state in the form of increased carbon and electron accumulation have a direct effect on the pathway's activity. Therefore, carbon sources used for PHB production should ideally have a high molecular weight and be more reduced than the organism's biomass. This will lead to the generation of an excess in both reducing agents (NAD(P)H) and carbon that can subsequently be shuttled towards PHB production. Moreover, the substrates should preferably produce acetoacetyl-CoA as part of their breakdown. This is necessary to bypass the extremely unfavorable first reaction of the PHB pathway. Based on these characteristics, LBPs such as *p*-coumarate and coniferyl alcohol appear to be ideal candidates for PHB production. Finally, under optimal metabolic conditions, it is expected that the catalytic efficiency of *phaB* may play a limiting role in the overall rate (Sim et al., 1997). Therefore, overexpression of *phaB* may be necessary to increase PHB production rates under such conditions. Most importantly, the generality of these design rules allows them to be applied to any PHB-producing microbe with similar metabolic features.

4.3.6 Selection of sodium butyrate as an ideal substrate for PHB production

To better understand how the choice of substrate impacts PHB production, butyrate ($C_4H_8O_2$) was tested since an annotated pathway was available, it bypasses the PhaA pathway, and is more reduced than acetate. Butyrate was assessed via metabolic modelling (*Section 4.3.4*), and PHB production was subsequently experimentally validated. After assessment with the GSMM to substantiate the hypotheses, we experimentally validated the growth and PHB production analyses on butyrate (Fig. 4.4A). Butyrate was compared to acetate on a carbon-to-carbon basis to test the impact on PHB titer from a more reduced substrate that bypasses the energy intensive keto-thiolase reaction (*phaA*). Significantly more PHB was produced from butyrate compared to virtually none from acetate, despite having the same carbon content (Fig. 4.4C). The percent carbon conversion from butyrate (10.83%) was lower than the LBPs (Table 4.3), which can be attributed to the higher molecular weights of the LBPs that likely leads to higher rates of NAD(P)H and acyl-CoA generation.

The approach taken to arrive at these findings highlights how experimental observations can be used to generate a broad hypothesis that can subsequently be narrowed down through the application of metabolic modeling frameworks. Furthermore, it illustrates the synergistic effect of combining a detailed modeling analysis of the pathway of interest with a coarse-grained genome scale analysis to test the generated hypothesis and to suggest subsequent validation experiments. As illustrated in this work, the advantage of utilizing detailed thermos-kinetic analysis is the ability of identifying specific metabolic factors that exert control over the production pathway of interest. Once those factors are identified, genome-scale metabolic modeling can be employed to predict how different

growth conditions influence the state of the identified factors. We believe such an approach can be generalized to other engineering applications where the production pathway of interest is highly connected to the rest of the metabolic network.

4.4. Conclusions

Novel design strategies for improved PHB production have been identified through an integrated experimental and computational approach. *R. palustris* was an ideal candidate for probing the metabolic elements that control PHB production due to its ability to utilize substrates of varying properties (Larimer et al., 2004; James B McKinlay and Harwood, 2011), the limited metabolic routes it can operate to maintain redox balance (James B. McKinlay et al., 2014), and its constant expression of *pha* genes across different conditions (James B. McKinlay et al., 2014; Ranaivoarisoa et al., 2019). Unique experimental findings from the metabolically versatile *R. palustris* motivated the application of metabolic modeling. These findings included 1) significantly higher PHB production rates from LBPs, 2) PHB production without stress induction, 3) growth and PHB production on coniferyl alcohol, 4) increased hydrogen production as PHB production peaks, 5) production of the copolymer PHBV, and 6) cytosolic space as a major limiting factor for PHB production. These findings led to the hypothesis that PHB production was driven by the metabolic state of the cell. Therefore, a metabolic modeling approach was taken to gain a deeper understanding of the underlying factors causing the discrepancies in observed PHB production. Three main design strategies were identified for optimizing PHB production in hosts with similar metabolic features.

First, PHB production efforts should utilize carbon sources that can bypass the thiolase reaction. Modeling results indicated that under normal Acetyl-CoA:CoA ratios, the first reaction in the PHB synthesis pathway was infeasible. This result explains, at least partly, why no PHB production was observed during growth on acetate. On the other hand, growth on butyrate and *p*-coumarate does not require this reaction for PHB production, as both substrates produce acetoacetyl-CoA as part of their consumption pathway. Although the assimilation route of coniferyl alcohol is not known, it is likely that breakdown of this substrate produces acetoacetyl-CoA as part of its consumption pathway, similar to *p*-coumarate. Second, carbon substrates used for PHB production should be more reduced than the cell's biomass. Model analysis indicates that activity of the acetoacetyl-CoA reductase (*phaB*) is highly dependent on the redox state of NADPH, especially under physiologically relevant NADPH:NADP ratios. The importance of this result is magnified due to the inherently low catalytic efficiency of this enzyme. Therefore, use of a highly reduced substrate or interruption of processes that require significant amounts of electrons (e.g. nitrogen fixation) is predicted to lead to a higher NADPH:NADP ratio and therefore enhance the rate through this reaction. Third, the utilized substrates should have high molecular weights, or a relatively large number of carbons. Growth measurements and model predictions indicate that the relatively large size of *p*-coumarate and coniferyl alcohol leads to a higher carbon uptake rate. At the observed uptake rates, catalytically inefficient enzymes within central metabolism, such as RuBisCO, are likely to operate close to their maximum capacity, leading to an increased production of storage metabolites like PHB. The increased uptake rate is also what leads to the predicted generation rates of NAD(P)H and acyl-CoAs being significantly higher during growth on *p*-coumarate.

Utilizing *R. palustris'* ability to consume a wide array of substrates, a number of carbon sources were screened to identify a carbon substrate that satisfies the identified design requirements. Due to the lack of annotation of consumption pathways associated with many substrates, butyrate was identified as the ideal candidate for model validation. Consistent with model predictions, butyrate consumption led to PHB production both before and after nitrogen starvation. However, the lower molecular weight of butyrate compared to *p*-coumarate likely lead to lower rates of NAD(P)H and acyl-CoA generation, which resulted in lower PHB titers despite butyrate being more reduced. As evident from the characteristics of *p*-coumarate and coniferyl alcohol, and from the measured PHB profiles associated with them, it appears that LBPs are ideal substrates for PHB production and can lead to an economically viable process for PHB production. Overall, this study showcases how an integrated experimental-modeling approach can identify a set of novel engineering design strategies associated with sustainable biopolymer production, thus advancing the replacement of petroleum-derived plastics. Most importantly, the generality of these design rules allows them to be applied to any PHB-producing microbe with similar metabolic features.

Table 4.1. Parameter values used in thermokinetic modeling.

Reaction (enzyme)	Parameter[a,b]	Value
Ketothiolase (PhaA)	$K_{accoa,1}$ (M)	3.78 x 10^{-9}
	$K_{accoa,2}$ (M)	8.4 x 10^{-4}
	K_{coa} (M)	3.14 x 10^{-5}
	$K_{aceaccoa}$ (M)	6.46 x 10^{-5}
	$\Delta_r G'^0$ (kJ/mol)	26.1
Reductase (PhaB)	$K_{aceaccoa}$ (M)	5.0 x 10^{-6}
	K_{NADPH} (M)	1.9 x 10^{-5}
	K_{3hbcoa} (M)	1.65 x 10^{-5}
	K_{NADP} (M)	3.1 x 10^{-5}
	$\Delta_r G'^0$ (kJ/mol)	-19.0

[a]Michaelis constants (Ki's) used were reported for the soil bacterium *C. necator* (Leaf and Srienc, 1998).

[b]Reaction standard Gibbs free energy ($\Delta_r G'^0$) values were obtained from eQuilibrator (Flamholz et al., 2012)

Table 4.2. Reported concentration ranges and cofactor ratios for metabolites in the PHB pathway.

Metabolite(s)	Concentration (or ratio)
Acetyl-CoA	20 – 760 µM (*E. coli*) (Bennett et al., 2009; Takamura and Nomura, 1988)
	920 µM (*C. kluyveri*) (Thauer et al., 1977)
Acetoacetyl-CoA	22 µM (*E. coli*) (Bennett et al., 2009)
3-hydroxybutyryl-CoA	0.021-3.0 mM (*C. necator)*
CoA	1.4-4.5 mM (*E. coli*) (Bennett et al., 2009)
	0.24 mM (*C. kluyveri)* (Thauer et al., 1977)
NADPH	0.121 mM (*E. coli*) (Bennett et al., 2009)
	1.4 mM (*C. kluyveri)* (Thauer et al., 1977)
NADP	0.0021 mM (*E. coli*) (Bennett et al., 2009)
	0.98 mM (*C. kluyveri)* (Thauer et al., 1977)
Acetyl-CoA/CoA	0.2-5.0 (*E. coli*) (Bennett et al., 2009; Gameiro et al., 2016; Park et al., 2016)
	3.8 (*C. kluyveri)* (Thauer et al., 1977)
NADPH/NADP	57.6 (*E. coli)* (Bennett et al., 2009)
	1.4 (*C. kluyveri)* (Thauer et al., 1977)
	1.4-7.5 (*R. palustris)* (Guzman et al., 2019)

Table 4.3. Carbon conversion efficiency to PHB from each substrate.

Substrate	Formula	Concentration Used (mM)	Carbon Invested (moles)*	Carbon Conversion to PHB (%)**
Sodium acetate	$C_2H_3NaO_2$	10	0.02	N/A
Sodium butyrate	$C_4H_7NaO_2$	5	0.02	10.83
p-Coumarate	$C_9H_7O_3^-$	1	0.009	68.4
Coniferyl alcohol	$C_{10}H_{12}O_3$	1	0.01	65.0

*This does not include 10mM sodium bicarbonate ($NaHCO_3$)

**The percent conversion to PHB includes 10mM sodium bicarbonate to account for total carbon invested

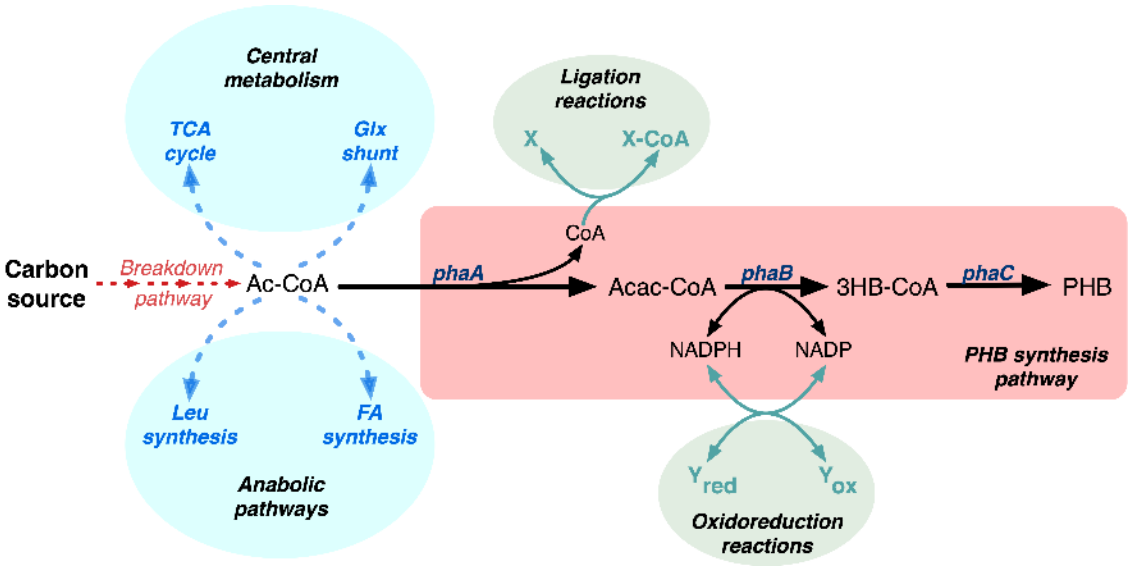

Fig. 4.1: PHB synthesis in the context of whole-cell metabolism. The pathway is connected to central metabolism through acetyl-CoA, the cofactor CoA, and the cofactor pair NADP/NADPH. The highly connected nature of these metabolites causes their concentration to be dependent on the activity of the overall processes.

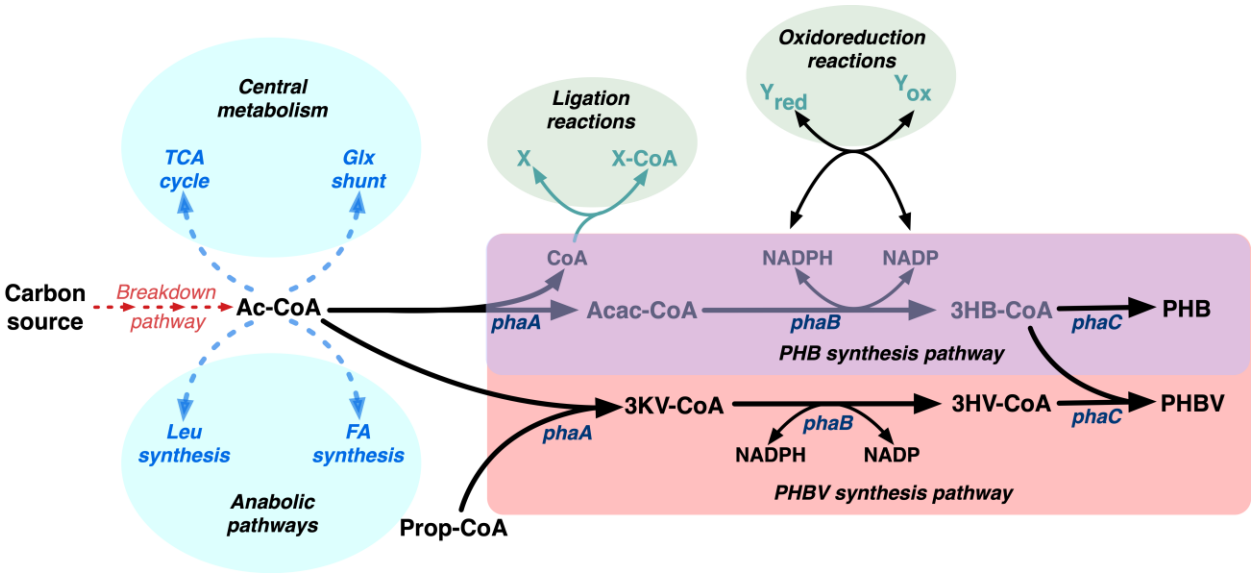

Fig. 4.2: PHB and PHBV synthesis in the context of whole-cell metabolism**.** Both PHB and PHV monomers are produced through the same *pha* enzymes. PHB synthesis starts with the condensation of two acetyl-CoA molecules while PHV requires condensation of acetyl-CoA and propionyl-CoA. The final polymer (PHBV) contains both monomers.

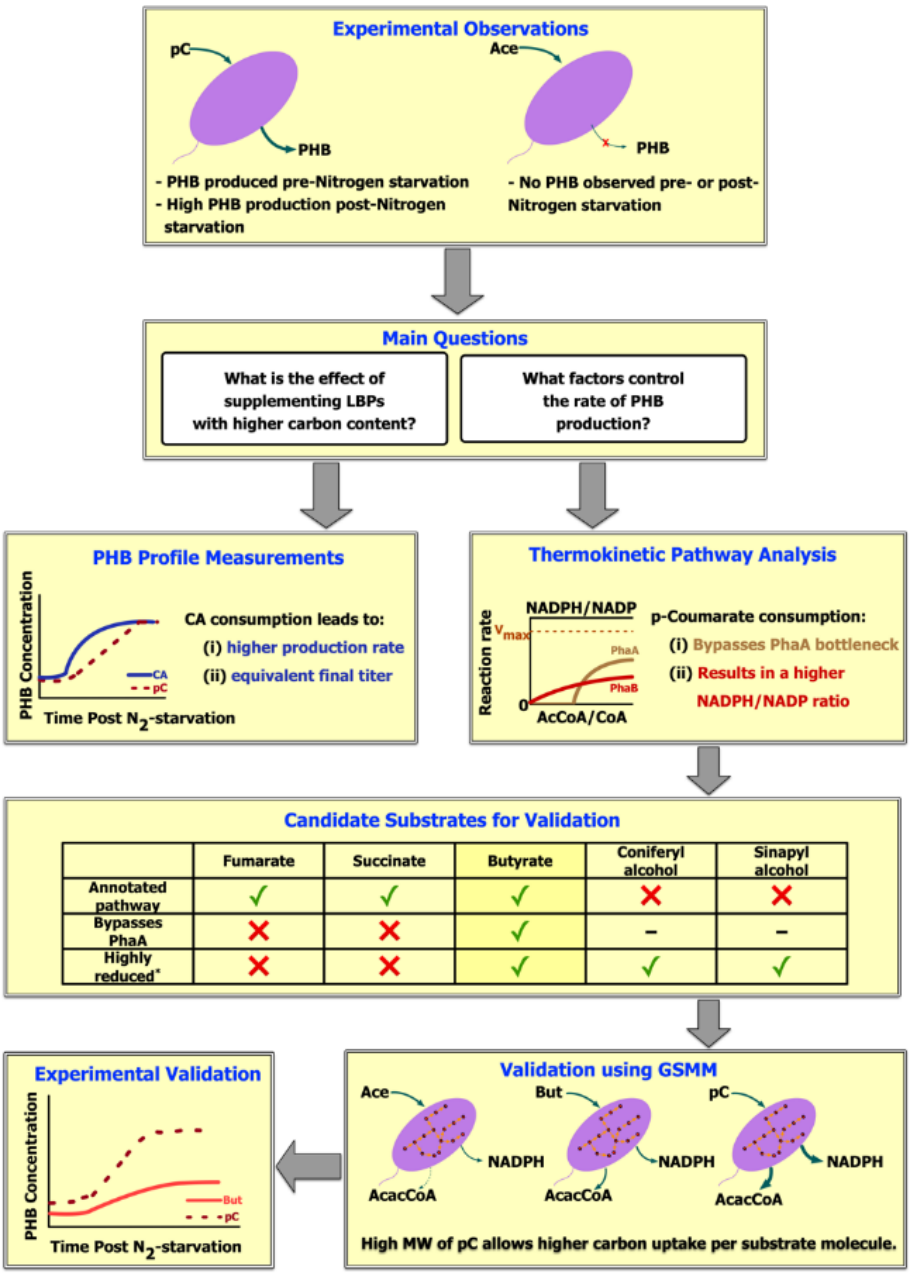

Fig. 4.3: Workflow followed to identify the metabolic factors controlling PHB production under different conditions.

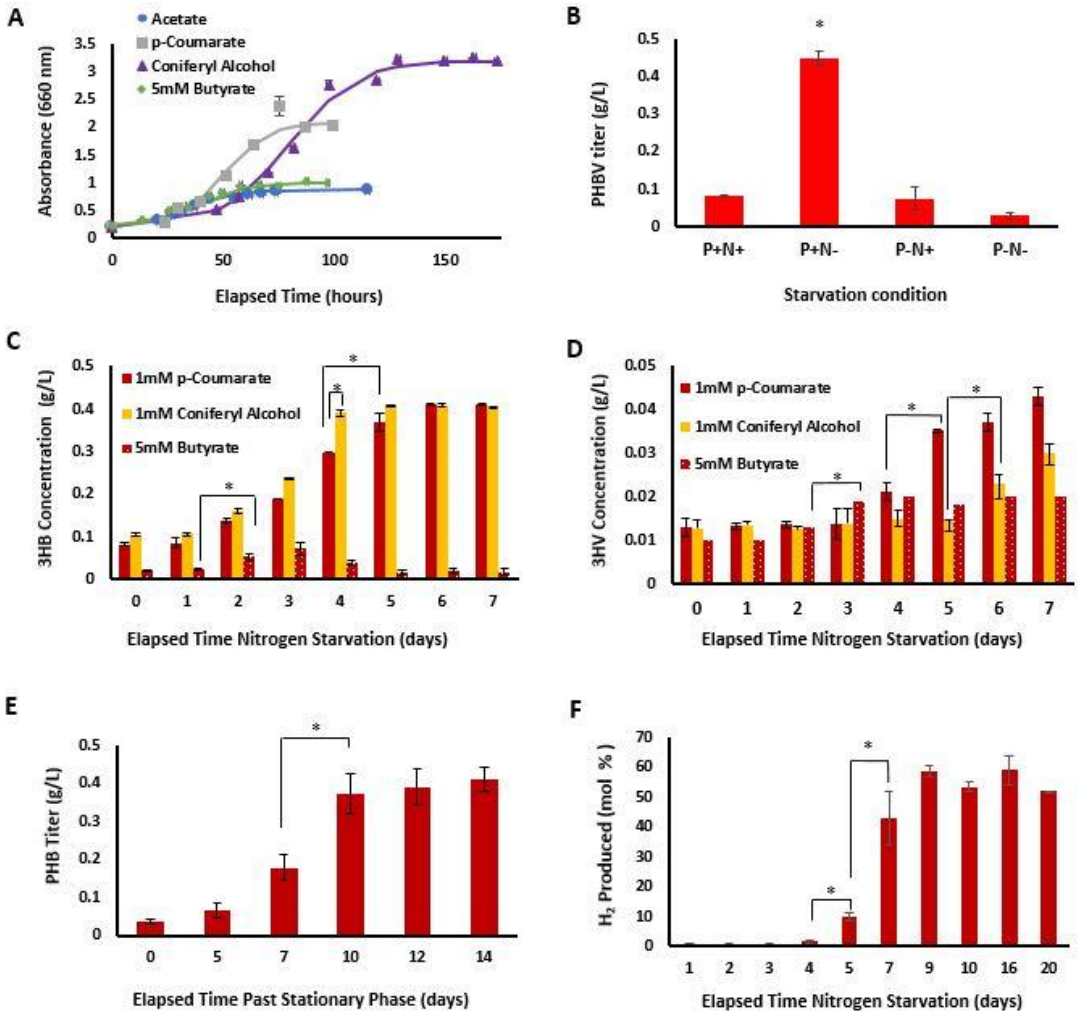

Fig. 4.4: Unique findings from experimental data that motivated application of the GSMM. (A) Anaerobic growth analyses. All substrates were supplemented with 10mM sodium bicarbonate. (B) Starvation condition analysis comparing nitrogen starvation, phosphorous starvation, and a combination of both nitrogen and phosphorus starvation from 1mM *p*-coumarate. (C) Comparison of 3HB titers on LBPs vs. butyrate. (D) Comparison of 3HV titers on LBPs vs. butyrate. (E) PHB production from 1mM *p*-coumarate from stationary phase (i.e. without resuspending in nitrogen-starved media). (F) H_2 production from 1mM *p*-coumarate after nitrogen starvation. All error bars represent the standard error for the population and are derived from the mean of biological triplicates for each data point. The (*) represents statistically significant at a 95% confidence level ($\alpha = 0.05$).

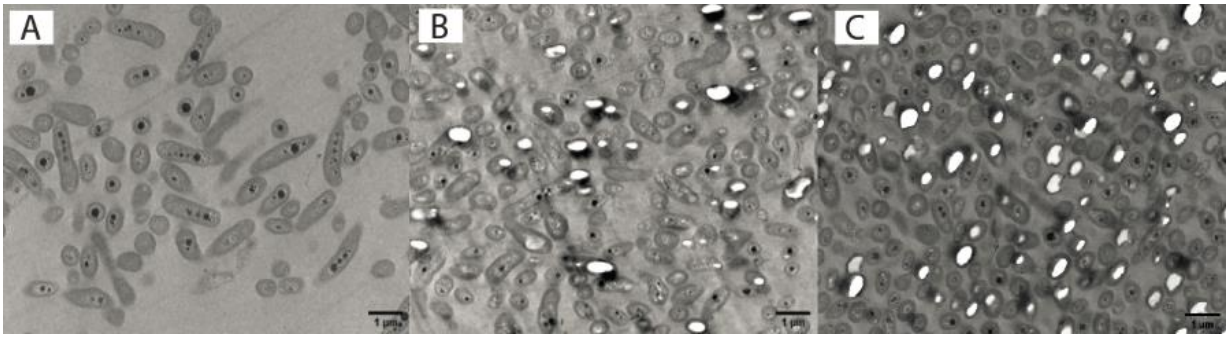

Fig. 4.5: Transmission Electron Microscopy (TEM). TEM images of *R. palustris* CGA009 cells grown anaerobically in photosynthetic media supplemented with (A) 10mM acetate and 10mM sodium bicarbonate, (B) 1mM *p*-coumarate and 10mM sodium bicarbonate, and (C) 1mM coniferyl alcohol and 10mM sodium bicarbonate. All samples were grown to mid-exponential phase, and subsequently nitrogen starved for five days. White inclusions inside the cytoplasm denote PHBV granules.

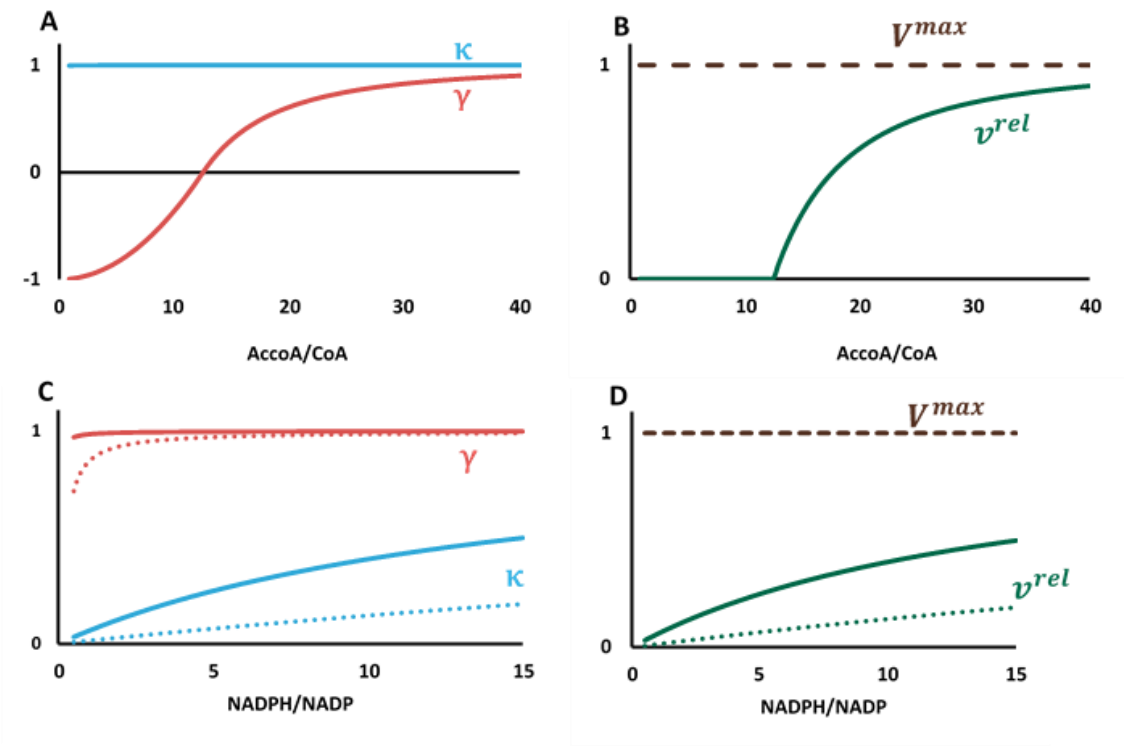

Fig. 4.6: Thermokinetic modeling of thiolase (*phaA*) and reductase (*phaB*) activity. Effect of the acetyl-CoA/CoA ratio on the *phaA*'s (A) thermodynamic driving force (γ) and substrate saturation (κ) and (B) Overall rate relative to V^{max}. Effect of the NADPH/NADP ratio on the *phaB*'s (C) thermodynamic driving force (γ) and substrate saturation (κ) and (D) Overall rate relative to V^{max}. Solid and dotted lines in (C) and (D) correspond to a 3-hydroxybutyryl-CoA concentration of 30 μM and 300 μM, respectively. The y-axis is unitless in all four panels.

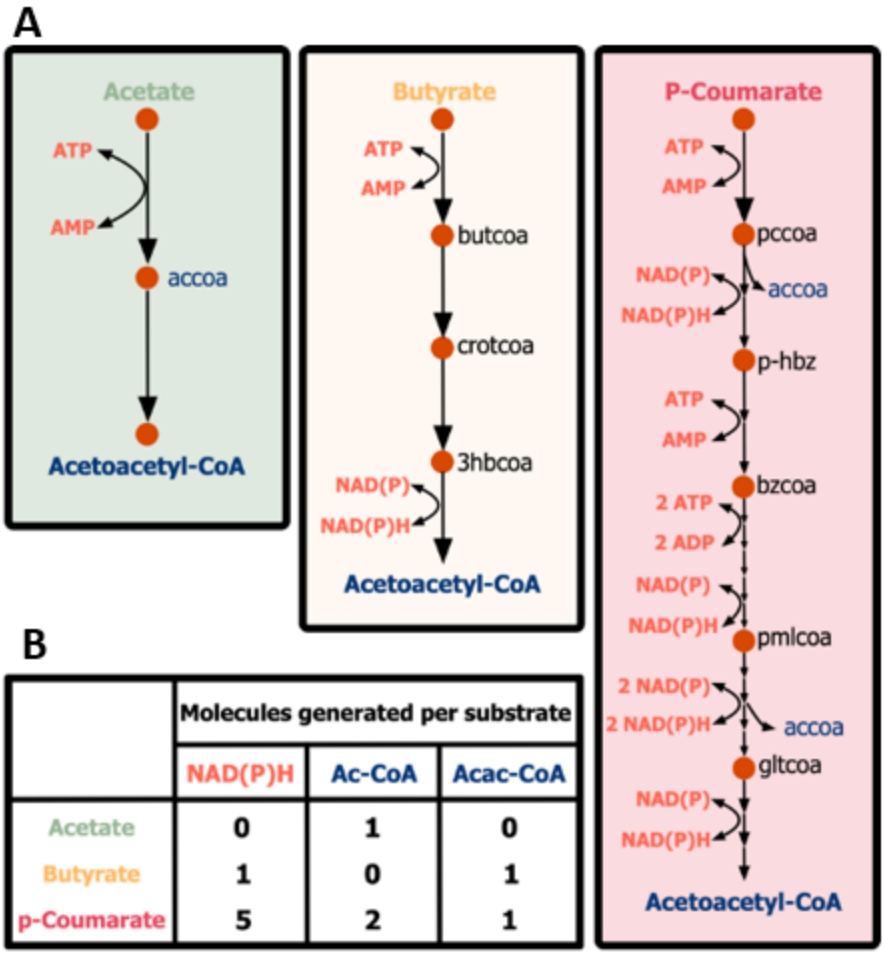

B

	Molecules generated per substrate		
	NAD(P)H	Ac-CoA	Acac-CoA
Acetate	0	1	0
Butyrate	1	0	1
p-Coumarate	5	2	1

Fig. 4.7: Substrate consumption of the three modeled carbon sources: acetate, butyrate, and *p*-coumarate depicting the (A) breakdown pathways and the (B) relevant cofactors and PHB precursors produced from each carbon source.

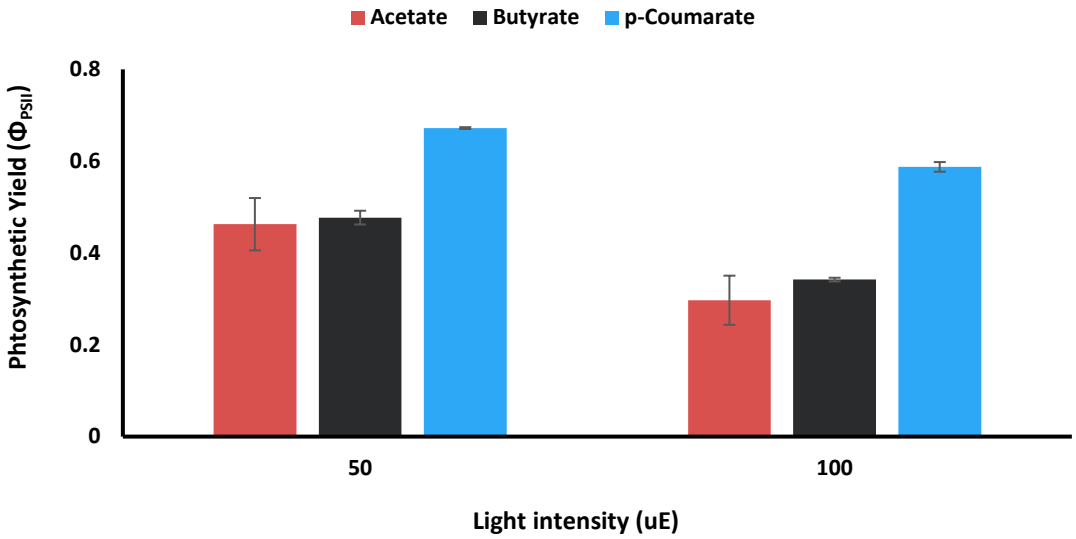

Fig. 4.8: Photosynthetic yields of *R. palustris* cells grown on different carbon sources as measured at 50 µE and 100 µE using PAM fluorometry.

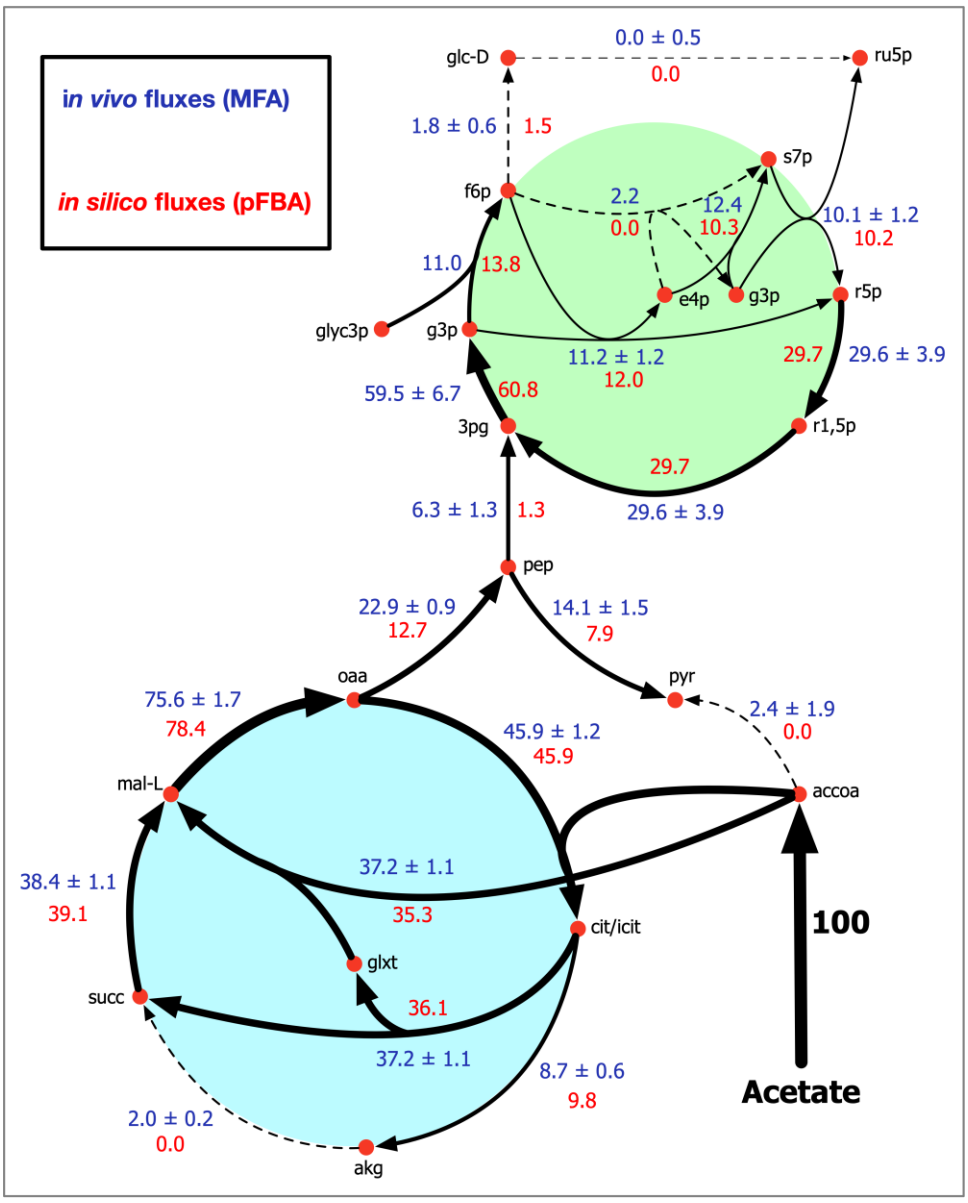

Fig. 4.9: Metabolic flux map showing predicted pFBA and experimentally obtained MFA reaction rates for growth on acetate.

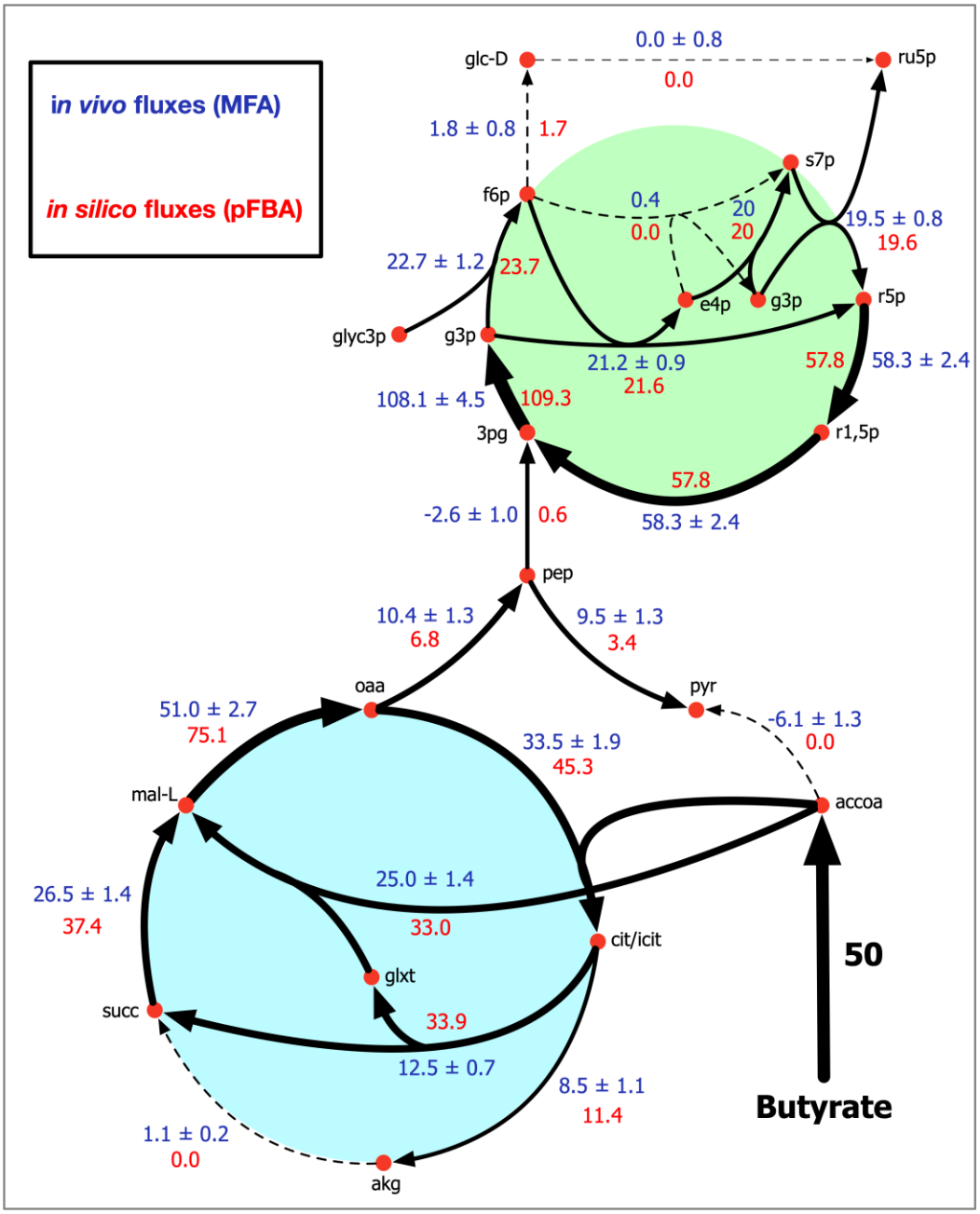

Fig. 4.10: Metabolic flux map showing predicted pFBA and experimentally obtained MFA reaction rates for growth on butyrate.

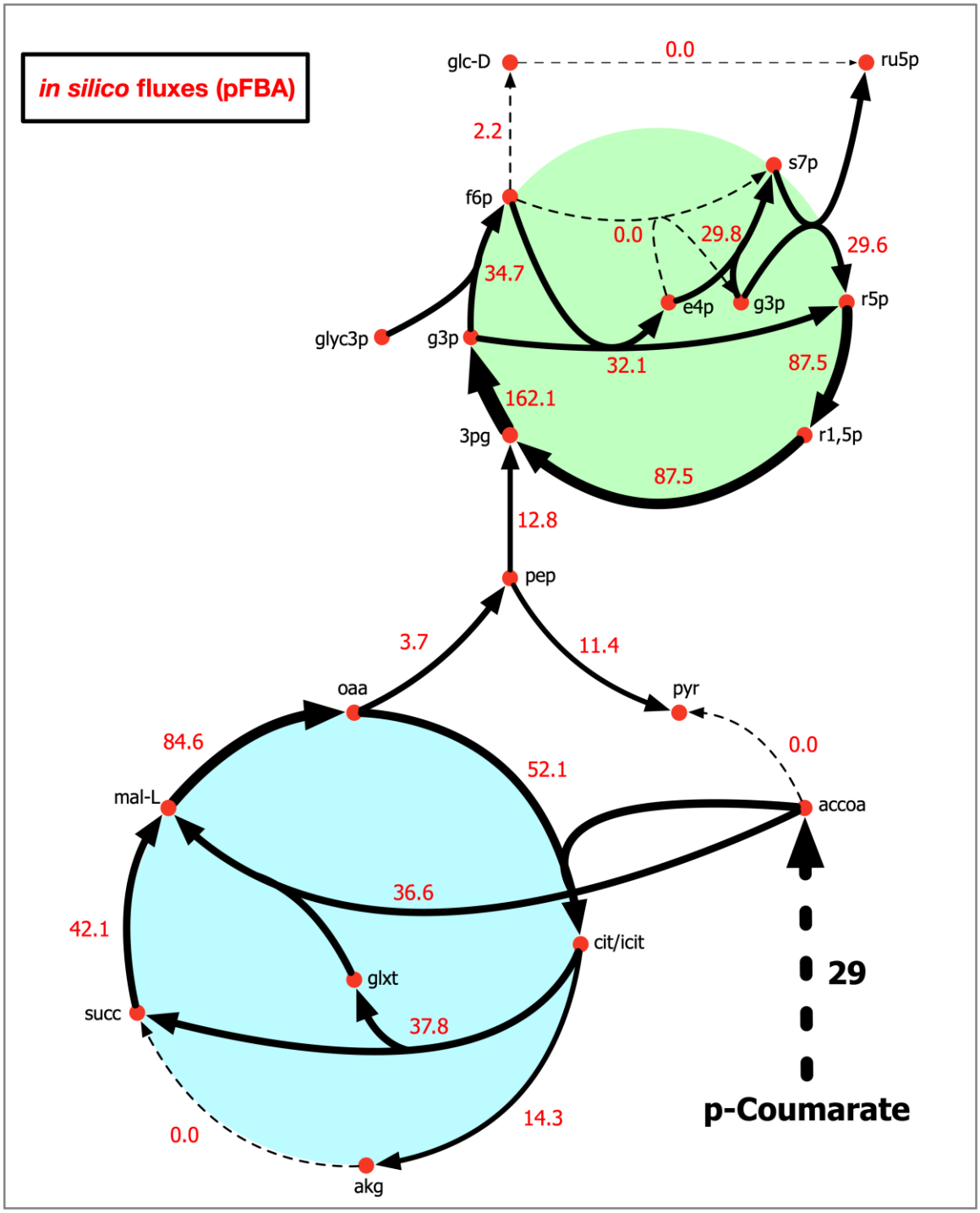

Fig. 4.11. Metabolic flux map showing predicted pFBA reaction rates for growth on *p*-coumarate**.** Dashed line implies that acetyl-CoA (acCoA) is produced in multiple steps along the pathway.

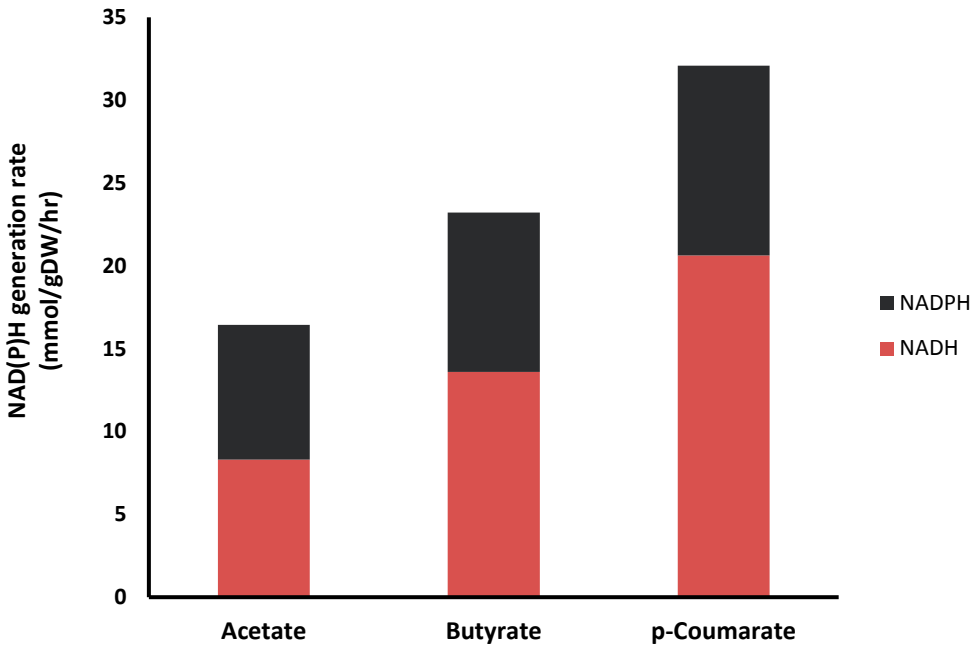

Fig. 4.12: Predicted reduction rates of the cofactors NAD and NADP during growth on acetate, butyrate, and *p*-coumarate.

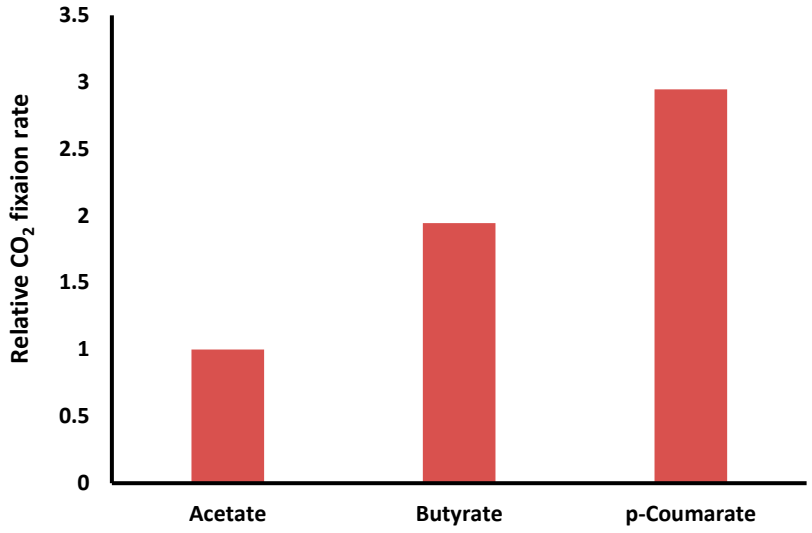

Fig. 4.13: Relative predicted rate of CO_2 fixation during growth on acetate, butyrate, and *p*-coumarate.

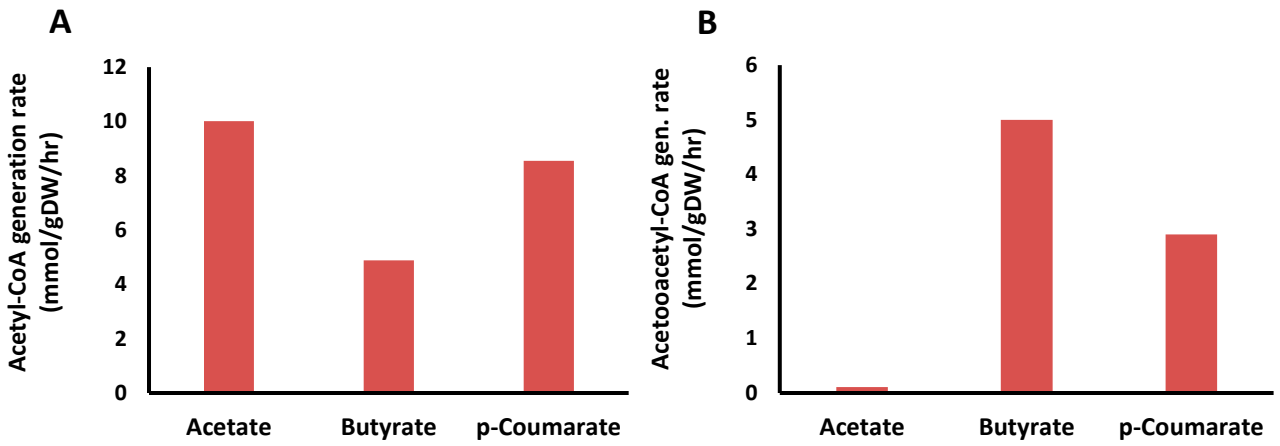

Fig. 4.14: Predicted generation rates of the first two substrates in the PHB pathway (acetyl-CoA (A) and acetoacetyl-CoA (B)) during growth on acetate, butyrate, and *p*-coumarate.

4.5 References

Alsiyabi, A., Immethun, C.M., Saha, R., 2019. Modeling the Interplay between Photosynthesis, CO2 Fixation, and the Quinone Pool in a Purple Non-Sulfur Bacterium. Sci. Rep. https://doi.org/10.1038/s41598-019-49079-z

Austin, S., Kontur, W.S., Ulbrich, A., Oshlag, J.Z., Zhang, W., Higbee, A., Zhang, Y., Coon, J.J., Hodge, D.B., Donohue, T.J., Noguera, D.R., 2015. Metabolism of Multiple Aromatic Compounds in Corn Stover Hydrolysate by Rhodopseudomonas palustris. Environ. Sci. Technol. https://doi.org/10.1021/acs.est.5b02062

Bennett, B.D., Kimball, E.H., Gao, M., Osterhout, R., Van Dien, S.J., Rabinowitz, J.D., 2009. Absolute metabolite concentrations and implied enzyme active site occupancy in Escherichia coli. Nat. Chem. Biol. https://doi.org/10.1038/nchembio.186

Bordel, S., Rodríguez, Y., Hakobyan, A., Rodríguez, E., Lebrero, R., Muñoz, R., 2019a. Genome scale metabolic modeling reveals the metabolic potential of three Type II methanotrophs of the genus Methylocystis. Metab. Eng. https://doi.org/10.1016/j.ymben.2019.04.001

Bordel, S., Rojas, A., Muñoz, R., 2019b. Reconstruction of a Genome Scale Metabolic Model of the polyhydroxybutyrate producing methanotroph Methylocystis parvus OBBP. Microb. Cell Fact. 18, 104. https://doi.org/10.1186/s12934-019-1154-5

Brown, B., Immethun, C., Wilkins, M., Saha, R., 2020. Rhodopseudomonas palustris CGA009 polyhydroxybutyrate production from a lignin aromatic and quantification via flow cytometry. Bioresour. Technol. Reports. https://doi.org/10.1016/j.biteb.2020.100474

Centeno-Leija, S., Huerta-Beristain, G., Giles-Gómez, M., Bolivar, F., Gosset, G., Martinez, A., 2014. Improving poly-3-hydroxybutyrate production in Escherichia coli by combining the increase in the NADPH pool and acetyl-CoA availability. Antonie Van Leeuwenhoek 105, 687–696. https://doi.org/10.1007/s10482-014-0124-5

Chen, G.-Q., Chen, X.-Y., Wu, F.-Q., Chen, J.-C., 2020. Polyhydroxyalkanoates (PHA) toward cost competitiveness and functionality. Adv. Ind. Eng. Polym. Res. https://doi.org/10.1016/j.aiepr.2019.11.001

Chen, G.-Q., Jiang, X.-R., 2017. Engineering bacteria for enhanced polyhydroxyalkanoates (PHA) biosynthesis. Synth. Syst. Biotechnol. 2, 192–197. https://doi.org/10.1016/j.synbio.2017.09.001

Chen, G.Q., 2009. A microbial polyhydroxyalkanoates (PHA) based bio- and materials industry. Chem. Soc. Rev. https://doi.org/10.1039/b812677c

Chen, G.Q., Zhang, J., 2018. Microbial polyhydroxyalkanoates as medical implant biomaterials. Artif. Cells, Nanomedicine Biotechnol. https://doi.org/10.1080/21691401.2017.1371185

Chohan, S.N., Copeland, L., 1998. Acetoacetyl Coenzyme A Reductase and

Polyhydroxybutyrate Synthesis in Rhizobium sp. Strain CC 1192. Appl. Environ. Microbiol. 64, 2859 LP – 2863. https://doi.org/10.1128/AEM.64.8.2859-2863.1998

Chohnan, S., Izawa, H., Nishihara, H., Takamura, Y., 1998. Changes in Size of Intracellular Pools of Coenzyme A and Its Thioesters in Escherichia coli K-12 Cells to Various Carbon Sources and Stresses. Biosci. Biotechnol. Biochem. https://doi.org/10.1271/bbb.62.1122

Cummins, P.L., Kannappan, B., Gready, J.E., 2018. Directions for optimization of photosynthetic carbon fixation: Rubisco's efficiency may not be so constrained after all. Front. Plant Sci. https://doi.org/10.3389/fpls.2018.00183

Flamholz, A., Noor, E., Bar-Even, A., Milo, R., 2012. eQuilibrator--the biochemical thermodynamics calculator. Nucleic Acids Res. 40, D770–D775. https://doi.org/10.1093/nar/gkr874

Fondi, M., Liò, P., 2015. Genome-Scale Metabolic Network Reconstruction BT - Bacterial Pangenomics: Methods and Protocols, in: Mengoni, A., Galardini, M., Fondi, M. (Eds.), . Springer New York, New York, NY, pp. 233–256. https://doi.org/10.1007/978-1-4939-1720-4_15

Gameiro, D., Pérez-Pérez, M., Pérez-Rodríguez, G., Monteiro, G., Azevedo, N.F., Lourenço, A., 2016. Computational resources and strategies to construct single-molecule metabolic models of microbial cells. Brief. Bioinform. https://doi.org/10.1093/bib/bbv096

Graham, L., Orenstein, J.M., 2007. Processing tissue and cells for transmission electron microscopy in diagnostic pathology and research. Nat. Protoc. 2, 2439–2450. https://doi.org/10.1038/nprot.2007.304

Guzman, M.S., Rengasamy, K., Binkley, M.M., Jones, C., Ranaivoarisoa, T.O., Singh, R., Fike, D.A., Meacham, J.M., Bose, A., 2019. Phototrophic extracellular electron uptake is linked to carbon dioxide fixation in the bacterium Rhodopseudomonas palustris. Nat. Commun. https://doi.org/10.1038/s41467-019-09377-6

Guzman, M.S., Rengasamy, K., Binkley, M.M., Jones, C., Ranaivoarisoa, T.O., Singh, R., Fike, D.A., Meacham, J.M., Bose, A., 2019. Phototrophic extracellular electron uptake is linked to carbon dioxide fixation in the bacterium Rhodopseudomonas palustris. Nat. Commun. https://doi.org/10.1038/s41467-019-09377-6

Harwood, C.S., Gibson, J., 1988. Anaerobic and aerobic metabolism of diverse aromatic compounds by the photosynthetic bacterium Rhodopseudomonas palustris. Appl. Environ. Microbiol. https://doi.org/10.1128/aem.54.3.712-717.1988

Islam, M.M., Saha, R., 2018. Computational Approaches on Stoichiometric and Kinetic Modeling for Efficient Strain Design BT - Synthetic Metabolic Pathways: Methods and Protocols, in: Jensen, M.K., Keasling, J.D. (Eds.), . Springer New York, New York, NY, pp. 63–82. https://doi.org/10.1007/978-1-4939-7295-1_5

Kim, M.-K., Harwood, C.S., 1991. Regulation of benzoate-CoA ligase in

Rhodopseudomonas palustris. FEMS Microbiol. Lett. 83, 199–203. https://doi.org/10.1111/j.1574-6968.1991.tb04440.x-i1

Kleiner, M., Wentrup, C., Lott, C., Teeling, H., Wetzel, S., Young, J., Chang, Y.J., Shah, M., VerBerkmoes, N.C., Zarzycki, J., Fuchs, G., Markert, S., Hempel, K., Voigt, B., Becher, D., Liebeke, M., Lalk, M., Albrecht, D., Hecker, M., Schweder, T., Dubilier, N., 2012. Metaproteomics of a gutless marine worm and its symbiotic microbial community reveal unusual pathways for carbon and energy use. Proc. Natl. Acad. Sci. U. S. A. https://doi.org/10.1073/pnas.1121198109

Kocharin, K., Chen, Y., Siewers, V., Nielsen, J., 2012. Engineering of acetyl-CoA metabolism for the improved production of polyhydroxybutyrate in Saccharomyces cerevisiae. AMB Express. https://doi.org/10.1186/2191-0855-2-52

Larimer, F.W., Chain, P., Hauser, L., Lamerdin, J., Malfatti, S., Do, L., Land, M.L., Pelletier, D.A., Beatty, J.T., Lang, A.S., Tabita, F.R., Gibson, J.L., Hanson, T.E., Bobst, C., Torres, J.L.T. y, Peres, C., Harrison, F.H., Gibson, J., Harwood, C.S., 2004. Complete genome sequence of the metabolically versatile photosynthetic bacterium Rhodopseudomonas palustris. Nat. Biotechnol. 22, 55–61. https://doi.org/10.1038/nbt923

Leaf, T.A., Srienc, F., 1998. Metabolic modeling of polyhydroxybutyrate biosynthesis. Biotechnol. Bioeng. https://doi.org/10.1002/(SICI)1097-0290(19980305)57:5<557::AID-BIT8>3.0.CO;2-F

Lee, I.Y., Kim, M.K., Park, Y.H., Lee, S.Y., 1996. Regulatory effects of cellular nicotinamide nucleotides and enzyme activities on poly(3-hydroxybutyrate) synthesis in recombinant Escherichia coli. Biotechnol. Bioeng. https://doi.org/10.1002/(SICI)1097-0290(19961220)52:6<707::AID-BIT8>3.0.CO;2-S

Lee, S., Kang, M., Bae, J.-H., Sohn, J.-H., Sung, B.H., 2019. Bacterial Valorization of Lignin: Strains, Enzymes, Conversion Pathways, Biosensors, and Perspectives. Front. Bioeng. Biotechnol. 7, 209. https://doi.org/10.3389/fbioe.2019.00209

Lewis, N.E., Hixson, K.K., Conrad, T.M., Lerman, J.A., Charusanti, P., Polpitiya, A.D., Adkins, J.N., Schramm, G., Purvine, S.O., Lopez-Ferrer, D., Weitz, K.K., Eils, R., König, R., Smith, R.D., Palsson, B., 2010. Omic data from evolved E. coli are consistent with computed optimal growth from genome-scale models. Mol. Syst. Biol. https://doi.org/10.1038/msb.2010.47

Li, Z., Yang, J., Loh, X.J., 2016. Polyhydroxyalkanoates: Opening doors for a sustainable future. NPG Asia Mater. https://doi.org/10.1038/am.2016.48

Lopar, M., Vrana Špoljarić, I., Atlić, A., Koller, M., Braunegg, G., Horvat, P., 2013. Five-step continuous production of PHB analyzed by elementary flux, modes, yield space analysis and high structured metabolic model. Biochem. Eng. J. https://doi.org/10.1016/j.bej.2013.07.003

Maxwell, K., Johnson, G.N., 2000. Chlorophyll fluorescence—a practical guide. J. Exp. Bot. 51, 659–668. https://doi.org/10.1093/jexbot/51.345.659

McKinlay, J.B., 2014. Systems Biology of Photobiological Hydrogen Production by Purple Non-sulfur Bacteria. pp. 155–176. https://doi.org/10.1007/978-94-017-8554-9_7

McKinlay, James B, Harwood, C.S., 2011. Calvin cycle flux, pathway constraints, and substrate oxidation state together determine the H2 biofuel yield in photoheterotrophic bacteria. MBio 2, e00323-10. https://doi.org/10.1128/mBio.00323-10

McKinlay, James B., Harwood, C.S., 2011. Calvin cycle flux, pathway constraints, and substrate oxidation state together determine the H2 biofuel yield in photoheterotrophic bacteria. MBio. https://doi.org/10.1128/mBio.00323-10

McKinlay, J.B., Harwood, C.S., 2010. Carbon dioxide fixation as a central redox cofactor recycling mechanism in bacteria. Proc. Natl. Acad. Sci. U. S. A. https://doi.org/10.1073/pnas.1006175107

McKinlay, James B., Oda, Y., Ruhl, M., Posto, A.L., Sauer, U., Harwood, C.S., 2014. Non-growing rhodopseudomonas palustris increases the hydrogen gas yield from acetate by shifting from the glyoxylate shunt to the tricarboxylic acid cycle. J. Biol. Chem. https://doi.org/10.1074/jbc.M113.527515

McKinlay, James B, Oda, Y., Rühl, M., Posto, A.L., Sauer, U., Harwood, C.S., 2014. Non-growing Rhodopseudomonas palustris Increases the Hydrogen Gas Yield from Acetate by Shifting from the Glyoxylate Shunt to the Tricarboxylic Acid Cycle* *Experimental aspects of this research were supported equally by the Division of Chemical Sciences,. J. Biol. Chem. 289, 1960–1970. https://doi.org/https://doi.org/10.1074/jbc.M113.527515

Medeiros Garcia Alcântara, J., Distante, F., Storti, G., Moscatelli, D., Morbidelli, M., Sponchioni, M., 2020. Current trends in the production of biodegradable bioplastics: The case of polyhydroxyalkanoates. Biotechnol. Adv. https://doi.org/10.1016/j.biotechadv.2020.107582

Noor, E., Flamholz, A., Liebermeister, W., Bar-Even, A., Milo, R., 2013a. A note on the kinetics of enzyme action: A decomposition that highlights thermodynamic effects. FEBS Lett. https://doi.org/10.1016/j.febslet.2013.07.028

Noor, E., Haraldsdóttir, H.S., Milo, R., Fleming, R.M.T., 2013b. Consistent Estimation of Gibbs Energy Using Component Contributions. PLoS Comput. Biol. https://doi.org/10.1371/journal.pcbi.1003098

O'Brien, E.J., Lerman, J.A., Chang, R.L., Hyduke, D.R., Palsson, B.Ø., 2013. Genome-scale models of metabolism and gene expression extend and refine growth phenotype prediction. Mol. Syst. Biol. 9, 693. https://doi.org/10.1038/msb.2013.52

Orth, J.D., Thiele, I., Palsson, B.O., 2010. What is flux balance analysis? Nat. Biotechnol. https://doi.org/10.1038/nbt.1614

Park, J.M., Kim, T.Y., Lee, S.Y., 2011. Genome-scale reconstruction and in silico analysis of the Ralstonia eutropha H16 for polyhydroxyalkanoate synthesis,

lithoautotrophic growth, and 2-methyl citric acid production. BMC Syst. Biol. https://doi.org/10.1186/1752-0509-5-101

Park, J.O., Rubin, S.A., Xu, Y.-F., Amador-Noguez, D., Fan, J., Shlomi, T., Rabinowitz, J.D., 2016. Metabolite concentrations, fluxes and free energies imply efficient enzyme usage. Nat. Chem. Biol. 12, 482–489. https://doi.org/10.1038/nchembio.2077

Phongjarus, N., Suvaphat, C., Srichai, N., Ritchie, R.J., 2018. Photoheterotrophy of photosynthetic bacteria (Rhodopseudomonas palustris) growing on oil palm and soybean cooking oils. Environ. Technol. Innov. https://doi.org/10.1016/j.eti.2018.03.002

Ranaivoarisoa, T.O., Singh, R., Rengasamy, K., Guzman, M.S., Bose, A., 2019. Towards sustainable bioplastic production using the photoautotrophic bacterium Rhodopseudomonas palustris TIE-1. J. Ind. Microbiol. Biotechnol. https://doi.org/10.1007/s10295-019-02165-7

Ritchie, R.J., 2013. The Use of Solar Radiation by the Photosynthetic Bacterium, Rhodopseudomonas palustris: Model Simulation of Conditions Found in a Shallow Pond or a Flatbed Reactor. Photochem. Photobiol. 89, 1143–1162. https://doi.org/https://doi.org/10.1111/php.12124

Ritchie, R.J., 2008. Fitting light saturation curves measured using modulated fluorometry. Photosynth. Res. 96, 201–215. https://doi.org/10.1007/s11120-008-9300-7

Ritchie, R.J., Larkum, A.W.D., 2012. Modelling photosynthesis in shallow algal production ponds. Photosynthetica. https://doi.org/10.1007/s11099-012-0076-9

Ritchie, R.J., Mekjinda, N., 2015. Measurement of photosynthesis using PAM technology in a purple sulfur bacterium Thermochromatium tepidum (Chromatiaceae). Photochem. Photobiol. 91, 350–358. https://doi.org/10.1111/php.12413

Sacomboio, E.N.M., Kim, E.Y.S., Correa, H.L.R., Bonato, P., Pedrosa, F.D.O., De Souza, E.M., Chubatsu, L.S., Müller-Santos, M., 2017. The transcriptional regulator NtrC controls glucose-6-phosphate dehydrogenase expression and polyhydroxybutyrate synthesis through NADPH availability in Herbaspirillum seropedicae. Sci. Rep. https://doi.org/10.1038/s41598-017-12649-0

Saha, R., Chowdhury, A., Maranas, C.D., 2014. Recent advances in the reconstruction of metabolic models and integration of omics data. Curr. Opin. Biotechnol. https://doi.org/10.1016/j.copbio.2014.02.011

Sekar, K., Tyo, K.E.J., 2015. Regulatory effects on central carbon metabolism from poly-3-hydroxybutryate synthesis. Metab. Eng. https://doi.org/10.1016/j.ymben.2015.01.003

Shen, R., Ning, Z.Y., Lan, Y.X., Chen, J.C., Chen, G.Q., 2019. Manipulation of polyhydroxyalkanoate granular sizes in Halomonas bluephagenesis. Metab. Eng. https://doi.org/10.1016/j.ymben.2019.03.011

Sim, S.J., Snell, K.D., Hogan, S.A., Stubbe, J.A., Rha, C., Sinskey, A.J., 1997. PHA

synthase activity controls the molecular weight and polydispersity of polyhydroxybutyrate in vivo. Nat. Biotechnol. https://doi.org/10.1038/nbt0197-63

Tajparast, M., Frigon, D., 2018. Predicting the accumulation of storage compounds by rhodococcus jostii RHA1 in the feast-famine growth cycles using genome-scale flux balance analysis. PLoS One. https://doi.org/10.1371/journal.pone.0191835

Takamura, Y., Nomura, G., 1988. Changes in the Intracellular Concentration of Acetyl-CoA and Malonyl-CoA in Relation to the Carbon and Energy Metabolism of Escherichia coli K12. Microbiology 134, 2249–2253. https://doi.org/10.1099/00221287-134-8-2249

Thauer, R.K., Jungermann, K., Decker, K., 1977. Energy conservation in chemotrophic anaerobic bacteria. Bacteriol. Rev. https://doi.org/10.1128/mmbr.41.1.100-180.1977

Tiryaki, O.N., Irmak, S., 2020. Evaluation of various corn variety kernels for hydrogen gas production by APR. Biomass and Bioenergy. https://doi.org/10.1016/j.biombioe.2020.105480

Tyo, K.E.J., Fischer, C.R., Simeon, F., Stephanopoulos, G., 2010. Analysis of polyhydroxybutyrate flux limitations by systematic genetic and metabolic perturbations. Metab. Eng. https://doi.org/10.1016/j.ymben.2009.10.005

Uchino, K., Saito, T., Gebauer, B., Jendrossek, D., 2007. Isolated poly(3-hydroxybutyrate) (PHB) granules are complex bacterial organelles catalyzing formation of PHB from acetyl coenzyme A (CoA) and degradation of PHB to acetyl-CoA. J. Bacteriol. https://doi.org/10.1128/JB.00752-07

Van Wegen, R.J., Lee, S.Y., Middelberg, A.P.J., 2001. Metabolic and kinetic analysis of poly(3-Hydroxybutyrate) production by recombinant Escherichia coli. Biotechnol. Bioeng. https://doi.org/10.1002/bit.1096

Wang, F., Lee, S.Y., 1997. Production of poly(3-hydroxybutyrate) by fed-batch culture of filamentation-suppressed recombinant Escherichia coli. Appl. Environ. Microbiol. 63, 4765–4769. https://doi.org/10.1128/AEM.63.12.4765-4769.1997

Wen, Q., Chen, Z., Tian, T., Chen, W., 2010. Effects of phosphorus and nitrogen limitation on PHA production in activated sludge. J. Environ. Sci. https://doi.org/10.1016/S1001-0742(09)60295-3

CHAPTER V

5. Heterologous Phasin Expression in *Rhodopseudomonas palustris* CGA009 for Bioplastic Production from Lignocellulosic Biomass

Abstract

Rhodopseudomonas palustris CGA009 is a metabolically robust microbe that can utilize lignin breakdown products to produce bioplastics. Our recent efforts suggest cytoplasmic space is a limiting factor for maximum production of the bioplastic poly(3-hydroxybutyrate-co-3-hydroxyvalerate) (PHBV) by *R. palustris.* The Phap1 phasin from the PHB-producing model bacterium *Cupriavidus necator* H16 was expressed in *R. palustris* with the aim of overproducing PHBV to foster smaller and more abundant granules and maximize the use of cytoplasmic space. Expression of *phaP1* yielded PHBV production from *R. palustris* aerobically (0.7 g/L), which does not occur in the wild-type strain, and led to a significantly higher PHBV titer than wild-type anaerobic production (0.41 g/L). The 3HV fractions were also significantly increased under both anaerobic and aerobic conditions, which boosts thermomechanical properties. Thus, heterologous phasin expression in *R. palustris* provides flexibility for industrial processing and fosters compositional changes in copolymers with better thermomechanical properties compared to PHB alone.

5.1. Introduction

Polyhydroxyalkanoates (PHAs) are biopolymers produced by bacteria that have the potential to replace conventional plastics due to their similar thermomechanical properties, biodegradability, and biocompatibility (Li et al., 2016; Muneer et al., 2020; Sabbagh and Muhamad, 2017). Due to these characteristics, PHAs have been applied in a wide variety of applications including therapeutics, packaging, and environmental rehabilitation (Bello-Gil et al., 2018; Draper and Rehm, 2012; Hungund et al., 2018; Parlane et al., 2017). Bacteria typically produce PHAs in response to stressful conditions, such as unbalanced growth, and store the granules inside the cytoplasm as a means of carbon and redox balance (Koller, 2020). The most commonly produced PHA by bacteria is called poly-3-hydroxybutyrate (PHB) and is thus the most extensively studied. However, market acceptance of PHAs is limited by their relatively high production costs compared to conventional plastics (Aramvash et al., 2018). PHA costs depend mainly on the carbon source, fermentation technology, and extraction processes (Chen et al., 2020; Medeiros Garcia Alcântara et al., 2020). Approximately half of the production cost for PHAs derives from the carbon source (Raza et al., 2018). Thus, engineering a microbe for PHA production from cheaper and renewable carbon sources is necessary to promote the valorization of PHAs.

Lignocellulosic biomass is considered to be the most economic carbon source in the world, and is thus an ideal candidate for cheaper production of bioplastics (Ponnusamy et al., 2019; Qian, 2013). Using inexpensive and renewable carbon sources for bioplastic production that do not compete with food production, such as lignocellulosic biowaste, could significantly reduce the costs of bioplastics while simultaneously closing the carbon

loop. Lignin is a heterogeneous network of cross-linked aromatics that accounts for nearly 30% of the organic carbon in plant biomass (Ponnusamy et al., 2019). The production of biopolymers from lignin is arguably one of the most promising routes for boosting the valorization of lignin (Rajesh Banu et al., 2019). Yet, one of the major challenges for valorizing lignin is developing an efficient bioconversion process to create value-added bioproducts from lignin breakdown products (LBPs), such as monolignols and hydroxycinnamic acids. Unfortunately, most microorganisms that can produce high-valued bioproducts cannot metabolize LBPs and are even inhibited by them. Thus, employing synthetic biology techniques and metabolic engineering to over-produce PHAs from microbes capable of catabolizing this cheaper and renewable carbon source is ideal. Efforts in synthetic biology and metabolic engineering offer opportunities for overproduction of PHAs (Koller, 2017; Raza et al., 2018), but there is still a need to engineer a microbe for more cost-competitive production of PHAs from lignocellulosic biomass.

Bacteria that produce PHAs utilize an ensemble of granule-associated proteins (GAPs) that help balance metabolic tradeoffs in cell growth, PHA production, and other functions. This system of GAPs includes polymerases, depolymerases, synthases (PhaC), phasin regulators (PhaR), and phasins (Choi et al., 2020; Pillai et al., 2019). Of these proteins, phasins are a fascinating class of small-molecular weight proteins that perform multiple functions for the cell. Phasins are employed by all PHA-producing bacteria and are the dominant protein surrounding the PHA granules (Mezzina and Pettinari, 2016). Although originally thought to simply create a boundary layer between the granule and the cytoplasm, phasins have been revealed to perform a number of additional functions such as controlling the size, shape, and abundance of granules in the cell (Sharma et al., 2016),

activating PHA depolymerization (Chen and Zhang, 2018), fostering granule segregation (Maestro et al., 2013), modulating expression of PHA synthases (Qi et al., 2000; Ushimaru et al., 2014), fostering localization of granules (Pfeiffer and Jendrossek, 2012), altering the composition of PHAs (Kawashima et al., 2015), and performing chaperone-like activities that contribute to cell fitness (Almeida et al., 2011). However, the roles and functions of phasins can differ between species, and even among multiple phasins expressed by the same bacterium. For example, *Cupriavidus necator* H16 (formerly known as *Ralstonia eutropha*) is a model bacterium for PHB production, and there have been seven different phasins discovered that perform distinct functions for the microbe (Sharma et al., 2016). *C. necator* has been extensively studied for PHB production and its phasins are arguably among the most characterized. For example, Phasin 1 (PhaP1) in *C. necator* has been shown to control the size and number of granules in the cytoplasm, impact PHB accumulation and degradation rates, foster localization of granules in the cytoplasm, and manipulate the copolymer compositions of PHAs (Kawashima et al., 2015; Kuchta et al., 2007; Pfeiffer and Jendrossek, 2012; Pötter et al., 2004; Sharma et al., 2016). Extensive characterization of *C. necator*'s phasins provides a platform for developing heterologous systems for PHA overproduction in other microbes.

Rhodopseudomonas palustris CGA009 (hereafter *R. palustris*) is a purple non-sulfur bacterium capable of fixing CO_2 and nitrogen or breaking down organic compounds for its carbon and nitrogen requirements, yielding several high-value product streams like bioplastics and biohydrogen (Brown et al., 2020a; Larimer et al., 2004; McKinlay et al., 2014). This makes *R. palustris* an excellent candidate for engineering towards industrial production. As a metabolically robust bacterium, *R. palustris*' genome includes pathways

for three of the four known microbial LBP degradation strategies, incorporating both aerobic and anaerobic photosynthetic catabolism (Larimer et al., 2004). Thus, *R. palustris* can break down numerous aromatic compounds derived from lignin while also potentially accomplishing complete degradation of these compounds to intermediates in the citric acid cycle that are important building blocks for bioplastic development. Our recent works show that *R. palustris* can utilize the major LBPs *p*-coumarate and coniferyl alcohol to produce bioplastics (Alsiyabi et al., 2021; Brown et al., 2020a). It was also revealed that *R. palustris* can create a copolymer of PHB called poly(3-hydroxybutyrate-co-3-hydroxyvalerate) (PHBV), which is a copolymer of the 3-hydroxybutyrate (3HB) and 3-hydroxyvalerate (3HV) monomers that has more ideal thermomechanical properties compared to PHB alone (Li et al., 2016).

In this study, *phaP1* from *C. necator* H16 was expressed in *Rhodopseudomonas palustris* CGA009 (hereafter *R. palustris*) with the aim of overproducing PHAs from lignocellulosic sources. *R. palustris'* ability to produce PHBV from lignocellulosic biomass renders it an ideal candidate for engineering toward industrial PHA production from lignin. However, our recent efforts also revealed that intracellular space may be a limiting factor for maximum PHBV production due to one large PHBV granule formed inside the cells (Alsiyabi et al., 2021). Thus, heterologous expression of *phap1* was implemented in *R. palustris* with the aim of overproducing PHBV from lignocellosic biomass by fostering smaller and more abundant granules to utilize more of the intracellular space.

5.2. Materials and Methods

5.2.1 Growth curves and PHBV production

R. palustris seed culture was grown on photosynthetic media (PM) supplemented with 20mM sodium acetate to an OD_{660} of approximately 0.5 as described previously (Brown et al., 2020a). All conditions employing the *phaP1* and Backbone (pBBR1MCS-2) strains were supplemented with kanamycin (300 μg/mL). Cultures were diluted to an OD_{660} of 0.2 in fresh PM supplemented with 1mM *p*-coumarate and 10mM sodium bicarbonate as the carbon sources in anaerobic and aerobic conditions. Anaerobic cultures were grown in sealed 14 mL Falcon™ round-bottom polystyrene tubes at 30°C with 100 μE white light and continuous shaking at 275 rpm. Aerobic cultures were grown in the dark using 250 mL flasks with no more than 50 mL of total culture volume in each flask, at 30°C, and with continuous shaking at 275 rpm. Growth data were fitted to a modified logarithmic growth model as described previously (Brown et al., 2020a). For anaerobic conditions, cultures were nitrogen starved at mid-exponential growth by resuspending the cell pellet in fresh PM without ammonium sulfate as a nitrogen source that was supplemented with 1mM *p*-coumarate and 10mM sodium bicarbonate. Anaerobic samples were harvested for PHBV extraction upon nitrogen starvation (day 0) and on each day after nitrogen starvation for 11 days. For aerobic conditions, samples were prepared for PHBV analysis at each time point designated in Fig. 5.3B.

5.2.2 PHBV quantification via gas-chromatography mass spectrometry (GC-MS)

PHBV extraction and quantification was conducted as described previously (Brown et al., 2020b). All harvested samples were washed twice with 1x phosphate buffered saline

(PBS), stored as cell pellets in -80°C until further processing, and extracted via acidic methanolysis. PHBV was quantified with conventional GC-MS as described (Brown et al., 2020b), using serial dilutions of sodium 3-hydroxybutyrate or (−)-methyl (R)-3-hydroxyvalerate (Sigma-Aldrich™) as external standards.

5.2.3 Isolation, amplification, and manipulation of DNA

C. necator was grown on rich media (17.5 g/L nutrient broth, 7.5 g/L yeast extract, 5 g/L $(NH_4)_2SO_4$) to an OD_{600} of approximately 1.0 (Nangle et al., 2020). *R. palustris* was grown as described in *Section 5.2.1*. Chromosomal DNA was extracted using a *Quick*-DNA Fungal/Bacterial kit per manufacturer instructions (Zymo Research). The plasmid was constructed using the Hot Fusion assembly method (Fu et al., 2014). The oligonucleotides and plasmids are summarized in Table 5.1. The oligonucleotides were purchased from Eurofins Genomics. Enzymes were purchased from Thermo Fisher Scientific.

5.2.4 Strain construction

The PSSBIO32-tonB-*phaP1* plasmid was constructed in NEB® 10-beta competent *E. coli*. *E. coli* was grown overnight (30°C with continuous shaking at 275 rpm), diluted to 0.025%, grown for 2 hrs, and washed twice with autoclaved H_2O (Tu et al., 2016). The washed cells were transformed with the Hot Fusion products via electroporation. The electroporated cells were allowed to rest at 30°C for 1 - 1.5 hours in Luria Broth (LB) (Miller, AMRESCO) at 30°C and 250 rpm in 14 mL BD Falcon™ round-bottom tubes without antibiotics, and subsequently plated onto LB plates supplemented with kanamycin (30 μg/mL). Colonies were selected and cultures were frozen as 15% glycerol stock at -

80°C until further processing. Fresh culture was subjected to the Invitrogen™ PureLink™ Quick Plasmid Miniprep kit (ThermoFisher) to remove the plasmid per manufacturer's instructions. PCR using designed sequencing oligonucleotides was conducted with the plasmids, and gel electrophoresis was used to check the amplicon size. If the amplicon was the expected size, the reaction was purified with the Invitrogen™ PureLink™ Quick PCR Purification Kit (ThermoFisher), and submitted to Eurofins Genomics for sequencing.

Sequence-verified plasmids were transformed into *R. palustris* following the same washing and electroporation steps. The transformed cells rested in Van Niel's Yeast Media (ATCC Medium 112) and were plated 24 hours later on Van Niel's Yeast Agar supplemented with kanamycin (300 μg/mL). Colonies were then streaked onto a new plate to supplement growth. Cells from this plate were lysed in water at 100°C for 25 minutes. PCR with the designed sequencing oligonucleotides was conducted again, followed by gel electrophoresis to check the amplicon size, purification, and submission for sequencing.

5.2.5 RT-PCR reactions

To validate expression of *phaP1*, RT-PCR was conducted for the wild type and *phaP1* strains under aerobic and anaerobic conditions using the designed oligonucleotides outlined in Table 5.1. Cultures were grown to mid-exponential on *p*-coumarate as shown in Fig. 5.1, saved with RNALater® solution per manufacture instructions, and stored in -80°C until further processing. RNA was extracted according to conventional chloroform-phenol extraction, and RNA samples were rid of DNA using the Invitrogen™ TURBO™ DNA-Free Kit (ThermoFisher). The RNA samples were purified using the Monarch® RNA Cleanup Kit (New England BioLabs). All samples were confirmed DNA-free due to a lack of a positive band via PCR with the RNA. Particular care was taken to assess

degradation of the RNA samples via bleach gels (Aranda et al., 2012). Only RNA samples that did not yield a DNA band or show degradation via a bleach gel were converted into cDNA using a High-Capacity cDNA Reverse Transcription Kit per manufacture instructions (ThermoFisher). All cDNA samples were tested via RT-PCR using GoTaq® Green Master Mix (Promega) and the *16S rRNA* housekeeping gene (*RPA_RNA55)* to ensure a positive band. If the housekeeping gene did not reveal a positive band from RT-PCR using a certain cDNA sample, that sample was considered too low of quality for further analysis.

5.2.6 Transmission Electron Microscopy (TEM)

TEM was conducted to visualize granules inside the wild type and *phaP1* strains grown on *p*-coumarate in both aerobic and anaerobic conditions as described previously (Alsiyabi et al., 2021). Briefly, the samples were fixed in a 2% glutaraldehyde and 1.5% paraformaldehyde in 100 mM sodium cacodylate buffer and submitted to the Nebraska Center for Biotechnology Morrison Microscopy Core Research Facility at the University of Nebraska-Lincoln. The samples were processed further by washing in sodium cacodylate buffer three times, and post-fixing in 1% osmium tetroxide in deionized water at room temperature for one hour. The samples were dehydrated through an ethanol series, embedded in Spurr medium, ultrathin section were cut using a Leica UC7 ultramicrotome, and the sections were stained with 1% uranyl acid and 1% lead citrate. Images were collected using a Hitachi H7500 TEM and taken without selection or bias.

5.2.7 Metabolic modeling

The trade-off plot between PHB and biomass production for the *phaP1* strain under aerobic conditions was generated by simulating (via flux balance analysis) aerobic growth on *p*-coumarate (Orth et al., 2010) using *R. palustris'* genome-scale metabolic model *iRpa940* (Alsiyabi et al., 2021, 2019). The maximal PHB and biomass generation rates were first determined by maximizing their respective reactions in the model. Next, biomass production was maximized while PHB production rate was set to increasing values between zero and maximal production. The maximum rate of carbon fixation was assumed to be equal to the rate in anaerobic growth (Alsiyabi et al., 2021). Furthermore, arbitrary uptake rates were set for *p*-coumarate and oxygen since the actual uptake rates are not known. However, the general observed trend in the trade-off plot should remain the same.

5.2.8 Statistical methods

Data points for growth curves and GC-MS data represent the averages of biological triplicates, and error bars are the calculated standard deviation from raw data based on the population. Independent, two-tailed *t* tests were used to calculate statistical significance at a 95% confidence interval ($\alpha = 0.05$), and the *p* value is listed where appropriate.

5.3. Results and Discussion

Our recent efforts suggested intracellular space is a limiting factor for maximum production of PHBV by *R. palustris* due to one large granule being formed inside the cells (Alsiyabi et al., 2021). PhaP1 leads to smaller and more abundant PHB granules in *C. necator*, and it was hypothesized that expression of *phaP1* would increase overall PHBV titers from *R. palustris*. Thus, *phaP1* was expressed in *R. palustris* with the aim of

overproducing PHBV from lignocellulosic sources by maximizing the use of intracellular space via producing smaller and more abundant granules.

5.3.1 Gene expression analysis for *phaP1*

Gene expression analysis was first conducted via RT-PCR to verify the expression of *phaP1* in the *phaP1* strain compared to the wild type strain. Fig. 5.1 depicts the expression bands for *phaP1* and *16S rRNA* in each condition. All conditions showed significant expression of the *16S rRNA* housekeeping gene. Furthermore, all conditions for the *phaP1* strain yielded expression of *phaP1*, whereas the wild type strain did not. In Fig. 5.1A, the positive and negative controls using *R. palustris* gDNA did not yield expression, which was to be expected since *phaP1* is naturally occurring in *C. necator*. In Fig. 5.1B, the controls for *16S rRNA* using *C. necator* gDNA did not yield expression since this occurs naturally in *R. palustris*.

5.3.2 Comparisons of growth and PHBV production

Analyses were conducted to assess the impacts on growth and PHBV production due to *phaP1* expression in *R. palustris*. In order to test whether aerobic PHBV production was fostered solely due to the stress of plasmid maintenance, the Backbone strain (i.e. without the *phap1* gene) was compared to the *phaP1* strain under aerobic conditions. Since wild type did not yield PHBV production aerobically, assessing the Backbone strain in aerobic conditions was ideal for deciphering if the stress of plasmid maintenance was the reason for the significant boost in PHBV production. Fig. 5.2 provides growth curves for the wild type, *phaP1,* and backbone strains. Fig. 5.3A depicts the 3HB and 3HV fractions produced anaerobically from the wild type and *phaP1* strains, while Fig. 5.3B depicts the

fractions for the *phaP1* and Backbone strains under aerobic conditions since wild type *R. palustris* did not yield PHBV production aerobically.

Under anaerobic conditions, there was no significant difference in maximum OD between the wild type and *phaP1* strains (p value = 0.395) using independent t tests (α = 0.05). There was also no statistical significance in maximum PHBV titers (i.e. 3HB + 3HV fractions) between the wild type and *phaP1* strains (p value = 0.137) in anaerobic conditions, but there was a significant difference in 3HV fractions between the strains. The *phaP1* strain generated a significantly higher 3HV fraction (0.25 g/L) compared to the wild type strain (0.04 g/L) under anaerobic conditions (p value = 0.00316). Increased production of 3HV is linked to increased propionyl-CoA pools, whereby β-ketothiolase conducts condensation of acetyl-coenzyme A (acetyl-CoA) and propionyl-CoA to form 3HV. Thus, it is hypothesized that expression of *phaP1* enables more efficient utilization of propionyl-CoA pools or performs stress mitigation in other ways (e.g. chaperone-like activities) that fostered higher 3HV fractions (Mezzina et al., 2017). Although the expression of *phaP1* did not yield higher 3HB production compared to the wild type strain, the 3HV fraction was higher and ultimately yields a bioplastic with more desirable thermomechanical properties compared to PHB alone (Li et al., 2016). Hence, heterologous phasin expression in *R. palustris* can be a strategy for producing bioplastics that have improved market applicability via altering the monomer fractions of the polymer as shown in other organisms (Kawashima et al., 2015).

There was also no significant difference in maximum OD between the wild type, *phaP1*, and backbone strains in aerobic conditions (p values > 0.05) using independent t tests (α = 0.05). Expression of *phaP1* yielded 3HB production from *R. palustris* aerobically

(0.7 g/L), which is significantly higher than the maximum anaerobic titer (0.41 g/L) for the wild-type strain (p value = 1.8 x 10^{-7}). The 3HV fraction generated aerobically from the *phaP1* strain (0.074 g/L) was also significantly higher than the wild type fraction (0.04 g/L) in anaerobic conditions (p value = 0.000126). In general, utilizing *phaP1* expression in *R. palustris* to foster aerobic PHBV production provides more flexibility for industrial processing. In aerobic bacteria the methyl citric acid cycle and the methylmalonyl-CoA pathways are major limiting factors inhibiting complete oxidation of propionic acid, thereby possibly limiting the 3HV fraction of PHBV. Thus, analysis and engineering of tradeoffs between these pathways under aerobic conditions could be a way forward to further improve the 3HV fractions from the *phaP1* strain under aerobic conditions (Steinbüchel and Lütke-Eversloh, 2003).

In order to test whether aerobic PHBV production was fostered solely due to the stress of plasmid maintenance, the Backbone strain was compared to the *phaP1* strain under aerobic conditions (Figs. 5.2 and 5.3). The Backbone strain produced a relatively small amount of 3HB (approximately 0.05 g/L maximum), and it is hypothesized that the stress of having to maintain the plasmid fostered this production (Fig. 5.3B). The 3HB production from the Backbone strain was merely 1/14 that of the production from the *phaP1* strain (0.7 g/L). Furthermore, the Backbone strain did not yield any 3HV production, compared to 0.074 g/L generated from the *phaP1* strain. Statistical comparison of the 3HB (p value = 1.243 x 10^{-6}) and 3HV (p value = 5.402 x 10^{-9}) fractions produced from the Backbone vs. the *phaP1* strains is significant, which supports the hypothesis that aerobic PHBV production is not solely due to the maintenance of the plasmid.

However, further analysis was conducted for the *phaP1* strain in aerobic conditions since it yielded a slower growth rate. It was hypothesized that the reduced growth rate could be due to tradeoffs in biomass and PHBV production. A genome-scale metabolic model of *R. palustris*, called *iRpa940*, was recently applied to compare tradeoffs in growth and PHB production from a variety of substrates including *p*-coumarate (Alsiyabi et al., 2021). Genome scale modeling synergizes results from the context of whole-cell metabolism, utilizing annotated breakdown pathways for the corresponding substrates. Since there was a lack of kinetic parameters and concentration ranges for PHBV production reactions in *R. palustris*, only tradeoffs corresponding to PHB were assessed previously. However, it is likely that the outcomes utilizing the model are very comparable between PHB and PHBV since the monomer products are produced by the same enzymes. Thus, this genome-scale metabolic model was employed here to assess the hypothesis that the *phaP1* strain had a reduced growth rate due to the new PHBV production compared to wild type *R. palustris* (Alsiyabi et al., 2021, 2019). As expected, the relationship between growth rate and PHBV production is linear (Fig. 5.3C) and reflects a direct negative correlation. Thus, since the *phaP1* strain produced PHBV under aerobic conditions compared to no production from the wild type strain, the *phaP1* strain had a lower growth rate to compensate for PHBV production.

In summary, expression of *phaP1* yielded increased 3HV fractions under both anaerobic and aerobic conditions, and also fostered PHBV production aerobically. Increased 3HV fractions are desirable since they create a bioplastic with increased tensile strength, impact strength, and flexibility that render it more applicable in a wider array of

applications (Heinrich et al., 2015). Engineering the production of PHBV aerobically also boosts the industrial production potential since it provides flexibility in processing.

5.3.3 Changes in PHBV granule formation

In addition to the gene expression, growth, and PHBV production analyses, TEM was conducted to test the hypothesis that expression of *phaP1* in *R. palustris* would boost PHBV production by fostering smaller and more abundant granules inside the cytoplasm. Fig. 5.4 depicts the TEM images of wild type cells (in the left column) versus *phaP1* cells (in the right column). Fig. 5.4A, B of the wild type and *phaP1* cells respectively in anaerobic conditions shows a discrepancy from the large, single granule produced in the wild type cells compared to smaller, and more numerous granules in the *phaP1* cells. There are some variations in terms of brightness between the PHBV granules, which can be attributed to the small granules getting replaced by embedding medium easier than the larger ones as well as variations in section thickness (Wahl et al., 2012). Furthermore, expression of *phaP1* appears to alter the subcellular localization of the PHBV granules in *R. palustris*, which has been shown in *C. necator* as well (Wahl et al., 2012). The granules in the cells from the *phaP1* strain are more dispersed inside the cytoplasm rather than remaining primarily at the poles. There is also a clear discrepancy between images taken of cells grown under aerobic conditions (Fig. 5.4C-F). Wild type *R. palustris* grown aerobically did not yield any PHBV titer, which is reflected in the lack of granules inside the cells (Fig. 5.4C, E). Expression of *phaP1* fostered PHBV production aerobically, which is supported by the granule formation observed in Fig. 5.4D, F. Ultimately, TEM analysis supports the hypothesis that expression of *phaP1* would foster changes in granule

formation inside the cytoplasm of *R. palustris* cells, which also likely contributes to the altered PHBV production capabilities in each condition.

5.4. Conclusions

In this study the Phap1 phasin from *C. necator* was expressed in *R. palustris* to overproduce PHBV by creating smaller and more abundant granules and use more intracellular space. Expression of *phaP1* yielded PHBV production from *R. palustris* aerobically (0.7 g/L), which does not occur in wild type, and to a significantly higher titer compared to wild type anaerobic production (0.41 g/L). The 3HV fractions were also significantly increased under both anaerobic and aerobic conditions. Thus, heterologous phasin expression in *R. palustris* provides flexibility for industrial processing and fosters compositional changes in copolymers with better thermomechanical properties compared to PHB alone.

Table 5.1. Bacterial strains, plasmids, and oligonucleotides used in this study.

Strain, plasmid, or oligonucleotide	Description	Source or reference
Strains		
Rhodopseudomonas palustris CGA009	Wild-type	*Rhodopseudomonas palustris* (Molisch) van Niel BAA-98™
phaP1	*R. palustris* expressing the PhaP1 phasin from *C. necator* H16	This study
Cupriavidus necator H16	Wild-type	DSM 428
Escherichia coli DH10B	NEB 10-beta Competent *E. coli* is a derivative of the popular DH10B. It is T1 phage resistant and endonuclease I (endA1) deficient for high-quality plasmid preparations.	New England Biolabs®, Inc.
Plasmids		
pBBR1MCS-2	Empty backbone; Mobilisable shuttle and expression vector	(Kovach et al., 1995)
pBBR1 ori; kan^R; P_{Lac}-phaP1		(Kovach et al., 1995)
Oligonucleotides for plasmid building		
H16 (F)	GAGTTTGGATCCTTAAGCACTCAGGCAGCCGTCGTCTTCTTTG	*C. necator* gDNA
H16 (R)	GAATTGTGAGCGGATAACAACTTAATTTGCTTGACCTTGAAGTTCACCAC	
rrnbTerm (R)	GTGCTTAAGGATCCAAACTCGAG	PSSBIO32-tonB, a derivative of pBBR1MCS-2
Lac01 (F)	TTGTTATCCGCTCACAATTCCACAC	
Sequencing Lac (F)	GAACGAAGTCTTGACGACCTG	PSSBIO32-tonB-*phaP1*, this study
Sequencing Lac (R)	GTTTGTGTCCACGACAGGTTTC	
Sequencing rrnb (F)	GCACCTCGCTAACGGATTCAC	
Sequencing rrnb (R)	CACCAAGGCGTTTGAAGGCGTC	
Oligonucleotides for RT-PCR		
16SrRNA (F)	CAGGACCGGTCGCAGAGACG	*R. palustris* cDNA
16SrRNA (R)	GACGTCATCCCCACCTTCCTC	
Phap1 (F)	CTGACCACCAAGGCGTTTGAAGG	*R. palustris* cDNA
Phap1 (R)	CAGCAGTTCCTGTGCGTCCTTG	

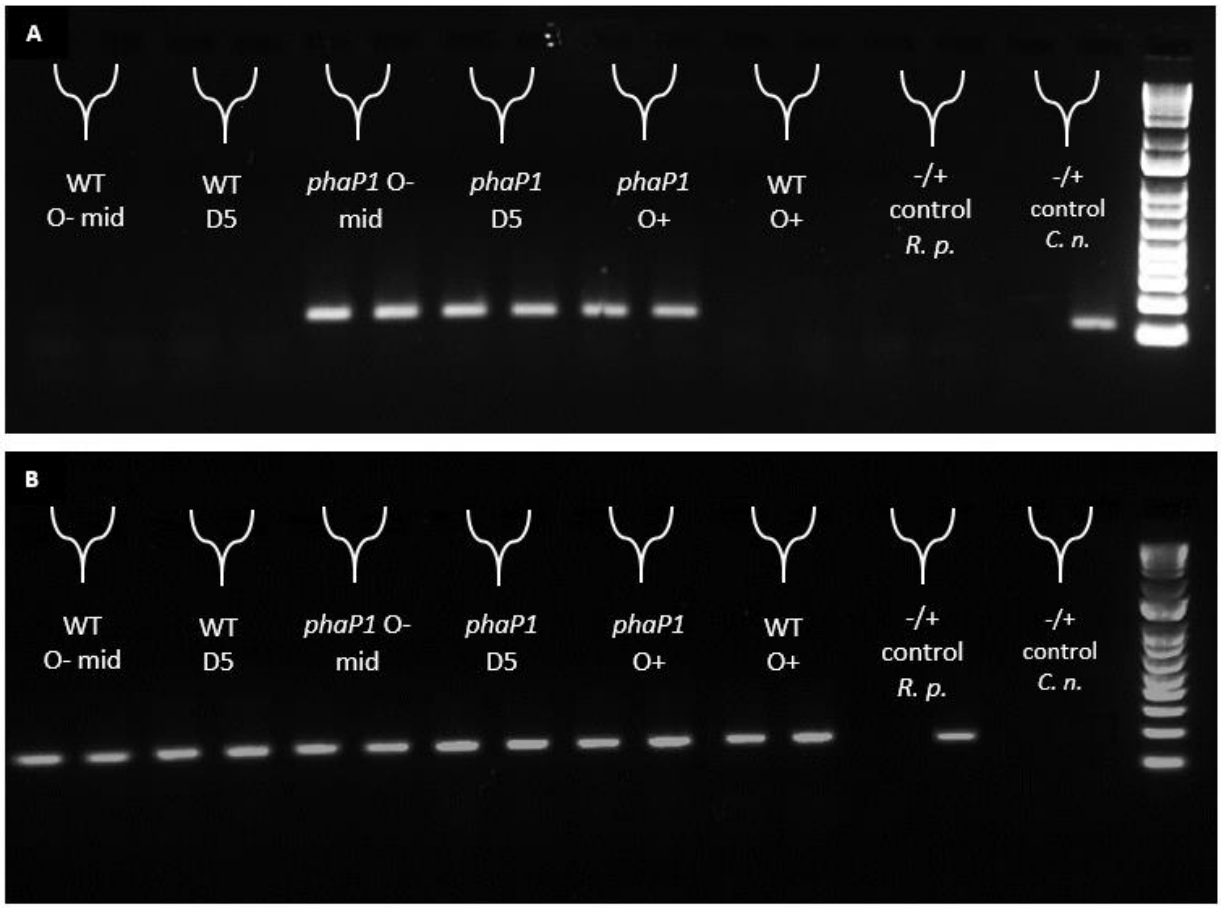

Fig. 5.1. Gene expression in the wild type (WT) vs. *phaP1* strains for (A) *phaP1* and (B) *16S rRNA*. The negative and positive controls represent water vs. gDNA for either *R. palustris* or *C. necator*.

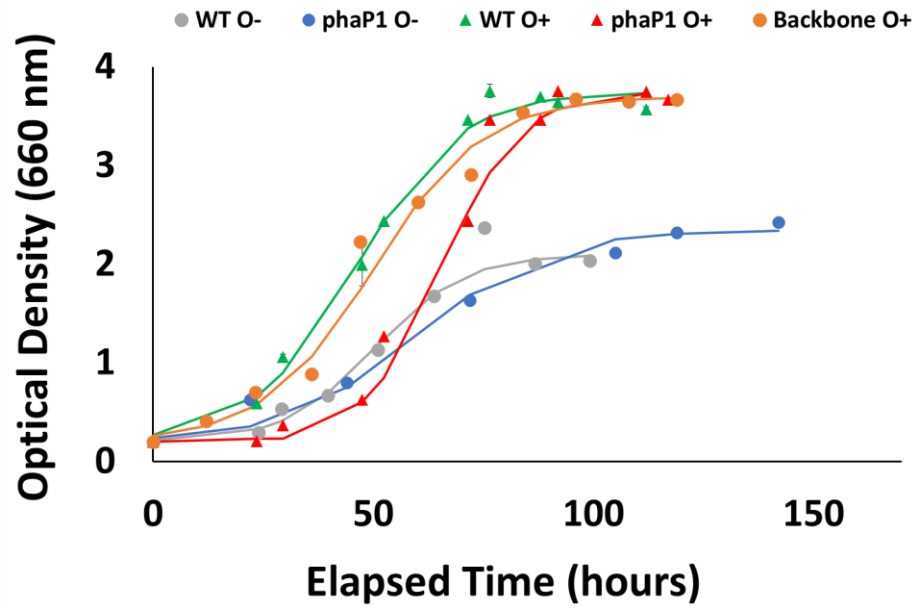

Fig. 5.2: Growth comparison between the wild type (WT), *phap1*, and Backbone strains. The Backbone strain was grown and tested aerobically only to serve as a control for assessing PHBV production. Data points are averages of biological triplicates, and errors bars are the calculated standard deviation. All conditions were grown on 1mM *p*-coumarate and 10mM sodium bicarbonate.

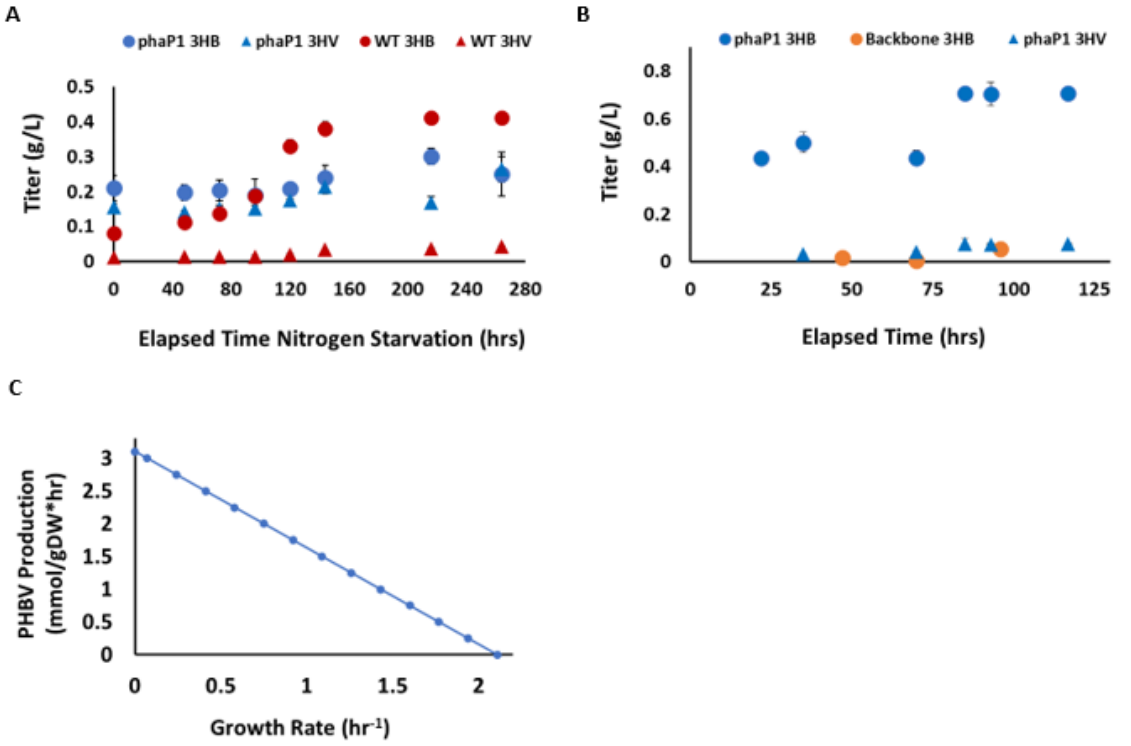

Fig. 5.3: PHBV production in (A) anaerobic conditions from the wild type (WT) and *phaP1* strains, (B) aerobic conditions from the *phaP1* and plasmid backbone (pBBR1MCS-2) strains (the WT strain yielded no PHBV under aerobic conditions), and (C) Trade-off pot comparing growth rate and PHBV production by the *phaP1* strain under aerobic conditions. PHBV production is broken down into the monomer components of 3HB and 3HV that can be measured via GC-MS. Data points represent biological triplicates, and error bars are the calculated standard deviation. All conditions were grown on 1mM *p*-coumarate and 10mM sodium bicarbonate.

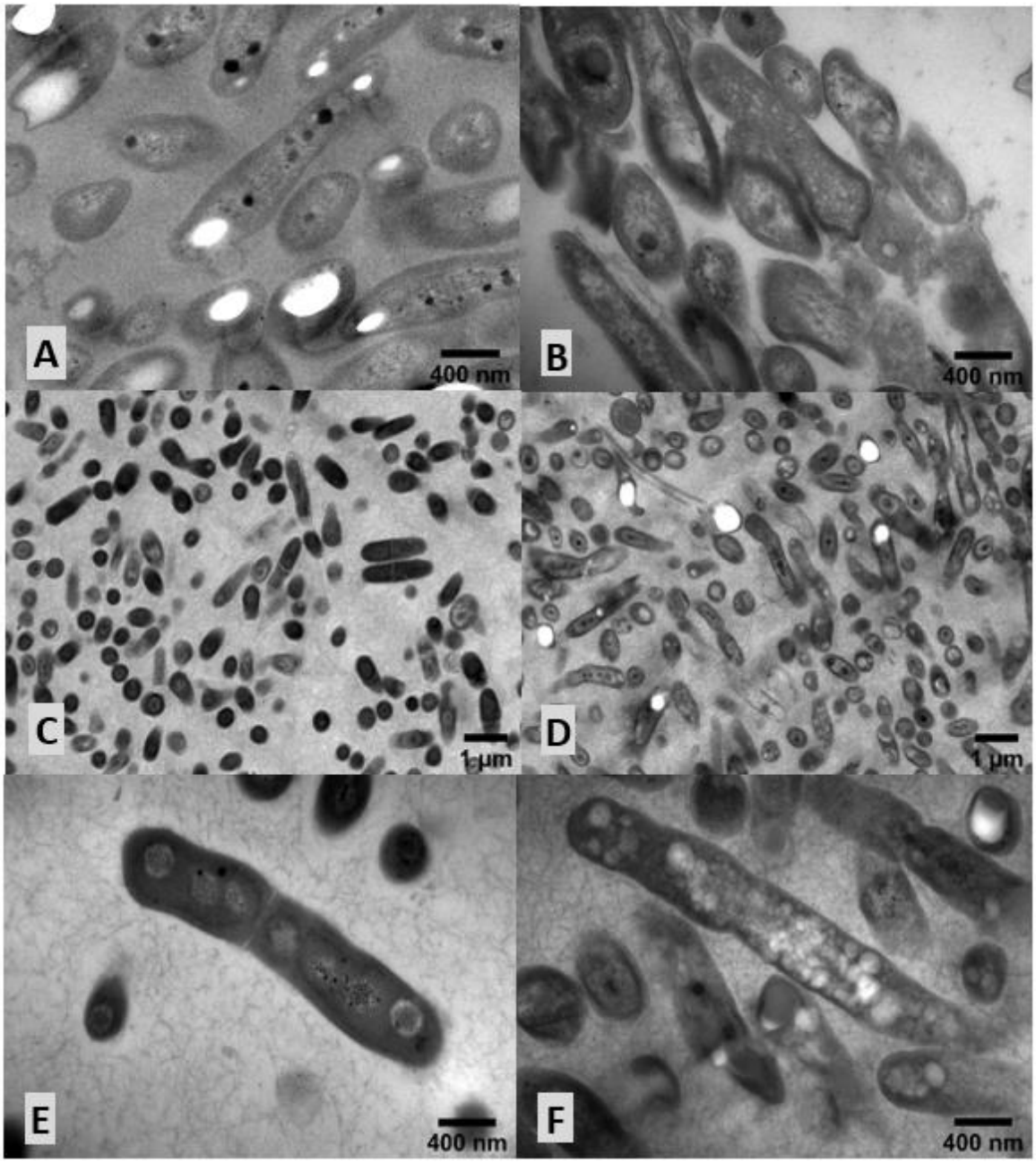

Fig. 5.4. TEM images of cells grown on *p*-coumarate for (A) wild type strain under anaerobic conditions, (B) *phaP1* strain under anaerobic conditions, (C) wild type strain under aerobic conditions, (D) *phaP1* strain under aerobic conditions, (E) wild type strain under aerobic conditions with higher magnification, and (G) *phaP1* strain under aerobic conditions with higher magnification. White inclusions inside the cytoplasm represent PHBV granules.

5.5 References

Almeida, de A., Catone, M. V, Rhodius, V.A., Gross, C.A., Pettinari, M.J., 2011. Unexpected stress-reducing effect of PhaP, a poly(3-hydroxybutyrate) granule-associated protein, in Escherichia coli. Appl. Environ. Microbiol. 77, 6622–6629. https://doi.org/10.1128/AEM.05469-11

Alsiyabi, A., Brown, B., Immethun, C., Wilkins, M., Saha, R., 2021. Synergistic Experimental and Computational Approach Identifies Novel Strategies for PHB Overproduction. https://doi.org/10.21203/rs.3.rs-334477/v1

Alsiyabi, A., Immethun, C.M., Saha, R., 2019. Modeling the Interplay between Photosynthesis, CO2 Fixation, and the Quinone Pool in a Purple Non-Sulfur Bacterium. Sci. Rep. https://doi.org/10.1038/s41598-019-49079-z

Aramvash, A., Moazzeni Zavareh, F., Gholami Banadkuki, N., 2018. Comparison of different solvents for extraction of polyhydroxybutyrate from Cupriavidus necator. Eng. Life Sci. https://doi.org/10.1002/elsc.201700102

Aranda, P.S., LaJoie, D.M., Jorcyk, C.L., 2012. Bleach gel: a simple agarose gel for analyzing RNA quality. Electrophoresis 33, 366–369. https://doi.org/10.1002/elps.201100335

Bello-Gil, D., Roig-Molina, E., Fonseca, J., Sarmiento-Ferrández, M.D., Ferrándiz, M., Franco, E., Mira, E., Maestro, B., Sanz, J.M., 2018. An enzymatic system for decolorization of wastewater dyes using immobilized CueO laccase-like multicopper oxidase on poly-3-hydroxybutyrate. Microb. Biotechnol. 11, 881–892. https://doi.org/10.1111/1751-7915.13287

Brown, B., Immethun, C., Wilkins, M., Saha, R., 2020a. Rhodopseudomonas palustris CGA009 polyhydroxybutyrate production from a lignin aromatic and quantification via flow cytometry. Bioresour. Technol. Reports 11, 100474. https://doi.org/https://doi.org/10.1016/j.biteb.2020.100474

Brown, B., Immethun, C., Wilkins, M., Saha, R., 2020b. Rhodopseudomonas palustris CGA009 polyhydroxybutyrate production from a lignin aromatic and quantification via flow cytometry. Bioresour. Technol. Reports. https://doi.org/10.1016/j.biteb.2020.100474

Chen, G.-Q., Chen, X.-Y., Wu, F.-Q., Chen, J.-C., 2020. Polyhydroxyalkanoates (PHA) toward cost competitiveness and functionality. Adv. Ind. Eng. Polym. Res. 3, 1–7. https://doi.org/https://doi.org/10.1016/j.aiepr.2019.11.001

Chen, G.Q., Zhang, J., 2018. Microbial polyhydroxyalkanoates as medical implant biomaterials. Artif. Cells, Nanomedicine Biotechnol. https://doi.org/10.1080/21691401.2017.1371185

Chen, Q., Wang, Q., Wei, G., Liang, Q., Qi, Q., 2011. Production in Escherichia coli of poly(3-hydroxybutyrate-co-3-hydroxyvalerate) with differing monomer compositions from unrelated carbon sources. Appl. Environ. Microbiol. 77, 4886–4893. https://doi.org/10.1128/AEM.00091-11

Choi, S.Y., Rhie, M.N., Kim, H.T., Joo, J.C., Cho, I.J., Son, J., Jo, S.Y., Sohn, Y.J., Baritugo, K.A., Pyo, J., Lee, Y., Lee, S.Y., Park, S.J., 2020. Metabolic engineering for the synthesis of polyesters: A 100-year journey from polyhydroxyalkanoates to non-natural microbial polyesters. Metab. Eng. https://doi.org/10.1016/j.ymben.2019.05.009

Draper, J.L., Rehm, B.H., 2012. Engineering bacteria to manufacture functionalized polyester beads. Bioengineered. https://doi.org/10.4161/bbug.19567

Heinrich, D., Raberg, M., Steinbüchel, A., 2015. Synthesis of poly(3-hydroxybutyrate-co-3-hydroxyvalerate) from unrelated carbon sources in engineered Rhodospirillum rubrum. FEMS Microbiol. Lett. 362. https://doi.org/10.1093/femsle/fnv038

Hungund, B.S., Umloti, S.G., Upadhyaya, K.P., Manjanna, J., Yallappa, S., Ayachit, N.H., 2018. Development and characterization of polyhydroxybutyrate biocomposites and their application in the removal of heavy metals. Mater. Today Proc. 5. https://doi.org/10.1016/j.matpr.2018.06.495

Kawashima, Y., Orita, I., Nakamura, S., Fukui, T., 2015. Compositional regulation of poly(3-hydroxybutyrate-co-3-hydroxyhexanoate) by replacement of granule-associated protein in Ralstonia eutropha. Microb. Cell Fact. 14, 187. https://doi.org/10.1186/s12934-015-0380-8

Koller, M., 2020. Advances in polyhydroxyalkanoate (PHA) production, volume 2. Bioengineering. https://doi.org/10.3390/bioengineering7010024

Koller, M., 2017. Advances in polyhydroxyalkanoate (PHA) production. Bioengineering. https://doi.org/10.3390/bioengineering4040088

Kovach, M.E., Elzer, P.H., Hill, D.S., Robertson, G.T., Farris, M.A., Roop, R.M. 2nd, Peterson, K.M., 1995. Four new derivatives of the broad-host-range cloning vector pBBR1MCS, carrying different antibiotic-resistance cassettes. Gene 166, 175–176. https://doi.org/10.1016/0378-1119(95)00584-1

Kuchta, K., Chi, L., Fuchs, H., Pötter, M., Steinbüchel, A., 2007. Studies on the Influence of Phasins on Accumulation and Degradation of PHB and Nanostructure of PHB Granules in Ralstonia eutropha H16. Biomacromolecules 8, 657–662. https://doi.org/10.1021/bm060912e

Larimer, F.W., Chain, P., Hauser, L., Lamerdin, J., Malfatti, S., Do, L., Land, M.L., Pelletier, D.A., Beatty, J.T., Lang, A.S., Tabita, F.R., Gibson, J.L., Hanson, T.E., Bobst, C., Torres Y Torres, J.L., Peres, C., Harrison, F.H., Gibson, J., Harwood, C.S., 2004. Complete genome sequence of the metabolically versatile photosynthetic bacterium Rhodopseudomonas palustris. Nat. Biotechnol. https://doi.org/10.1038/nbt923

Li, Z., Yang, J., Loh, X.J., 2016. Polyhydroxyalkanoates: Opening doors for a sustainable future. NPG Asia Mater. https://doi.org/10.1038/am.2016.48

Maestro, B., Galán, B., Alfonso, C., Rivas, G., Prieto, M.A., Sanz, J.M., 2013. A New Family of Intrinsically Disordered Proteins: Structural Characterization of the Major

Phasin PhaF from Pseudomonas putida KT2440. PLoS One 8. https://doi.org/10.1371/journal.pone.0056904

McKinlay, J.B., Oda, Y., Ruhl, M., Posto, A.L., Sauer, U., Harwood, C.S., 2014. Non-growing rhodopseudomonas palustris increases the hydrogen gas yield from acetate by shifting from the glyoxylate shunt to the tricarboxylic acid cycle. J. Biol. Chem. https://doi.org/10.1074/jbc.M113.527515

Medeiros Garcia Alcântara, J., Distante, F., Storti, G., Moscatelli, D., Morbidelli, M., Sponchioni, M., 2020. Current trends in the production of biodegradable bioplastics: The case of polyhydroxyalkanoates. Biotechnol. Adv. https://doi.org/10.1016/j.biotechadv.2020.107582

Mezzina, M.P., Álvarez, D.S., Egoburo, D.E., Peña, R.D., Nikel, P.I., Pettinari, M.J., 2017. A new player in the biorefineries field: Phasin PhaP enhances tolerance to solvents and boosts ethanol and 1,3-propanediol synthesis in Escherichia coli. Appl. Environ. Microbiol. 83. https://doi.org/10.1128/AEM.00662-17

Mezzina, M.P., Pettinari, M.J., 2016. Phasins, Multifaceted Polyhydroxyalkanoate Granule-Associated Proteins. Appl. Environ. Microbiol. 82, 5060 LP – 5067. https://doi.org/10.1128/AEM.01161-16

Muneer, F., Rasul, I., Azeem, F., Siddique, M.H., Zubair, M., Nadeem, H., 2020. Microbial Polyhydroxyalkanoates (PHAs): Efficient Replacement of Synthetic Polymers. J. Polym. Environ. 28, 2301–2323. https://doi.org/10.1007/s10924-020-01772-1

Nangle, S.N., Ziesack, M., Buckley, S., Trivedi, D., Loh, D.M., Nocera, D.G., Silver, P.A., 2020. Valorization of CO₂ through lithoautotrophic production of sustainable chemicals in Cupriavidus necator bioRxiv 2020.02.08.940007. https://doi.org/10.1101/2020.02.08.940007

Orth, J.D., Thiele, I., Palsson, B.O., 2010. What is flux balance analysis? Nat. Biotechnol. https://doi.org/10.1038/nbt.1614

Parlane, N.A., Gupta, S.K., Rubio-Reyes, P., Chen, S., Gonzalez-Miro, M., Wedlock, D.N., Rehm, B.H.A., 2017. Self-Assembled Protein-Coated Polyhydroxyalkanoate Beads: Properties and Biomedical Applications. ACS Biomater. Sci. Eng. https://doi.org/10.1021/acsbiomaterials.6b00355

Pfeiffer, D., Jendrossek, D., 2012. Localization of poly(3-Hydroxybutyrate) (PHB) granule-associated proteins during PHB granule formation and identification of two new phasins, phap6 and phap7, in Ralstonia eutropha H16. J. Bacteriol. 194. https://doi.org/10.1128/JB.00779-12

Pillai, A.B., Kumar, A.J., Kumarapillai, H., 2019. Synthetic Biology and Metabolic Engineering Approaches for Improved Production and Recovery of Bacterial Polyhydroxyalkanoates, in: Next Generation Biomanufacturing Technologies, ACS Symposium Series. American Chemical Society, pp. 181-207 SE–9. https://doi.org/doi:10.1021/bk-2019-1329.ch009

Ponnusamy, V.K., Nguyen, D.D., Dharmaraja, J., Shobana, S., Banu, J.R., Saratale, R.G., Chang, S.W., Kumar, G., 2019. A review on lignin structure, pretreatments, fermentation reactions and biorefinery potential. Bioresour. Technol. 271, 462–472. https://doi.org/https://doi.org/10.1016/j.biortech.2018.09.070

Pötter, M., Müller, H., Reinecke, F., Wieczorek, R., Fricke, F., Bowien, B., Friedrich, B., Steinbüchel, A., 2004. The complex structure of polyhydroxybutyrate (PHB) granules: Four orthologous and paralogous phasins occur in Ralstonia eutropha. Microbiology. https://doi.org/10.1099/mic.0.26970-0

Qi, Q., Steinbüchel, A., Rehm, B.H.A., 2000. In vitro synthesis of poly(3-hydroxydecanoate): Purification and enzymatic characterization of type II polyhydroxyalkanoate synthases PhaC1 and PhaC2 from Pseudomonas aeruginosa. Appl. Microbiol. Biotechnol. 54. https://doi.org/10.1007/s002530000357

Qian, E.W., 2013. Pretreatment and Saccharification of Lignocellulosic Biomass, in: Research Approaches to Sustainable Biomass Systems. https://doi.org/10.1016/B978-0-12-404609-2.00007-6

Rajesh Banu, J., Kavitha, S., Yukesh Kannah, R., Poornima Devi, T., Gunasekaran, M., Kim, S.-H., Kumar, G., 2019. A review on biopolymer production via lignin valorization. Bioresour. Technol. 290, 121790. https://doi.org/https://doi.org/10.1016/j.biortech.2019.121790

Raza, Z.A., Abid, S., Banat, I.M., 2018. Polyhydroxyalkanoates: Characteristics, production, recent developments and applications. Int. Biodeterior. Biodegrad. https://doi.org/10.1016/j.ibiod.2017.10.001

Sabbagh, F., Muhamad, I.I., 2017. Production of poly-hydroxyalkanoate as secondary metabolite with main focus on sustainable energy. Renew. Sustain. Energy Rev. https://doi.org/10.1016/j.rser.2016.11.012

Sharma, P.K., Fu, J., Spicer, V., Krokhin, O. V, Cicek, N., Sparling, R., Levin, D.B., 2016. Global changes in the proteome of Cupriavidus necator H16 during poly-(3-hydroxybutyrate) synthesis from various biodiesel by-product substrates. AMB Express 6. https://doi.org/10.1186/s13568-016-0206-z

Steinbüchel, A., Lütke-Eversloh, T., 2003. Metabolic engineering and pathway construction for biotechnological production of relevant polyhydroxyalkanoates in microorganisms. Biochem. Eng. J. 16, 81–96. https://doi.org/https://doi.org/10.1016/S1369-703X(03)00036-6

Tu, Q., Yin, J., Fu, J., Herrmann, J., Li, Y., Yin, Y., Stewart, A.F., Müller, R., Zhang, Y., 2016. Room temperature electrocompetent bacterial cells improve DNA transformation and recombineering efficiency. Sci. Rep. 6, 24648. https://doi.org/10.1038/srep24648

Ushimaru, K., Motoda, Y., Numata, K., Tsuge, T., 2014. Phasin proteins activate aeromonas caviae polyhydroxyalkanoate (PHA) synthase but not ralstonia eutropha PHA synthase. Appl. Environ. Microbiol. 80. https://doi.org/10.1128/AEM.04179-13

Wahl, A., Schuth, N., Pfeiffer, D., Nussberger, S., Jendrossek, D., 2012. PHB granules are attached to the nucleoid via PhaM in Ralstonia eutropha. BMC Microbiol. 12, 262. https://doi.org/10.1186/1471-2180-12-262

https://doi.org/10.1007/s002530000357

Qian, E.W., 2013. Pretreatment and Saccharification of Lignocellulosic Biomass, in: Research Approaches to Sustainable Biomass Systems. https://doi.org/10.1016/B978-0-12-404609-2.00007-6

Rajesh Banu, J., Kavitha, S., Yukesh Kannah, R., Poornima Devi, T., Gunasekaran, M., Kim, S.-H., Kumar, G., 2019. A review on biopolymer production via lignin valorization. Bioresour. Technol. 290, 121790. https://doi.org/https://doi.org/10.1016/j.biortech.2019.121790

Raza, Z.A., Abid, S., Banat, I.M., 2018. Polyhydroxyalkanoates: Characteristics, production, recent developments and applications. Int. Biodeterior. Biodegrad. https://doi.org/10.1016/j.ibiod.2017.10.001

Sabbagh, F., Muhamad, I.I., 2017. Production of poly-hydroxyalkanoate as secondary metabolite with main focus on sustainable energy. Renew. Sustain. Energy Rev. https://doi.org/10.1016/j.rser.2016.11.012

Sharma, P.K., Fu, J., Spicer, V., Krokhin, O. V, Cicek, N., Sparling, R., Levin, D.B., 2016. Global changes in the proteome of Cupriavidus necator H16 during poly-(3-hydroxybutyrate) synthesis from various biodiesel by-product substrates. AMB Express 6. https://doi.org/10.1186/s13568-016-0206-z

Steinbüchel, A., Lütke-Eversloh, T., 2003. Metabolic engineering and pathway construction for biotechnological production of relevant polyhydroxyalkanoates in microorganisms. Biochem. Eng. J. 16, 81–96. https://doi.org/https://doi.org/10.1016/S1369-703X(03)00036-6

Tu, Q., Yin, J., Fu, J., Herrmann, J., Li, Y., Yin, Y., Stewart, A.F., Müller, R., Zhang, Y., 2016. Room temperature electrocompetent bacterial cells improve DNA transformation and recombineering efficiency. Sci. Rep. 6, 24648. https://doi.org/10.1038/srep24648

Ushimaru, K., Motoda, Y., Numata, K., Tsuge, T., 2014. Phasin proteins activate aeromonas caviae polyhydroxyalkanoate (PHA) synthase but not ralstonia eutropha PHA synthase. Appl. Environ. Microbiol. 80. https://doi.org/10.1128/AEM.04179-13

Wahl, A., Schuth, N., Pfeiffer, D., Nussberger, S., Jendrossek, D., 2012. PHB granules are attached to the nucleoid via PhaM in Ralstonia eutropha. BMC Microbiol. 12, 262. https://doi.org/10.1186/1471-2180-12-262

CHAPTER VI

6. Conclusions and Future Work

The research presented in this dissertation further developed the metabolically robust *R. palustris* as a biotechnology chassis to produce PHAs from lignocellulosic biomass. Multiple approaches were taken that fostered production of PHB and PHBV from lignin breakdown products, optimized a high-throughput method for quantifying PHB production, and discovered novel engineering design strategies for the overproduction of PHB from *R. palustris* and other microbes with similar metabolisms. A summary of the major findings is outlined in the summary of results, and recommendations for future research and innovation of also proposed.

6.1 Summary of results

(1) For production of PHB from the LBP *p*-coumarate at shake flask scale (250 mL), results revealed that *R. palustris* produces PHB to a maximum titer of 0.41g/L with a 68% carbon conversion efficiency. Since typical PHB extraction involves lysing the cells with toxic solvents, this study optimized a high-throughput quantification method involving flow cytometry and Nile Red or BODIPY 493/503 lipophilic stains. Using a permeabilizer technique, this method yielded high linear correlations with a wide range of both PHB titers a cell counts, which enables the quantification of production on a per-biomass basis. Furthermore, being able to take quick and reliable quantification of PHB production utilizing these stains is advantageous because it could provide leverage for optimal timing during industrial fermentation processing and also yield flexibility for

synthetic biology approaches that use fluorescent proteins (e.g., green or red fluorescent proteins).

(2) This study delivers an integrated experimental and computational modeling approach to decipher metabolic factors controlling PHB production and offers engineering design strategies to boost production. It was shown for the first time that *R. palustris* produces PHBV, a copolymer of PHB with more ideal thermomechanical properties than PHB alone. PHBV production from the LBPs *p*-coumarate and coniferyl alcohol was significantly higher than acetate, and combined experimental results of growth, PHBV production, H_2 production, and TEM suggested there were key characteristics about substrate choice that could foster PHB-overproduction from a metabolic standpoint. To obtain a systems-level understanding of factors driving PHB yield, a model-driven investigation was performed. The model yielded several engineering design strategies including utilizing reduced, high molecular weight substrates that bypass the thiolase reaction (*phaA*) in the PHB production pathway. Butyrate was selected based on the results obtained, and was used to validate the design strategies. Not only does this study employ *R. palustris* as a model organism for deciphering these key design strategies based on its robust metabolism, but the results could be expanded to other microbes with similar metabolisms for the over-production of PHB.

(3) The *phap1* phasin gene from the PHB-producing model bacterium *Cupriavidus necator* H16 was expressed in *R. palustris* with the aim of overproducing PHBV to foster smaller and more abundant granules and maximize the use of intracellular space. Expression of *phaP1* yielded PHBV production from *R. palustris* aerobically (0.7 g/L),

which does not occur in the wild-type strain, and led to a significantly higher PHBV titer than wild-type anaerobic production (0.41 g/L). The 3HV fractions were also significantly increased under both anaerobic and aerobic conditions, which boosts thermomechanical properties. Thus, heterologous phasin expression in *R. palustris* provides flexibility for industrial processing and fosters compositional changes in copolymers with better thermomechanical properties compared to PHB alone.

6.2 Recommendations for future work

(1) Production of PHB from pretreated lignocellulosic biomass is more ideal than isolated LBPs since lignocellosic biomass is a common agricultural waste, generally easier to obtain, and less costly than purified LBPs. Pretreated lignocellulosic biomass is often colored, such as dark alkaline pretreated liquor, which makes it difficult to decipher biomass and PHBV concentrations with conventional methods. Thus, this renders the need to optimize this high-throughput quantification method with flow cytometry for *R. palustris* on lignin from pretreated lignocellulosic biomass in the future.

(2) Since the design strategies discovered in this combined experimental and biology strategy can be expanded to other PHB-producing microbes with similar metabolisms, the results could be assessed on a model organism (such as *C. necator*) for the over-production of PHB. Thus, employing synthetic biology techniques to enlarge the size of the cells could be implemented in the future.

(3) The aerobic PHBV production provides more flexibility for industrial processing such that co-culture systems can be engineered with other aerobic microbes that enhance production efficiency. For example, engineering a co-culture system

between *C. necator* and *R. palustris* on lignocellosic biomass could be ideal since *C. necator* consumes the sugars from hydrolysates while *R. palustris* catabolizes the LBPs. Additionally, this study showed that 3HV fractions can be increased in both aerobic and anaerobic environments, and more investigation is necessary to understand the fundamental mechanisms for how this occurs. Design and engineering towards upscaled production is also necessary to further valorize the system for industrial scale production. Lastly, the native phasins employed by *R. palustris* have yet to be experimentally validated or characterized, which could also be a potential avenue for engineering the overproduction of PHBV from lignin and for manipulating the 3HV fractions of the copolymer.